Title
Design of Electrospun Hydrogel Fibers Containing Multivalent Peptide Conjugates for Cardiac Tissue Engineering

Author
Rode, Nikhil Ajit

Publication Date
2014

Peer reviewed|Thesis/dissertation

Design of Electrospun Hydrogel Fibers Containing Multivalent Peptide Conjugates for Cardiac Tissue Engineering

By

Nikhil Ajit Rode

A dissertation submitted in partial satisfaction of the

requirements for the degree of

Doctor of Philosophy

in

Engineering – Materials Science and Engineering

in the

Graduate Division

of the

University of California, Berkeley

Committee in charge:

Professor Kevin Healy, Chair

Professor Ting Xu

Professor Song Li

Fall 2014

Design of Electrospun Hydrogel Fibers Containing Multivalent Peptide Conjugates for Cardiac Tissue Engineering

Nikhil Ajit Rode

Abstract

Design of Electrospun Hydrogel Fibers Containing Multivalent Peptide Conjugates for Cardiac Tissue Engineering

by

Nikhil Ajit Rode

Doctor of Philosophy in Engineering - Materials Science and Engineering

University of California, Berkeley

Professor Kevin Healy, Chair

A novel material was designed using biomimetic engineering principles to recreate the chemical and physical environment of the extracellular matrix for cardiac tissue engineering applications. In order to control the chemical and specific bioactive signals provided by the material, a multivalent conjugate of a RGD-containing cell-binding peptide with hyaluronic acid was synthesized. These conjugates were characterized using in-line size exclusion chromatography with static multi-angle light scattering, UV absorbance, and differential refractive index measurements (SEC-MALS-UV-RI) to determine their molecular weight and valency, as well as the distributions of each. These conjugates were electrospun with poly(ethylene glycol) and poly(ethylene glycol) diacrylate to create a nanofibrous hydrogel material embedded with bioinstructive macromolecules. This electrospinning process was explored and optimized to create well-formed nanofibers. The diameter and orientation of the fibers was controlled to closely mimic the nanostructure of the extracellular matrix of the myocardium. Further characterization of the material was performed to ensure that its mechanical properties resemble those found in the myocardium. The availability of the peptides embedded in the hydrogel material was confirmed by measuring peptides released by trypsin incubation and was found to be sufficient to cause cell adhesion. This material was capable of supporting cell culture, maintaining the viability of cultured fibroblasts and cardiomyocytes, and preserving cardiomyocyte functionality. In this way, this material shows promise of serving as a biomimetic *in vitro* scaffold for generation of functional myocardial tissue, with possible applications as an *in vivo* cardiac patch for repair of the damage myocardium post-myocardial infarction.

Dedication

For my family, my friends, and all those that believed in me.

Table of Contents

Chapter 1

Motivation, goals, and hypothesis

1.1. Motivation and goals

The need for regeneration and replacement of damaged tissues, as well as for *in vitro* platforms for use in tissue modeling and drug testing, have led to the formation of the field of tissue engineering. In order to generate these constructs, a material is needed to serve as a scaffold for physical support and chemical signaling. The extracellular matrix, as the natural environment for cell growth and function, is the obvious choice for use as a scaffold. However, using natural materials wholesale causes problems with sourcing, variation, potential immunogenicity, and an overly complex and poorly defined environment. Thus, rather than use the material itself, the extracellular matrix is often used as a design reference. The important functionality of the extracellular matrix can be re-engineered from the bottom up using natural and synthetic polymer materials. Specific signals and properties can be included in the material to create a completely defined environment, allowing for the interrogation of the mechanisms underlying the interactions between cells and their environments and easing the regulatory process for translating the material to the clinic.

One aspect of material design for tissue engineering that has only recently been focused on is the role of non-chemical cues, such as material architecture. To address the role of structure in tissue generation, a number of controlled architectures have been created, including physically and chemically patterned surfaces, porous polymers, and networks of nanofibers. Nanofibrous materials are of particular interest, as that closely resembles the architecture of the extracellular matrix. The focus of this dissertation, then, is the generation and characterization of a novel biomaterial that can mimic the extracellular matrix structurally and chemically while providing a defined platform for tissue generation *ex vivo*.

The main goals of the project were:

- Engineer a defined, synthetic hydrogel material for *in vitro* cell culture and *in vivo* tissue regeneration (Chapter 4)
- Impart on this hydrogel a nanofibrous morphology that will mimic the extracellular matrix architecture through the process of electrospinning (Chapters 5 and 6)
- Assess the capability of this material to support cell growth and function with particular focus on cardiomyocyte adhesion, viability and contractility (Chapter 7)

1.2. Hypothesis

The central hypothesis for the development of this material was that materials in which specific biological function has been engineered to recreate the important function of the extracellular matrix, which have physiologically relevant mechanical properties, and which closely mimic the structure of the extracellular matrix, will induce tissue-specific cell function and serve as an *ex vivo* scaffold for tissue-like construct generation.

1.3. Specific aims

The specific aims of this dissertation were:

a) Synthesis and characterization of a multivalent peptide-biomacromolecule conjugate to present bioactive ligands
b) Electrospinning of a hydrogel containing these multivalent conjugates to create a stable nanofibrous hydrogel material capable of presenting specifically engineered cell-instructive signals
c) Optimization of the electrospinning protocol to generate nanofibers with properties that closely mimic the extracellular matrix, such as their diameter, alignment, and modulus
d) Assessment of this nanofibrous hydrogel material to support cell culture, induce alignment, and maintain cardiomyocyte contractility

1.4. Dissertation layout

This dissertation applies biomaterials design principles for the generation of a biomimietic electrospun hydrogel scaffold. This material was evaluated based on its physical, mechanical, and chemical properties, and on its ability to serve as a scaffold for tissue growth. In ***Chapter 1***, the motivations, goals, hypothesis, and specific aims of the dissertation are outlines. ***Chapter 2*** reviews the current state of biomimetic materials design for tissue engineering. It covers the rationale behind and the goals of biomimetic material design, as well as the properties of the extracellular matrix that guide design. The role of nonchemical signals in tissue engineering in particular is addressed. The chapter concludes with a broad overview of the materials and processing methods currently used in tissue engineering, and some of their applications. ***Chapter 3*** focuses primarily on one of those processing methods, electrospinning. An overview of the process and of the underlying physics, as well as the various processing parameters involved and their effects on the resultant material, is provided. Lastly, the chapter reviews the use of electrospinning in tissue engineering, the various natural and synthetic polymers that have been successfully electrospun, and their tissue engineering applications. ***Chapter 4*** describes the synthesis of a multivalent peptide-polymer conjugate, as well as a methodology for its characterization using in-line size exclusion chromatography, UV light absorbance, multi-angle static light scattering, and differential refractometry. This method allows for the measurement of the molecular weight, valency, and polydispersity of the sample, amongst

other properties, in an absolute way, without need of a standard and using a minimal amount of material. In ***Chapter 5***, this multivalent conjugate is electrospun along with a carrier polymer and crosslinked into a nanofibrous hydrogel. A phase diagram of this process is created to ensure proper material morphology. The effect of the concentration of poly(ethylene glycol) diacrylate on the distribution of the diameters of the nanofibers is described. Finally, the ability of various electrospinning targets to generate aligned nanofibers is assessed. In ***Chapter 6***, the nanofibrous materials generated in Chapter 5 are physically and chemically characterized to assess their ability to mimic the extracellular matrix. The effect of photoinitiator, poly(ethylene glycol) diacrylate concentration, and fiber alignment on material modulus is measured. The availability of the embedded peptides on the surface of the material is characterized by the action of trypsin to cleave a fluorescently marked peptide. The dissertation concludes with ***Chapter 7***, which evaluates the capability of the material to serve as scaffold for tissue engineering. The ability of the material to align adhered cells in the direction of fiber alignment is assessed, as is the capability of cardiomyocytes to generate force and contract on the material.

Chapter 2

Introduction to scaffold design in tissue engineering

2.1. Introduction to tissue engineering

In recent years, the need for repair or replacement of damaged organs and tissues has vastly outpaced the availability of organs from donor sources[1]. Biomaterials, and in particular tissue engineering, have become an important tool in addressing this clinical need. Tissue engineering is a relatively young field combining the expertise of molecular biology, bioengineering, and materials science to address the problem of tissue damage and organ failure through the development of an implantable scaffold. This scaffold, when combined with soluble signaling factors, will allow for cells to develop structurally and functionally as if they were in their native tissue[2]. Cells may either be developed on the scaffold *ex vivo* on the scaffold pre-implantation, or recruited *in situ* post-implantation. The scaffold must provide both the proper chemical and mechanical environment until the tissue is mature and stable[3], at which point it will ideally degrade, leaving only new biological material[4].

The extracellular matrix (ECM) has a complex chemistry and structure that is lacking in most biomaterials. Even the most complexly engineered synthetic biomaterials will fail to capture the full spectrum of signals provided to cells by the ECM. Initially, biomaterials used in tissue repair served mainly as space filling or structural materials intended to aid in wound healing. Ideal biomaterials were believed to be biologically inert, non-cell binding and non-inflammatory. However, recent advances have begun refining biomaterials to be cell-instructive and interact with the body in positive ways, rather than trying to minimize impact. One method to accomplish this is designing materials that more closely mimic the important aspects of the cell-ECM interaction for a given application and cell type[5]. In this way, biomaterials can serve not only a passive structural and macromechanical purpose in tissue repair, but also an active chemical and biological role.

This chapter provides an overview of the current state of scaffold material design for tissue engineering with a focus on materials engineered to mimic the ECM. The principles and goals of biomimetic scaffold design are presented, as are the guiding properties of the ECM itself, namely its composition, structure, and mechanics. The role of mechanics and structure in tissue engineering are explored. Finally, an overview of commonly used materials and processing methods for tissue scaffold generation is provided.

2.2. Biomimicry and the extracellular matrix

2.2.1. The need for biomimetic materials

The extracellular matrix is an incredibly complex material consisting of myriad structural proteins, polysaccharides, proteoglycans, and soluble and tethered growth factors. This material provides physical and chemical cues to cells in a spatially and temporally controlled way while simultaneously acting as a structural support for tissue growth. Each component of the ECM has specific adhesion and signaling interactions that varies with cell type. A diagram of some of these interactions is shown in Figure 2.1. Communication between the cells and ECM is multidirectional, with cells degrading and depositing ECM, as well as migrating through it.

Modern materials used as tissue scaffolds attempt to harness the natural processes of tissue growth and wound healing to occur in a synthetic, controlled environment. As the natural ECM has specifically evolved to serve in this function, it is used as a guide and reference for biomaterial design. Thus, engineers in the tissue engineering field try to recapitulate as many of these cell-ECM interactions as possible using biomimetic materials. The goal of biomimetic design is to create a material that can mimic the native ECM in all structural, chemical, and mechanical aspects pertaining to a specific subset of tissue and cell types.

The structural and mechanical properties of biomimetic materials are largely dictated by polymer choice and processing methods, with specific chemical interactions engineered in depending on the design specifications. These chemical interactions consist mainly of specific macromolecular recognition and binding motifs included to induce specific behavior in cells. The main method in which this has been achieved is the inclusion of either proteins or protein fragments in the material. These signals can be tethered to the material to increase cell/material interaction, or released to allow for cellular internalization.

In addition, specific enzymatic degradation has recently been included in biomaterial design to allow for the cells to influence their environment as they would in the natural ECM. In this way, cells are capable of migrating through the material and depositing their own ECM proteins. In time, this will ideally result in the complete replacement of the synthetic material with natural ECM and the generation of a functional tissue construct.

In order to make biomimetic material use practical, the complex environment of the ECM has been broken down into component building blocks that can be included in functional material design. These include specific binding peptides, included growth factors, and enzymatically degradable crosslinking agents. In this way, biomimetic materials can be synthesized that contain only the necessary signals for a given application or cell type, cutting down both complexity of synthesis and material cost. In addition, this bottom-up approach allows for the underlying mechanisms of cell/material interaction to be elucidated, increasing the library of future building blocks available[6].

2.2.2. Composition of the extracellular matrix

The composition of the extracellular matrix varies from tissue to tissue, as well as within different parts of the same tissue. The ECM's components can be broken down into three main categories: structural proteins, glycoproteins, and polysaccharides and proteoglycans. A list of the most prevalent and important components of the ECM is presenting in Table 2.1. The structural proteins dominate the mechanical properties of the ECM. The most prominent component of the ECM, making up almost one third of the total protein mass in the body, is collagen[7]. Collagens are a family of fibrillar proteins that bind a number of cell surface receptors, including many integrins. The abundance of collagen in the body makes it an attractive protein for biomimetic materials engineering[8]. Collagen itself has been used extensively in bone tissue engineering[9], as have peptides that are capable of mimicking its structure[8] and cell-binding properties. The other major structural protein of the ECM is elastin, which as its name would suggest provides tissue elasticity. Elastin is found predominantly in tissues that regularly undergo strain, such as the skin and arteries.

Glycoproteins are the component of the ECM that most strongly interacts with cells chemically. They are proteins that have been decorated with short oligosaccharides and contain multiple domains that can bind both to cell surface receptors and to other components of the ECM, such as structural proteins. Glycoproteins serve myriad functions, such as controlling ECM organization and moderating cell/ECM interaction. Three of the most common glycoproteins utilized in biomimetic tissue engineering are fibronectin, vitronectin, and laminin. Fibronectin is a high molecular weight integrin-binding protein that will also bind to collagen, fibrin, and other ECM molecules. Vitronectin will also bind integrins and promotes cell adhesion and spreading. The laminin family of proteins is highly diverse and will bind integrins and other cell surface receptors as well as collagen and heparin and have effects on cell differentiation, survival, and morphology.

Polysaccharides and glycosaminoglycans (GAGs) such as hyaluronic acid and heparin are another important component of the ECM. They consist of repeating disaccharide units and strongly bind water. Whereas structural proteins like collagen and elastin provide tensile strength to tissues, GAGs provide compressive strength by resisting the expulsion of water. Some GAGs, such as heparin, will bind growth factors. In the body, this slows their degradation and increases their local concentrations in tissue. In addition, the binding of multiple growth factors to a single GAG creates multivalent interaction with cells. This multivalent interaction has been exploited in biomaterials design to both localize delivered peptides and growth factors and to increase their potency[10]. Swollen hyaluronic acid and GAG hydrogels serve as a space filling matrix in tissues like the eye and synovial fluid. Hyaluronic acid is responsible for the low coefficient of friction and compressive strength of cartilage.

2.2.3. Structure of the extracellular matrix

The nanostructure of the ECM in soft tissues is largely defined by structural proteins. Collagen self-organizes into a rod like structure with a diameter of about 1.5 nm that can be up to 300 nm long[11]. These molecules arrange side by side and offset length-wise to form larger fibrils, which can have diameters of hundreds of nanometers and lengths up to the millimeter range. In structural tissues such as ligament or tendon, these fibrils arrange themselves into collagen fibers with a diameter of roughly 10 micrometers. Space-filling molecules such as hyaluronic acid take the form of a loosely associated hydrogel. Some proteins, such as aggrecan, are large bottlebrush-like molecules that add to the compressive strength of tissues. Together with structural proteins, this makes the ECM effectively a reinforced hydrogel (Figure 2.2).

In many tissues, these fibers form an aligned matrix with which cells will align. The myocardial ECM, for example, consists of aligned collagen fibrils. Collagen type I and III form thick struts that connect myocytes within muscle fibers, as well as different muscle fibers. A looser network of collagen IV runs perpendicular to these collagen fibers. This collagen network serves the dual function of aligning myocytes into myofibrils and connecting different myofibrils mechanically[12]. The ECM is broken down into three levels; the epimysium, perimysium, and endomysium. The epimysium consists of collagen fibers that surround the epicardium and endocardium. As the heart muscle stretches, the collagen fibers of the epimysium align until fully parallel, at which point they resist further stretching, serving as a limit on muscle stretch[13]. The perimysium consists of coiled collagen fibers that surround myocytes. These fibers serve to align myocytes, as well as to transmit contractile forces throughout the myocardium. Endomysial

collagen serves mainly as cell to cell connections and transmits force between cells within a myofibril.

The structure of the ECM varies from tissue to tissue, as well as spatially within a tissue. For example, in articular cartilage, the deep zone, which interfaces with the underlying bone, consists of collagen fibrils arranged perpendicular to the surface of the bone and a high concentration of proteoglycans. In this zone, the resident chrondrocytes are arranged in a columnar orientation parallel to the collagen[14]. Further from the bone is the transitional zone, in which the collagen fibrils are thinner and more disorganized. Chrondrocytes here are more spherical, with no preferred orientation. At the articular surface, collagen fibrils are arranged parallel to the surface and perpendicular to the deep zone collagen. Consequentially, the chondrocytes in this region exhibit a flattened, spread morphology.

2.3. Scaffold design principles

The overarching goal of scaffold design for tissue engineering can be stated thusly: to fabricate a material that, when combined with cells either *ex vivo* or *in vivo*, will produce a functional tissue construct for repair or replacement of damaged tissues. The exact criteria for succeeding at this goal will vary between target tissues. Broadly speaking, the best way to accomplish this goal is to engineer a scaffold that will mimic the native environment of healthy tissue as closely as possible. Practically, a small number of factors can be isolated and accounted for, simplifying the engineering problem of recreating the incredibly complex chemical and physical environment of the ECM.

A number of parameters in scaffold design, material choice, and processing are available to create functional tissue scaffolds (Table 2.2). The first is the architecture of the material. On the macroscopic scale, this involves the shape of the tissue scaffold to arrange the new tissue into a properly formed organ. On the microscopic scale, material porosity, patterning, architecture, and anisotropy will affect the scaffold's performance (Figure 2.3). The mechanical modulus of the material can be tailored using the crosslinking density of hydrogel materials. The chemical environment of the scaffold can be controlled by the inclusion of immobilized binding signals or released growth factors. And finally, the temporal properties of the material can be controlled by changing its rate of degradation, either specific or hydrolytic.

Materials used as a scaffold must serve as a functional synthetic extracellular matrix. They must allow for cellular attachment, proliferation, and in the case of pluripotent or multipotent cell types, differentiation[15]. They must organize cells into the proper three dimensional architecture[16]. The mechanical properties of the scaffold material must resemble that of the ECM in the appropriate tissue. Scaffolds designed for specific tissue types may have additional requirements, such as directionality for heart tissue[17] or strength for bone tissue[18]. When cells are encapsulated within the material itself, additional requirements of nutrient and waste diffusion, gelation kinetics and toxicity, and cell-mediated degradability must be addressed[19]. Scaffolds that are designed to be implanted, rather than be used *in vitro*, must be non-immunogenic, degradable, and allow for rapid vascularization[20,21]. These requirements are summarized in Table 2.3.

2.4. The role of mechanics and microstructure in tissue engineering

2.4.1. Stiffness

There exists an enormous variety in modulus of tissues[22]. The modulus of the ECM can vary from the order of 0.1 kPa in tissue such as the brain, to 30 kPa in demineralized bone. In the extreme case, mineralized ECM in bone can have a modulus of over 20 GPa[23]. In addition, natural ECM is viscoelastic[24], and cells will experience the frequency-dependent mechanical behavior of the substrate[25]. The stiffness of the substrate has recently been shown to have a profound effect on the behavior of cells in both two dimensional and three dimensional culture[26]. The mechanism of the effect of substrate stiffness on cell activity is mediated by cell surface receptors such as integrins[27]. On stiffer substrates, cells are capable of generating a greater amount of tensile force[28]. Varying the tension on the cell, either through use of a stiffer substrate or an actively stretching substrate, will cause reorganization of the cytoskeleton and changes in cell contractility[29,30], as well as directly influencing protein expression[31,32].

Perhaps the most profound and well known example of substrate stiffness effecting cellular behavior was shown by the Discher lab[33]. They demonstrated that the differentiation of mesenchymal stem cells (MSCs) can be biased toward a certain lineage by the substrate stiffness independently of any soluble factors in the media. Namely, MSCs tended to differentiate into a cell type whose native ECM most closely resembled that of the scaffold on which they were cultured, with soft scaffolds enhancing neurogenic differentiation, stiff scaffolds enhancing osteogenic differentiation, and intermediate stiffnesses favoring myogenic differentiation. This work implies that when designing materials for use as a tissue scaffold, especially when undifferentiated cells are being used, care must be taken to match the mechanical properties of the material with that of the tissue-specific ECM.

This has been demonstrated in heart tissue engineering with terminally differentiated cells as well. Culture of rat cardiomyocytes on substrates with stiffness matching that of the myocardial ECM resulted in optimal performance in terms of cell morphology and function. Softer substrates resulted in reduced cell contractility and lowered cell elongation and number, while stiffer substrates had increased fibroblast density and poor excitability[34]. Indeed, the stiffer substrate of the myocardial scar tissue after myocardial infarction has been implicated in reducing the contractile ability of surviving cardiomyocytes[35], which could cause further expansion of the noncontractile area.

There are few synthetic biomaterials that can provide the structural integrity necessary for repairing soft connective tissues like muscle while matching their mechanical properties[36]. This mismatch in stiffness between the tissue and the material can lead to[37] graft failure. One class of materials that provides the necessary range of moduli are hydrogels, which can be mechanically tailored by varying their properties, such as crosslinking density[38].

2.4.2. Roughness and surface topography

Scaffold nanostructure is of utmost importance, as it can greatly increase the surface area over which the cells will interact with the material[39]. The micro- and nanostructure of a material will affect cell adhesion, cytoskeletal arrangement, force transduction, protein expression, and differentiation[6,40]. Alteration of surface geometry, such as the diameter of nanotubes on the

substrate, independent of surface chemistry, can induce changes in cell shape and spreading, which in turn will affect the differentiation of stem cells[41]. Even subtle differences, such as the difference between sharply edged features and rounded features on the substrate, can change cell morphology and protein expression[42]. For a patterned substrate, many properties such as feature size, height, and pitch[43] will all change cellular response. Surprisingly, cells will also respond differently to patterns that are completely ordered and symmetric, versus imperfectly ordered substrates[44,45]. Different cell types will adhere to and interact with substrate surface morphologies in different ways[46].

One commonly used method to exploit the cellular sensitivity to surface morphology is the patterning of grooves or pits on the substrate. These patterns can be created using common photolithographic microfabrication methods used in the semiconductor industry[47], or through means such as nanoimprint lithography[48], laser ablation[49] or electron beam lithography[50]. Patterns of pits and pillars can make a surface resistant to cell binding, with potential applications in materials for which cell attachment is undesirable, such as the surface of a stent[51]. Controlling cellular adhesion through surface patterning can be applied to individual cells. In this way, cell shape can be regulated using patterned surfaces[52]. Altering cell shape has direct effects on behavior such as stem cell differentiation[53,54].

Anisotropic surface patterns, such as long gratings or aligned fibers, can be used to induce alignment of cells[48]. In the presence of long grooves, cells will alter their morphology, becoming elongated along the direction of the grooves. The degree of alignment depends on both the depth and width of the grooves[51]. This is caused by the restructuring of the cell cytoskeleton. Actin filaments predominantly run from the cell edge to the nucleus. An anisotropic substrate with limited available binding locations will tend to cause the actin filaments to run along the grooves. This is true for grooved substrates with depth of as little as 30 nm[55].

2.4.3. Porosity

The capacity for a material to assist in the regeneration of functional tissue has been shown to be dependent on the porosity of the scaffold material[56]. Adding pores to the microstructure of a material will mechanically weaken the material, but provide a large number of potential benefits. A material with a large degree of pore volume will allow for the delivery of a significantly higher number of cells than materials for which cells are restrained to the outer surface. Porosity assists in simulating the ECM architecture and allows for cells to infiltrate the material. An interconnected pore structure is also necessary for the diffusion of nutrients to cells growing within the interior of the material and provides an available avenue for vascularization to occur. In addition, smaller pores can be used as reservoirs for the controlled release of growth factor or other signaling molecules.

The size of the pores will determine what function they are capable of serving, and how various cell types will interact with the porous structure[57]. For example, small pores with a diameter of 5 microns will assist in neovascularization, while larger pores will promote the ingrowth of fibroblasts or other cell types[16]. Pores in the 20-125 micron range will promote skin regeneration, while larger pores in the 100-350 micron range will promote bone regeneration. Factors other than size, such as shape and tortuosity can affect tissue ingrowth into porous materials.

One factor that must be considered in conjunction with material porosity is material degradability. For non-degradable materials, infiltration of cells into the material interior is entirely dependent on the initial porosity. Without porosity, cells will be constrained to the surface of the material. Over time, deposition of proteins and growth of cells will shrink and possibly occlude the pore structure. Materials with surface degradability will experience the opposite progression. Over time, the internal pore structure will expand as the material degrades away, increasing both pore size and interconnectivity.

2.5. Materials in tissue engineering

Biodegradable polymers have become the standard in tissue engineering because of their low incidence of chronic inflammation[58]. These can be broken down into two main categories: synthetic polymer-based materials and natural polymer-based materials. Synthetic polymers allow for a large diversity of chemical and physical properties due to the number of possible monomers and the capability to combine them into copolymers. These materials are easily synthesized in large quantities and possess controllable and consistent properties, but lack innate biological signals. Commonly used synthetic polymers in tissue engineering include poly(ethylene glycol)[59,60], polyesters such as poly(lactic acid) and poly(glycolic acid)[61,62], and polyurethanes[63,64] A more comprehensive list is presented in Table 2.4. Here, we will focus on polyesters and synthetic hydrogels. Natural polymers used in tissue engineering include hydrogels made of polysaccharides such as hyaluronic acid[65,66] or chondroitin sulfate[67,68], or proteins such as collagen[69,70,71], fibrin[72,73,74], and elastin[75,76] Table 2.5). These natural polymers offer the advantage of inherent biological properties such as cell adhesion and signaling and cell-mediated degradability, and unlike synthetic materials which require extra modification[77]. In addition, natural materials readily mimic the mechanical properties of the natural ECM, whereas the majority of synthetic polymeric materials have a much higher modulus.

2.5.1. Polyesters

Polyesters are a group of synthetic polymers containing an ester functional group in their main chain. Polylactic acid (pLA) and its copolymer with polyglycolic acid, pLGA, are some of the most common synthetic polymers used in tissue engineering, having been used in applications for skin, cartilage, bone, ligament, tendon, nerve, bladder and liver regeneration[20]. They are strong and hydrolytically degradable[78], and their degradation products can be excreted through the natural metabolic pathway[79]. This makes them ideal for use in applications in which mechanical stability is key, such as repair of bone defects[80]. However, they are highly hydrophobic and release high quantities of acid when degrading, which may have adverse reactions with nearby tissue[81]. Their hydrophobicity and harsh processing conditions makes them less viable for applications involving cell encapsulation[1]. In addition, the high stiffness of polyesters inhibits their use in repair of soft tissues.

The hydrophobic properties of polyesters allow for the rapid adsorption and spreading of proteins, either from the media or secreted by cells. While this creates an uncontrolled surface chemistry for the material, it does provide an easy avenue for cell attachment. To create a controlled surface chemistry, functional groups have been added to pLGA pre-polymerization with functionalized monomers, or post-polymerization using plasma treatment[82,83], surface hydrolysis[84], chemical grafting[85], or physical adsorption[86,87]. These modifications help change

polyester tissue scaffolds from passive materials to bioactive, instructional, and defined substrates.

2.5.2. Hydrogels

A hydrogel material is made up of a hydrophilic polymer that has been crosslinked and swollen with many times its own weight of water. They are of great interest to the tissue engineering community due to their hydrophilicity and biocompatibility[88]. Hydrogel networks can be formed by chemically crosslinking monomers or oligomers that have multiple functional groups such as acrylates or methacrylates[89]. They can also be made via physical[90], hydrophobic[91], or ionic[92,93] crosslinking. The crosslinking kinetics can be tailored to make the material injectable, crosslinking *in situ* to allow for minimally invasive implantation of tissue scaffolds with or without cells[59,94,95,96]. The mechanical performance of hydrogel materials will depend on intrinsic material properties such as polymer identity, concentration, mesh size, temperature, and pH, and may change over time due to degradation[97]. As a polymer network swollen with water, hydrogels have excellent mass transport properties, allowing for exchange of oxygen and nutrients for cells embedded within the gel.

Synthetic hydrogel materials can be functionalized with small peptides to modulate or enhance their functionality. Due to their hydrophilic nature, cell-excreted ECM proteins do not readily adhere to hydrogel scaffolds, rendering them non-cell adhesive and decreasing cell viability[98]. Modification of the hydrogel with a cell adhesive peptide[99] or protein[100] can aid in the adhesion of cells to the material. Methods of modification include covalent attachment, incorporation into the hydrogel, entrapment of protein or macromolecular conjugates, and specific binding (Figure 2.4). Hydrogel functionalization can also change cellular behavior on the material, such as altering migration[101] or promoting differentiation of stem cells into particular lineages[102,103]. By using an interpenetrating or semi-interpenetrating polymer network, the presentation of these peptides can be controlled independently of hydrogel mechanics[104,105]. Inclusion of a natural polymer in a synthetic polymer hydrogel can also impart functionality to an otherwise inert material.

Natural hydrogels can be created using polysaccharides such as alginate[106], chitosan[107], or hyaluronic acid, as well as from proteins such as collagen[108], and combinations thereof[109]. These materials have the benefit of already containing cell-binding and cell-instructive residues, reducing the need to engineer in specific functionality. In addition, as components of the ECM, they will naturally tend toward more ECM-like morphologies and nanostructures. These natural hydrogels also benefit from reduced cytotoxicity and minimal inflammation and foreign body reaction after implantation. As a drawback, many of these materials are difficult to control, with variations between batches and sources in purity and molecular weight.

2.5.3. Decellularized extracellular matrix

The material most capable of mimicking the ECM is, as would be expected, the ECM itself. To produce a tissue scaffold from the ECM, excised tissue undergoes a decellularization process by which all cellular material is removed. This can be achieved by chemical means using acids and bases[110], surfactants and detergents[111], by solvents such as alcohols or acetone[112], biologically using enzymes[113], or physically[114]. The resulting material can either be solubilized and processed to create a scaffold, or used in its native architecture. Using the latter method,

decellularized ECM can be used as a material that perfectly mimics the chemical and structural environment of healthy tissue. As such, it is capable of supporting cell migration, differentiation, arrangement, and function. The ECM can be harvested from allogeneic or xenogeneic sources, and from a variety of tissues, including skin, bladder, intestine, and the heart[115]. Decellularized ECM has been used in the repair of tendon, breast, liver, respiratory tract, nerve, and adipose tissues.

There are, however, two major drawbacks to using decellularized ECM as a tissue scaffold. First, as biological material from an external source, decellularized ECM will trigger an immune reaction when implanted. Fortunately, if the decellularization is complete, the immune response can be minimized due to the highly conserved nature of ECM proteins. If the decellularization process is incomplete, or if fragmented DNA is left over entrapped in the ECM, it could cause a severe response and ultimately tissue rejection. Complete and thorough removal of the cellular material often causes disruption of the architecture of the ECM, as well as crosslinking of the ECM components[116]. Secondly, decellularized ECM materials must be sterilized prior to implantation, which could further damage the material structure and change its mechanical properties.

2.5.4. Small molecules in tissue engineering

Materials can be designed to release small molecules such as growth factors in a controlled way through either enzymatic or hydrolytic degradation[117,118]. This can be used to either deliver these molecules to the host post-implantation[119] or to provide a steady supply of a soluble factor to cells growing within the material[120,121]. Growth factors can be physically encapsulated within the implant material[122], associated with binding sites within the material[123], or covalently conjugated to the material itself[124,125].

2.6. Processing methods for tissue scaffold generation

With the wide variety of available materials and the large number of structural factors important in tissue scaffold design, there is a suitable large variety of processing methods for creating these materials. For two dimensional surfaces, such as would be presented from a glass, ceramic, metal, or non-hydrogel material, the most common processing method is photolithography, as is used in the semiconductor industry. Microcontact printing and two-dimensional self-assembly are other methods of creating patterned surfaces. Processing bulk hydrogels can impart desired structure for three dimensional tissue scaffolds. Without these processes, bulk hydrogels consist of a mesh-like network of interconnecting polymer chains. The density of the network is determined by the length of the connecting multifunctional monomers, as well as the presence of bifunctional monomers, which can serve to lengthen the distance between crosslinks. Tight polymer networks with only a short distance between crosslinks will give rise to a stiffer gel with more restrictive diffusive properties. The most common three dimensional processing methods for tissue scaffold materials are self assembly of polymers or proteins, salt leaching and solvent casting, 3D printing, and electrospinning. A list of these processing methods is presented in Table 2.6.

2.6.1. Photolithography

Borrowed from the semiconductor industry, photolithography is the best way to impart control of the morphology of metal, metal oxide, or polymer surfaces (Figure 2.5). First, the material surface is cleaned, and a layer of photoactive resist is deposited through spin coating. This photoresist is then exposed to light through a mask representing the pattern desired on the material surface. For positive photoresist, the areas exposed to light become soluble in a "developer" solvent, and the resulting structure directly follows the exposure mask. Negative photoresist becomes crosslinked and insoluble in the developer, inverting the mask pattern. In either case, post-exposure, the surface is exposed to a developer solvent, removing the photoresist over a patterned area. The entire surface is then etched, either using a wet, solvent-based or dry, plasma-based etching procedure. The exposed surface becomes etched, while portions of the surface still covered in the photoresist is left untouched, or the photoresist itself becomes etched, depending on the etching method. After this process, the photoresist is removed, leaving a structured surface that either directly or inversely mimics the photomask used. Photolithography can be used to create features in the sub-micron scale.

Photolithographic techniques have been applied to many different materials and applications. It has been applied to materials such as titanium oxide[42], silicon[43], poly(dimethyl siloxane)[126], and hydrogels[127]. Use of photolithography allows for the creation of organized, defined surface morphology. Morphologies created have varied from aligned grooves[128], pits[45], and columns[129].

2.6.2. Microcontact printing

Evolving out of the photolithographic technique, microcontact printing and soft lithography creates a controlled, patterned chemical surface with minimal changes to the structure of the biomaterial surface (Figure 2.6). Patterned surfaces in a soft material such as poly(dimethyl siloxane) are created using traditional photolithographic methods. This surface is then coated in a desired substance, such as protein or other surface-coating molecule, or cells themselves. This coated, patterned surface can be used as a stamp to apply the substance to a scaffold surface in a way that maintains the pattern. These PDMS masters can be used many times, reducing the cost of manufacturing patterned surfaces compared to direct photolithography.

This technique can be used to control cell attachment. Features on the scale of 20-100 microns can be used to control the arrangement of cells and regulate cell-cell contact and alignment, while sub-micron features can be used to control the binding of individual cells to the surface and the structure of their focal adhesions.

2.6.3. Self-assembly

The process of self-assembly of biomaterials can be broken down into two major categories; two dimensional and three dimensional self-assembly. In two dimensional self-assembly, the material surface is exposed to a molecule that will self-assemble along the surface, presenting a functionalized two dimensional surface. The most common two dimensional self-assembled surfaces are created via thiol-terminated molecules assembling on a gold substrate, or silane terminated molecules on a glass or silicon substrate (Figure 2.7). These molecules

normally take the form of a silane or thiol on one end, a long hydrocarbon chain, and a functional group on the other end to functionalize the surface. The functionalization of the surface can vary from hydroxyl, methyl, carboxyl, or amine groups, as well as oligomers[130]. These groups can change properties such as surface hydrophobicity, which has effects on protein adsorption, and thus cell binding[131]. Spatial control over surface modification using thiol terminated molecules can be controlled by the selective deposition of gold on the material surface.

In three dimensions, self-assembly can be used to generate complex material architecture simply by mixing the components. This is most commonly accomplished by using amphiphilic molecules, with spatially separated hydrophilic and hydrophobic components. These can be either block copolymers or peptide amphiphiles. These molecules will spontaneously form superstructures through the association of their hydrophobic regions to shield them from the aqueous environment. Depending on the specific molecular architecture, namely the relative lengths of the hydrophilic and hydrophobic regions, these molecules may self-assemble into micelles, vesicles, sheets, fibers, or tubes[132] (Figure 2.8). Self-assembly of peptide amphiphiles into nanofibers can be used to create self-supporting 3D matrices at low material concentrations[133]. These fibers present a greatly increased surface density of peptide compared to other nanofiber generation methods, due to the maximized "pinning density" of peptides on the surface[134]. The major downside to using self-assembly in material processing is the severely limited number of materials that will undergo this process, and the relatively strict design parameters under which self-assembly is viable.

2.6.4. Salt leaching

Salt leaching is one of the earliest and simplest methods by which to introduce porosity and nanostructure to biomaterials. In this process, polymer and salt crystals are combined in a mold. Once the polymer has set or been crosslinked, the entrapped salt is dissolved away in a solvent such as water or alcohol. The void space where the salt crystals resided is retained, resulting in the generation of a porous scaffold. The degree of porosity and pore diameter can be controlled by changing the relative quantity and size of the salt crystals. A large variety of materials are compatible with salt leaching, including hydrogels[135], proteins[136], polysaccharides[137], and hydrophobic polymers[138], and these materials have been applied in regeneration of bone, skin, cartilage, and other tissues. Materials formed using salt-leaching, however, are limited in their thickness, as the embedded salt particles must be reached and dissolved by the solvent. In addition, specific measures must be taken to ensure pore interconnectivity. One such strategy is fusing the salt particles before the addition of the polymer. As the porous polymer network forms the negative of the salt inclusions, formation of a connected network within the salt particles results in a connected network of pores in the polymer. This improves the vascularization of the material, which can be inhibited if some of the pores are inaccessible[139].

2.6.5. 3D printing

For whole organ tissue engineering where macroscopic organization is critical, 3D printing presents a cheap, simple, and quick by which scaffolds may be fabricated. The process is elegant in its simplicity. A three dimensional CAD design is fed to a printer with a nozzle capable of movement in three dimensions. The printer recreates the computed design by layer-by-layer deposition of polymer or other scaffold material. In this way, ceramics, hydrogels,

hydrophobic polymers, proteins, and even cells themselves can be printed into whatever form is desired. In fact, the printing process can simultaneously deposit the scaffolding material with one nozzle and cells or cell clusters with another nozzle, pre-seeding the construct with a spatially defined distribution of cells[140]. While it is an incredibly simple and straightforward process, it does lack power. On the macroscale, materials can be printed into whatever tissue architecture is desired. However, 3D printed materials lack control over the micro and nanostructure, with a spatial resolution on the order of 50 microns[141].

2.6.6. Aligned nanofiber generation

Several methods exist for producing aligned polymer nanofibers for tissue scaffolds. Among them are fiber drawing, extrusion, and templating[142]. Fiber drawing consists of mechanically stretching polymer droplets to create high aspect ratio fibers. This method can create fibers with diameters as low as 50 nanometers[143] and hundreds of millimeters long[144]. These fibers can be manually aligned after synthesis, or aligned during the drawing process by means such as a rapidly rotating system. For polymer fiber extrusion, rather than having polymer stretched into fiber form, the polymer is compressed and forced through a die. The fiber cross-section can be designed by altering the die structure. Fiber extrusion has been used to create fibers with diameters in the range of 100-200 nanometers and several microns in length[145]. These fibers can be aligned during the extrusion process again through the use of a rotating system that uses centrifugal force to push the polymer through the die. In the templating process, polymer is injected into a template made of alumina with an aligned nanopore network. The alumina mold is then destroyed to release the polymer nanofibers. Aligned fibers with diameters ranging from 25 to 400 nanometers and up to several hundred microns in length have been fabricated using this method[146].

One of the most widely used processes for nanofiber generation is electrospinning. In this process, a polymer solution is charged at high voltage as it is fed to a needle tip. Electrostatic forces cause the formation of a cone-like morphology at the needle tip and the ejection of a thin jet from the cone's tip. This jet is attracted to a target that is either grounded or charged oppositely the polymer solution. Over the course of the polymer's flight, the solvent evaporates, resulting in the deposition of dry polymer fibers. Electrospinning has been used to create fibers with a vast range of diameters and morphologies, and is capable of producing both aligned and unaligned fiber mats. A wide array of materials, including proteins, hydrophobic polymers, polysaccharides, and hydrogels have been electrospun. In addition, it is an easily scalable process capable of large scale production of nanofibers. A more in depth discussion of the electrospinning process, its underlying physics and guiding parameters, and applications in tissue engineering is presented in Chapter 3.

2.7. References

1. Drury, J. L.; Mooney, D. J., Hydrogels for tissue engineering: scaffold design variables and applications. *Biomaterials* **2003,** *24* (24), 4337-4351.

2. Rosso, F.; Giordano, A.; Barbarisi, M.; Barbarisi, A., From cell-ECM interactions to tissue engineering. *J Cell Physiol* **2004,** *199* (2), 174-180.

3. Putnam, A. J.; Mooney, D. J., Tissue engineering using synthetic extracellular matrices. *Nat Med* **1996,** *2* (7), 824-826.

4. Rozario, T.; DeSimone, D. W., The extracellular matrix in development and morphogenesis: A dynamic view. *Dev Biol* **2010,** *341* (1), 126-140.

5. Dvir, T.; Timko, B. P.; Kohane, D. S.; Langer, R., Nanotechnological strategies for engineering complex tissues. *Nat Nanotechnol* **2011,** *6* (1), 13-22.

6. Griffith, L. G.; Swartz, M. A., Capturing complex 3D tissue physiology in vitro. *Nat Rev Mol Cell Bio* **2006,** *7* (3), 211-224.

7. Frantz, C.; Stewart, K. M.; Weaver, V. M., The extracellular matrix at a glance. *J Cell Sci* **2010,** *123* (24), 4195-4200.

8. Lee, H. J.; Lee, J. S.; Chansakul, T.; Yu, C.; Elisseeff, J. H.; Yu, S. M., Collagen mimetic peptide-conjugated photopolymerizable PEG hydrogel. *Biomaterials* **2006,** *27* (30), 5268-5276.

9. Ber, S.; Kose, G. T.; Hasirci, V., Bone tissue engineering on patterned collagen films: an in vitro study. *Biomaterials* **2005,** *26* (14), 1977-1986.

10. Wall, S. T.; Saha, K.; Ashton, R. S.; Kam, K. R.; Schaffer, D. V.; Healy, K. E., Multivalency of Sonic hedgehog conjugated to linear polymer chains modulates protein potency. *Bioconjugate Chem* **2008,** *19* (4), 806-812.

11. Gautieri, A.; Vesentini, S.; Redaelli, A.; Buehler, M. J., Hierarchical Structure and Nanomechanics of Collagen Microfibrils from the Atomistic Scale Up. *Nano Lett* **2011,** *11* (2), 757-766.

12. Caulfield, J. B.; Borg, T. K., Collagen Network of the Heart. *Lab Invest* **1979,** *40* (3), 364-372.

13. Robinson, T. F.; Cohengould, L.; Factor, S. M., Skeletal Framework of Mammalian Heart-Muscle - Arrangement of Inter and Pericellular Connective-Tissue Structures. *Lab Invest* **1983,** *49* (4), 482-498.

14. Sophia Fox, A. J.; Bedi, A.; Rodeo, S. A., The basic science of articular cartilage: structure, composition, and function. *Sports Health* **2009,** *1* (6), 461-8.

15. Hollister, S. J., Porous scaffold design for tissue engineering. *Nat Mater* **2005,** *4* (7), 518-524.

16. Yang, S. F.; Leong, K. F.; Du, Z. H.; Chua, C. K., The design of scaffolds for use in tissue engineering. Part 1. Traditional factors. *Tissue Eng* **2001,** *7* (6), 679-689.

17. Senel-Ayaz, H. G.; Perets, A.; Govindaraj, M.; Brookstein, D.; Lelkes, P. I., Textile-Templated Electrospun Anisotropic Scaffolds for Tissue Engineering and Regenerative

Medicine. *2010 Annual International Conference of the Ieee Engineering in Medicine and Biology Society (Embc)* **2010**, 255-258.

18. Bose, S.; Vahabzadeh, S.; Bandyopadhyay, A., Bone tissue engineering using 3D printing. *Mater Today* **2013,** *16* (12), 496-504.

19. Lim, F., Microencapsulation of Living Cells and Tissues. *Artif Organs* **1984,** *8* (1), 112-112.

20. Kim, B. S.; Park, I. K.; Hoshiba, T.; Jiang, H. L.; Choi, Y. J.; Akaike, T.; Cho, C. S., Design of artificial extracellular matrices for tissue engineering. *Prog Polym Sci* **2011,** *36* (2), 238-268.

21. Lovett, M.; Lee, K.; Edwards, A.; Kaplan, D. L., Vascularization Strategies for Tissue Engineering. *Tissue Eng Part B-Re* **2009,** *15* (3), 353-370.

22. Reilly, G. C.; Engler, A. J., Intrinsic extracellular matrix properties regulate stem cell differentiation. *J Biomech* **2010,** *43* (1), 55-62.

23. Rho, J. Y.; Ashman, R. B.; Turner, C. H., Youngs Modulus of Trabecular and Cortical Bone Material - Ultrasonic and Microtensile Measurements. *J Biomech* **1993,** *26* (2), 111-119.

24. Pan, W. X.; Petersen, E.; Cai, N.; Ma, G.; Lee, J. R.; Feng, Z. Q.; Liao, K.; Leong, K. W., Viscoelastic properties of human mesenchymal stem cells. *2005 27th Annual International Conference of the IEEE Engineering in Medicine and Biology Society, Vols 1-7* **2005**, 4854-4857.

25. Galbraith, C. G.; Yamada, K. M.; Galbraith, J. A., Polymerizing actin fibers position integrins primed to probe for adhesion sites. *Science* **2007,** *315* (5814), 992-995.

26. Pek, Y. S.; Wan, A. C. A.; Ying, J. Y., The effect of matrix stiffness on mesenchymal stem cell differentiation in a 3D thixotropic gel. *Biomaterials* **2010,** *31* (3), 385-391.

27. Carvalho, R. S.; Schaffer, J. L.; Gerstenfeld, L. C., Osteoblasts induce osteopontin expression in response to attachment on fibronectin: Demonstration of a common role for integrin receptors in the signal transduction processes of cell attachment and mechanical stimulation. *J Cell Biochem* **1998,** *70* (3), 376-390.

28. McBeath, R.; Pirone, D. M.; Nelson, C. M.; Bhadriraju, K.; Chen, C. S., Cell shape, cytoskeletal tension, and RhoA regulate stem cell lineage commitment. *Dev Cell* **2004,** *6* (4), 483-95.

29. Giannone, G.; Sheetz, M. P., Substrate rigidity and force define form through tyrosine phosphatase and kinase pathways. *Trends Cell Biol* **2006,** *16* (4), 213-223.

30. Ahmed, I.; Ponery, A. S.; Nur-E-Kamal, A.; Kamal, J.; Meshel, A. S.; Sheetz, M. P.; Schindler, M.; Meiners, S., Morphology, cytoskeletal organization, and myosin dynamics of

mouse embryonic fibroblasts cultured on nanofibrillar surfaces. *Mol Cell Biochem* **2007,** *301* (1-2), 241-249.

31. Tamada, M.; Sheetz, M. P.; Sawada, Y., Activation of a signaling cascade by cytoskeleton stretch. *Dev Cell* **2004,** *7* (5), 709-718.

32. Ingber, D. E., Tensegrity: The architectural basis of cellular mechanotransduction. *Annu Rev Physiol* **1997,** *59*, 575-599.

33. Engler, A. J.; Sen, S.; Sweeney, H. L.; Discher, D. E., Matrix elasticity directs stem cell lineage specification. *Cell* **2006,** *126* (4), 677-689.

34. Bhana, B.; Iyer, R. K.; Chen, W. L.; Zhao, R.; Sider, K. L.; Likhitpanichkul, M.; Simmons, C. A.; Radisic, M., Influence of substrate stiffness on the phenotype of heart cells. *Biotechnol Bioeng* **2010,** *105* (6), 1148-60.

35. Engler, A. J.; Carag-Krieger, C.; Johnson, C. P.; Raab, M.; Tang, H. Y.; Speicher, D. W.; Sanger, J. W.; Sanger, J. M.; Discher, D. E., Embryonic cardiomyocytes beat best on a matrix with heart-like elasticity: scar-like rigidity inhibits beating. *J Cell Sci* **2008,** *121* (Pt 22), 3794-802.

36. Freed, L. E.; Engelmayr, G. C.; Borenstein, J. T.; Moutos, F. T.; Guilak, F., Advanced Material Strategies for Tissue Engineering Scaffolds. *Adv Mater* **2009,** *21* (32-33), 3410-3418.

37. Freed, L. E.; Guilak, F.; Guo, X. E.; Gray, M. L.; Tranquillo, R.; Holmes, J. W.; Radisic, M.; Sefton, M. V.; Kaplan, D.; Vunjak-Novakovic, G., Advanced tools for tissue engineering: Scaffolds, bioreactors, and signaling. *Tissue Eng* **2006,** *12* (12), 3285-3305.

38. Pelham, R. J.; Wang, Y. L., Cell locomotion and focal adhesions are regulated by substrate flexibility. *P Natl Acad Sci USA* **1997,** *94* (25), 13661-13665.

39. Stevens, M. M.; George, J. H., Exploring and engineering the cell surface interface. *Science* **2005,** *310* (5751), 1135-1138.

40. Saha, K.; Pollock, J. F.; Schaffer, D. V.; Healy, K. E., Designing synthetic materials to control stem cell phenotype. *Curr Opin Chem Biol* **2007,** *11* (4), 381-387.

41. Oh, S.; Brammer, K. S.; Li, Y. S. J.; Teng, D.; Engler, A. J.; Chien, S.; Jin, S., Stem cell fate dictated solely by altered nanotube dimension. *P Natl Acad Sci USA* **2009,** *106* (7), 2130-2135.

42. Andersson, A. S.; Backhed, F.; von Euler, A.; Richter-Dahlfors, A.; Sutherland, D.; Kasemo, B., Nanoscale features influence epithelial cell morphology and cytokine production. *Biomaterials* **2003,** *24* (20), 3427-3436.

43. Teixeira, A. I.; Nealey, P. F.; Murphy, C. J., Responses of human keratocytes to micro- and nanostructured substrates. *J Biomed Mater Res A* **2004,** *71A* (3), 369-376.

44. Curtis, A. S. G.; Gadegaard, N.; Dalby, M. J.; Riehle, M. O.; Wilkinson, C. D. W.; Aitchison, G., Cells react to nanoscale order and symmetry in their surroundings. *Ieee T Nanobiosci* **2004,** *3* (1), 61-65.

45. Bettinger, C. J.; Langer, R.; Borenstein, J. T., Engineering Substrate Topography at the Micro- and Nanoscale to Control Cell Function. *Angew Chem Int Edit* **2009,** *48* (30), 5406-5415.

46. Price, R. L.; Ellison, K.; Haberstroh, K. M.; Webster, T. J., Nanometer surface roughness increases select osteoblast adhesion on carbon nanofiber compacts. *J Biomed Mater Res A* **2004,** *70A* (1), 129-138.

47. Khademhosseini, A.; Langer, R.; Borenstein, J.; Vacanti, J. P., Microscale technologies for tissue engineering and biology. *P Natl Acad Sci USA* **2006,** *103* (8), 2480-2487.

48. Yim, E. K. F.; Reano, R. M.; Pang, S. W.; Yee, A. F.; Chen, C. S.; Leong, K. W., Nanopattern-induced changes in morphology and motility of smooth muscle cells. *Biomaterials* **2005,** *26* (26), 5405-5413.

49. Vaidya, R.; Tender, L. M.; Bradley, G.; O'Brien, M. J.; Cone, M.; Lopez, G. P., Computer-controlled laser ablation: A convenient and versatile tool for micropatterning biofunctional synthetic surfaces for applications in biosensing and tissue engineering. *Biotechnol Progr* **1998,** *14* (3), 371-377.

50. Norman, J.; Desai, T., Methods for fabrication of nanoscale topography for tissue engineering scaffolds. *Ann Biomed Eng* **2006,** *34* (1), 89-101.

51. Wilkinson, C. D. W.; Riehle, M.; Wood, M.; Gallagher, J.; Curtis, A. S. G., The use of materials patterned on a nano- and micro-metric scale in cellular engineering. *Mat Sci Eng C-Bio S* **2002,** *19* (1-2), 263-269.

52. Chen, C. S.; Mrksich, M.; Huang, S.; Whitesides, G. M.; Ingber, D. E., Micropatterned surfaces for control of cell shape, position, and function. *Biotechnol Progr* **1998,** *14* (3), 356-363.

53. McBeath, R.; Pirone, D. M.; Nelson, C. M.; Bhadriraju, K.; Chen, C. S., Cell shape, cytoskeletal tension, and RhoA regulate stem cell lineage commitment. *Dev Cell* **2004,** *6* (4), 483-495.

54. Kilian, K. A.; Bugarija, B.; Lahn, B. T.; Mrksich, M., Geometric cues for directing the differentiation of mesenchymal stem cells. *P Natl Acad Sci USA* **2010,** *107* (11), 4872-4877.

55. Wojciak-Stothard, B.; Curtis, A.; Monaghan, W.; MacDonald, K.; Wilkinson, C., Guidance and activation of murine macrophages by nanometric scale topography. *Exp Cell Res* **1996,** *223* (2), 426-35.

56. Cima, L. G.; Vacanti, J. P.; Vacanti, C.; Ingber, D.; Mooney, D.; Langer, R., Tissue Engineering by Cell Transplantation Using Degradable Polymer Substrates. *J Biomech Eng-T Asme* **1991,** *113* (2), 143-151.

57. Wei, G. B.; Ma, P. X., Structure and properties of nano-hydroxyapatite/polymer composite scaffolds for bone tissue engineering. *Biomaterials* **2004,** *25* (19), 4749-4757.

58. Nair, L. S.; Laurencin, C. T., Biodegradable polymers as biomaterials. *Prog Polym Sci* **2007,** *32* (8-9), 762-798.

59. Burdick, J. A.; Anseth, K. S., Photoencapsulation of osteoblasts in injectable RGD-modified PEG hydrogels for bone tissue engineering. *Biomaterials* **2002,** *23* (22), 4315-4323.

60. Zhu, J. M., Bioactive modification of poly(ethylene glycol) hydrogels for tissue engineering. *Biomaterials* **2010,** *31* (17), 4639-4656.

61. Patrick, C. W.; Chauvin, P. B.; Hobley, J.; Reece, G. P., Preadipocyte seeded PLGA scaffolds for adipose tissue engineering. *Tissue Eng* **1999,** *5* (2), 139-151.

62. Ma, P. X., Scaffolds for tissue fabrication. *Mater Today* **2004,** *7* (5), 30-40.

63. McBane, J. E.; Sharifpoor, S.; Cai, K. H.; Labow, R. S.; Santerre, J. P., Biodegradation and in vivo biocompatibility of a degradable, polar/hydrophobic/ionic polyurethane for tissue engineering applications. *Biomaterials* **2011,** *32* (26), 6034-6044.

64. Jia, L.; Prabhakaran, M. P.; Qin, X. H.; Kai, D.; Ramakrishna, S., Biocompatibility evaluation of protein-incorporated electrospun polyurethane-based scaffolds with smooth muscle cells for vascular tissue engineering. *J Mater Sci* **2013,** *48* (15), 5113-5124.

65. Kim, I. L.; Mauck, R. L.; Burdick, J. A., Hydrogel design for cartilage tissue engineering: A case study with hyaluronic acid. *Biomaterials* **2011,** *32* (34), 8771-8782.

66. Collins, M. N.; Birkinshaw, C., Hyaluronic acid based scaffolds for tissue engineering-A review. *Carbohyd Polym* **2013,** *92* (2), 1262-1279.

67. Muzzarelli, R. A. A.; Greco, F.; Busilacchi, A.; Sollazzo, V.; Gigante, A., Chitosan, hyaluronan and chondroitin sulfate in tissue engineering for cartilage regeneration: A review. *Carbohyd Polym* **2012,** *89* (3), 723-739.

68. Li, Q.; Williams, C. G.; Sun, D. D. N.; Wang, J.; Leong, K.; Elisseeff, J. H., Photocrosslinkable polysaccharides based on chondroitin sulfate. *J Biomed Mater Res A* **2004,** *68A* (1), 28-33.

69. Cen, L.; Liu, W.; Cui, L.; Zhang, W. J.; Cao, Y. L., Collagen tissue engineering: Development of novel biomaterials and applications. *Pediatr Res* **2008,** *63* (5), 492-496.

70. Wang, Y.; Silvent, J.; Robin, M.; Babonneau, F.; Meddahi-Pelle, A.; Nassif, N.; Guille, M. M. G., Controlled collagen assembly to build dense tissue-like materials for tissue engineering. *Soft Matter* **2011,** *7* (20), 9659-9664.

71. Parenteau-Bareil, R.; Gauvin, R.; Berthod, F., Collagen-Based Biomaterials for Tissue Engineering Applications. *Materials* **2010,** *3* (3), 1863-1887.

72. Ye, Q.; Zund, G.; Benedikt, P.; Jockenhoevel, S.; Hoerstrup, S. P.; Sakyama, S.; Hubbell, J. A.; Turina, M., Fibrin gel as a three dimensional matrix in cardiovascular tissue engineering. *Eur J Cardio-Thorac* **2000,** *17* (5), 587-591.

73. Ahmed, T. A. E.; Dare, E. V.; Hincke, M., Fibrin: A versatile scaffold for tissue engineering applications. *Tissue Eng Part B-Re* **2008,** *14* (2), 199-215.

74. Colombini, A.; Ceriani, C.; Banfi, G.; Brayda-Bruno, M.; Moretti, M., Fibrin in Intervertebral Disc Tissue Engineering. *Tissue Eng Part B Rev* **2014**.

75. Daamen, W. F.; Veerkamp, J. H.; van Hest, J. C. M.; van Kuppevelt, T. H., Elastin as a biomaterial for tissue engineering. *Biomaterials* **2007,** *28* (30), 4378-4398.

76. Rnjak-Kovacina, J.; Wise, S. G.; Li, Z.; Maitz, P. K. M.; Young, C. J.; Wang, Y. W.; Weiss, A. S., Tailoring the porosity and pore size of electrospun synthetic human elastin scaffolds for dermal tissue engineering. *Biomaterials* **2011,** *32* (28), 6729-6736.

77. Rosso, F.; Marino, G.; Giordano, A.; Barbarisi, M.; Parmeggiani, D.; Barbarisi, A., Smart materials as scaffolds for tissue engineering. *J Cell Physiol* **2005,** *203* (3), 465-470.

78. Gunatillake, P. A.; Adhikari, R., Biodegradable synthetic polymers for tissue engineering. *Eur Cell Mater* **2003,** *5*, 1-16; discussion 16.

79. Seal, B. L.; Otero, T. C.; Panitch, A., Polymeric biomaterials for tissue and organ regeneration. *Mat Sci Eng R* **2001,** *34* (4-5), 147-230.

80. Kim, S. S.; Park, M. S.; Jeon, O.; Choi, C. Y.; Kim, B. S., Poly(lactide-co-glycolide)/hydroxyapatite composite scaffolds for bone tissue engineering. *Biomaterials* **2006,** *27* (8), 1399-1409.

81. Meyer, F.; Wardale, J.; Best, S.; Cameron, R.; Rushton, N.; Brooks, R., Effects of lactic acid and glycolic acid on human osteoblasts: A way to understand PLGA involvement in PLGA/calcium phosphate composite failure. *J Orthop Res* **2012,** *30* (6), 864-871.

82. Nakagawa, M.; Teraoka, F.; Fujimoto, S.; Hamada, Y.; Kibayashi, H.; Takahashi, J., Improvement of cell adhesion on poly(L-lactide) by atmospheric plasma treatment. *J Biomed Mater Res A* **2006,** *77A* (1), 112-118.

83. Yamaguchi, M.; Shinbo, T.; Kanamori, T.; Wang, P. C.; Niwa, M.; Kawakami, H.; Nagaoka, S.; Hirakawa, K.; Kamiya, M., Surface modification of poly(L: -lactic acid) affects initial cell attachment, cell morphology, and cell growth. *J Artif Organs* **2004,** *7* (4), 187-93.

84. Khang, G.; Lee, S. J.; Jeon, J. H.; Lee, J. H.; Lee, H. B., Interaction of fibroblast cell onto physicochemically treated PLGA surfaces. *Polym-Korea* **2000,** *24* (6), 869-876.

85. Ma, Z. W.; Gao, C. Y.; Shen, J. C., Surface modification of poly-L-lactic acid (PLLA) membrane by grafting acrylamide: an effective way to improve cytocompatibility for chondrocytes. *J Biomat Sci-Polym E* **2003,** *14* (1), 13-25.

86. Sailynoja, E.; Koskinen, M.; Salonen, J.; Holmlund, P.; Sodergard, A.; Koskinen, M., Immobilization of a biologically active coating on a hydrophobic L-lactide-epsilon-caprolactone copolymer. *Journal of Materials Science-Materials in Medicine* **1999,** *10* (12), 703-705.

87. Ma, Z. W.; Gao, C. Y.; Gong, Y. H.; Ji, J.; Shen, J. C., Immobilization of natural macromolecules on poly-L-lactic acid membrane surface in order to improve its cytocompatibility. *J Biomed Mater Res* **2002,** *63* (6), 838-847.

88. Hoffman, A. S., Hydrogels for biomedical applications. *Adv Drug Deliver Rev* **2002,** *54* (1), 3-12.

89. Cruise, G. M.; Scharp, D. S.; Hubbell, J. A., Characterization of permeability and network structure of interfacially photopolymerized poly(ethylene glycol) diacrylate hydrogels. *Biomaterials* **1998,** *19* (14), 1287-1294.

90. Boucard, N.; Viton, C.; Agay, D.; Mari, E.; Roger, T.; Chancerelle, Y.; Domard, A., The use of physical hydrogels of chitosan for skin regeneration following third-degree burns. *Biomaterials* **2007,** *28* (24), 3478-3488.

91. Jeong, B.; Bae, Y. H.; Kim, S. W., Thermoreversible gelation of PEG-PLGA-PEG triblock copolymer aqueous solutions. *Macromolecules* **1999,** *32* (21), 7064-7069.

92. Gacesa, P., Alginates. *Carbohyd Polym* **1988,** *8* (3), 161-182.

93. Chenite, A.; Chaput, C.; Wang, D.; Combes, C.; Buschmann, M. D.; Hoemann, C. D.; Leroux, J. C.; Atkinson, B. L.; Binette, F.; Selmani, A., Novel injectable neutral solutions of chitosan form biodegradable gels in situ. *Biomaterials* **2000,** *21* (21), 2155-2161.

94. Temenoff, J. S.; Mikos, A. G., Injectable biodegradable materials for orthopedic tissue engineering. *Biomaterials* **2000,** *21* (23), 2405-2412.

95. Ravichandran, R.; Venugopal, J. R.; Sundarrajan, S.; Mukherjee, S.; Sridhar, R.; Ramakrishna, S., Minimally invasive injectable short nanofibers of poly(glycerol sebacate) for cardiac tissue engineering. *Nanotechnology* **2012,** *23* (38).

96. Pollock, J. F.; Healy, K. E., Mechanical and swelling characterization of poly(N-isopropyl acrylamide-co-methoxy poly(ethylene glycol) methacrylate) sol-gels. *Acta Biomater* **2010,** *6* (4), 1307-1318.

97. Anseth, K. S.; Bowman, C. N.; BrannonPeppas, L., Mechanical properties of hydrogels and their experimental determination. *Biomaterials* **1996,** *17* (17), 1647-1657.

98. Hubbell, J. A., Bioactive biomaterials. *Curr Opin Biotech* **1999,** *10* (2), 123-129.

99. Nuttelman, C. R.; Tripodi, M. C.; Anseth, K. S., Synthetic hydrogel niches that promote hMSC viability. *Matrix Biol* **2005,** *24* (3), 208-218.

100. Lu, Y.; Mapili, G.; Suhali, G.; Chen, S. C.; Roy, K., A digital micro-mirror device-based system for the microfabrication of complex, spatially patterned tissue engineering scaffolds. *J Biomed Mater Res A* **2006,** *77A* (2), 396-405.

101. Shin, H.; Zygourakis, K.; Farach-Carson, M. C.; Yaszemski, M. J.; Mikos, A. G., Attachment, proliferation, and migration of marrow stromal osteoblasts cultured on biomimetic hydrogels modified with an osteopontin-derived peptide. *Biomaterials* **2004,** *25* (5), 895-906.

102. Shin, H.; Temenoff, J. S.; Bowden, G. C.; Zygourakis, K.; Farach-Carson, M. C.; Yaszemski, M. J.; Mikos, A. G., Osteogenic differentiation of rat bone marrow stromal cells cultured on Arg-Gly-Asp modified hydrogels without dexamethasone and beta-glycerol phosphate. *Biomaterials* **2005,** *26* (17), 3645-3654.

103. Hwang, N. S.; Varghese, S.; Zhang, Z.; Elisseeff, J., Chondrogenic differentiation of human embryonic stem cell-derived cells in arginine-glycine-aspartate modified hydrogels. *Tissue Eng* **2006,** *12* (9), 2695-2706.

104. Kim, S.; Healy, K. E., Synthesis and characterization of injectable poly(N-isopropylacrylamide-co-acrylic acid) hydrogels with proteolytically degradable cross-links. *Biomacromolecules* **2003,** *4* (5), 1214-1223.

105. Li, Y. J.; Chung, E. H.; Rodriguez, R. T.; Firpo, M. T.; Healy, K. E., Hydrogels as artificial matrices for human embryonic stem cell self-renewal. *J Biomed Mater Res A* **2006,** *79A* (1), 1-5.

106. Smidsrod, O.; Skjakbraek, G., Alginate as Immobilization Matrix for Cells. *Trends Biotechnol* **1990,** *8* (3), 71-78.

107. Suh, J. K. F.; Matthew, H. W. T., Application of chitosan-based polysaccharide biomaterials in cartilage tissue engineering: a review. *Biomaterials* **2000,** *21* (24), 2589-2598.

108. Lee, C. R.; Grodzinsky, A. J.; Spector, M., The effects of cross-linking of collagen-glycosaminoglycan scaffolds on compressive stiffness, chondrocyte-mediated contraction, proliferation and biosynthesis. *Biomaterials* **2001,** *22* (23), 3145-3154.

109. Park, S. N.; Park, J. C.; Kim, H. O.; Song, M. J.; Suh, H., Characterization of porous collagen/hyaluronic acid scaffold modified by 1-ethyl-3-(3-dimethylaminopropyl)carbodiimide cross-linking. *Biomaterials* **2002,** *23* (4), 1205-1212.

110. Rosario, D. J.; Reilly, G. C.; Salah, E. A.; Glover, M.; Bullock, A. J.; MacNeil, S., Decellularization and sterilization of porcine urinary bladder matrix for tissue engineering in the lower urinary tract. *Regen Med* **2008,** *3* (2), 145-156.

111. Ott, H. C.; Matthiesen, T. S.; Goh, S. K.; Black, L. D.; Kren, S. M.; Netoff, T. I.; Taylor, D. A., Perfusion-decellularized matrix: using nature's platform to engineer a bioartificial heart. *Nat Med* **2008,** *14* (2), 213-221.

112. Flynn, L. E., The use of decellularized adipose tissue to provide an inductive microenvironment for the adipogenic differentiation of human adipose-derived stem cells. *Biomaterials* **2010,** *31* (17), 4715-4724.

113. Bolland, F.; Korossis, S.; Wilshaw, S. P.; Ingham, E.; Fisher, J.; Kearney, J. N.; Southgate, J., Development and characterisation of a full-thickness acellular porcine bladder matrix for tissue engineering. *Biomaterials* **2007,** *28* (6), 1061-1070.

114. Remlinger, N. T.; Czajka, C. A.; Juhas, M. E.; Vorp, D. A.; Stolz, D. B.; Badylak, S. F.; Gilbert, S.; Gilbert, T. W., Hydrated xenogeneic decellularized tracheal matrix as a scaffold for tracheal reconstruction. *Biomaterials* **2010,** *31* (13), 3520-3526.

115. Crapo, P. M.; Gilbert, T. W.; Badylak, S. F., An overview of tissue and whole organ decellularization processes. *Biomaterials* **2011,** *32* (12), 3233-3243.

116. Gilbert, T. W.; Sellaro, T. L.; Badylak, S. F., Decellularization of tissues and organs. *Biomaterials* **2006,** *27* (19), 3675-3683.

117. Richardson, T. P.; Peters, M. C.; Ennett, A. B.; Mooney, D. J., Polymeric system for dual growth factor delivery. *Nat Biotechnol* **2001,** *19* (11), 1029-1034.

118. Sokolsky-Papkov, M.; Agashi, K.; Olaye, A.; Shakesheff, K.; Domb, A. J., Polymer carriers for drug delivery in tissue engineering. *Adv Drug Deliver Rev* **2007,** *59* (4-5), 187-206.

119. Bhattarai, N.; Gunn, J.; Zhang, M. Q., Chitosan-based hydrogels for controlled, localized drug delivery. *Adv Drug Deliver Rev* **2010,** *62* (1), 83-99.

120. Ferreira, L. S.; Gerecht, S.; Fuller, J.; Shieh, H. F.; Vunjak-Novakovic, G.; Langer, R., Bioactive hydrogel scaffolds for controllable vascular differentiation of human embryonic stem cells. *Biomaterials* **2007,** *28* (17), 2706-2717.

121. Park, H.; Temenoff, J. S.; Tabata, Y.; Caplan, A. I.; Raphael, R. M.; Jansen, J. A.; Mikos, A. G., Effect of dual growth factor delivery on chondrogenic differentiation of rabbit marrow mesenchymal stem cells encapsulated in injectable hydrogel composites. *J Biomed Mater Res A* **2009,** *88A* (4), 889-897.

122. Whitaker, M. J.; Quirk, R. A.; Howdle, S. M.; Shakesheff, K. M., Growth factor release from tissue engineering scaffolds. *J Pharm Pharmacol* **2001,** *53* (11), 1427-1437.

123. Jeon, O.; Song, S. J.; Kang, S. W.; Putnam, A. J.; Kim, B. S., Enhancement of ectopic bone formation by bone morphogenetic protein-2 released from a heparin-conjugated poly(L-lactic-co-glycolic acid) scaffold. *Biomaterials* **2007,** *28* (17), 2763-2771.

124. Ma, Z. W.; Gao, C. Y.; Gong, Y. H.; Shen, J. C., Cartilage tissue engineering PLLA scaffold with surface immobilized collagen and basic fibroblast growth factor. *Biomaterials* **2005,** *26* (11), 1253-1259.

125. Fan, V. H.; Au, A.; Tamama, K.; Littrell, R.; Richardson, L. B.; Wright, J. W.; Wells, A.; Griffith, L. G., Tethered epidermal growth factor provides a survival advantage to mesenchymal stem cells. *Stem Cells* **2007,** *25* (5), 1241-1251.

126. Vozzi, G.; Flaim, C.; Ahluwalia, A.; Bhatia, S., Fabrication of PLGA scaffolds using soft lithography and microsyringe deposition. *Biomaterials* **2003,** *24* (14), 2533-2540.

127. Hahn, M. S.; Taite, L. J.; Moon, J. J.; Rowland, M. C.; Ruffino, K. A.; West, J. L., Photolithographic patterning of polyethylene glycol hydrogels. *Biomaterials* **2006,** *27* (12), 2519-2524.

128. Lee, M. R.; Kwon, K. W.; Jung, H.; Kim, H. N.; Suh, K. Y.; Kim, K.; Kim, K. S., Direct differentiation of human embryonic stem cells into selective neurons on nanoscale ridge/groove pattern arrays. *Biomaterials* **2010,** *31* (15), 4360-4366.

129. Dalby, M. J.; Riehle, M. O.; Sutherland, D. S.; Agheli, H.; Curtis, A. S. G., Changes in fibroblast morphology in response to nano-columns produced by colloidal lithography. *Biomaterials* **2004,** *25* (23), 5415-5422.

130. Faucheux, N.; Schweiss, R.; Lutzow, K.; Werner, C.; Groth, T., Self-assembled monolayers with different terminating groups as model substrates for cell adhesion studies. *Biomaterials* **2004,** *25* (14), 2721-2730.

131. Prime, K. L.; Whitesides, G. M., Adsorption of Proteins onto Surfaces Containing End-Attached Oligo(Ethylene Oxide) - a Model System Using Self-Assembled Monolayers. *J Am Chem Soc* **1993,** *115* (23), 10714-10721.

132. Zhang, S. G., Fabrication of novel biomaterials through molecular self-assembly. *Nat Biotechnol* **2003,** *21* (10), 1171-1178.

133. Cui, H. G.; Webber, M. J.; Stupp, S. I., Self-Assembly of Peptide Amphiphiles: From Molecules to Nanostructures to Biomaterials. *Biopolymers* **2010,** *94* (1), 1-18.

134. Silva, G. A.; Czeisler, C.; Niece, K. L.; Beniash, E.; Harrington, D. A.; Kessler, J. A.; Stupp, S. I., Selective differentiation of neural progenitor cells by high-epitope density nanofibers. *Science* **2004,** *303* (5662), 1352-1355.

135. Chiu, Y. C.; Larson, J. C.; Isom, A.; Brey, E. M., Generation of Porous Poly(Ethylene Glycol) Hydrogels by Salt Leaching. *Tissue Eng Part C-Me* **2010,** *16* (5), 905-912.

136. Zhang, X. H.; Cao, C. B.; Ma, X. L.; Li, Y. A., Optimization of macroporous 3-D silk fibroin scaffolds by salt-leaching procedure in organic solvent-free conditions. *Journal of Materials Science-Materials in Medicine* **2012,** *23* (2), 315-324.

137. Pezeshki-Modaress, M.; Rajabi-Zeleti, S.; Zandi, M.; Mirzadeh, H.; Sodeifi, N.; Nekookar, A.; Aghdami, N., Cell-loaded gelatin/chitosan scaffolds fabricated by salt-leaching/lyophilization for skin tissue engineering: In vitro and in vivo study. *J Biomed Mater Res A* **2014,** *102* (11), 3908-17.

138. Sadiasa, A.; Nguyen, T. H.; Lee, B. T., In vitro and in vivo evaluation of porous PCL-PLLA 3D polymer scaffolds fabricated via salt leaching method for bone tissue engineering applications. *J Biomat Sci-Polym E* **2014,** *25* (2), 150-167.

139. Rouwkema, J.; Rivron, N. C.; van Blitterswijk, C. A., Vascularization in tissue engineering. *Trends Biotechnol* **2008,** *26* (8), 434-441.

140. Mironov, V.; Boland, T.; Trusk, T.; Forgacs, G.; Markwald, R. R., Organ printing: computer-aided jet-based 3D tissue engineering. *Trends Biotechnol* **2003,** *21* (4), 157-161.

141. Gross, B. C.; Erkal, J. L.; Lockwood, S. Y.; Chen, C. P.; Spence, D. M., Evaluation of 3D Printing and Its Potential Impact on Biotechnology and the Chemical Sciences. *Anal Chem* **2014,** *86* (7), 3240-3253.

142. Beachley, V.; Katsanevakis, E.; Zhang, N.; Wen, X. J., Highly Aligned Polymer Nanofiber Structures: Fabrication and Applications in Tissue Engineering. *Biomedical Applications of Polymeric Nanofibers* **2012,** *246*, 171-212.

143. Nain, A. S.; Sitti, M.; Jacobson, A.; Kowalewski, T.; Amon, C., Dry Spinning Based Spinneret Based Tunable Engineered Parameters (STEP) Technique for Controlled and Aligned Deposition of Polymeric Nanofibers. *Macromol Rapid Comm* **2009,** *30* (16), 1406-1412.

144. Xing, X.; Wang, Y.; Li, B., Nanofibers drawing and nanodevices assembly in poly(trimethylene terephthalate). *Opt Express* **2008,** *16* (14), 10815-22.

145. Cheng, F. Y.; Tang, W.; Li, C. S.; Chen, J.; Liu, H. K.; Shen, P. W.; Dou, S. X., Conducting poly(aniline) nanotubes and nanofibers: Controlled synthesis and application in lithium/poly(aniline) rechargeable batteries. *Chem-Eur J* **2006,** *12* (11), 3082-3088.

146. Grimm, S.; Giesa, R.; Sklarek, K.; Langner, A.; Gosele, U.; Schmidt, H. W.; Steinhart, M., Nondestructive replication of self-ordered nanoporous alumina membranes via cross-linked polyacrylate nanofiber arrays. *Nano Lett* **2008,** *8* (7), 1954-1959.

2.8. Tables

Table 2.1. List of major components of the mammalian ECM.

Structural Proteins	**Glycoproteins**	**Polysaccharides**
Collagens	Fibronectin	Hyaluronic Acid
Elastin	Laminin	Heparin/Heparin Sulfate
	Vitronectin	Chondroitin/Chondroitin Sulfate

Table 2.2. Available parameters in biomimetic material design.

- Structural architecture/microstructure
- Anisotropy and alignment
- Porosity
- Material modulus
- Embedded or localized signaling molecules
- Release of soluble signaling molecules
- Non-specific hydrolytic degradability
- Specific cell-mediated degradability

Table 2.3. Summary of design requirements for tissue scaffolds

- Provide structural support for three dimensional tissue growth
- Provide mechanical support for structural tissues until replaced by biological tissue
- Allow for cellular attachment and proliferation
- Allow for diffusion of nutrients to and waste from encapsulated or embedded cells
- Guide differentiation of stem cells into desired tissue
- Spatially organize and orient cells into functional tissue construct
- Give rise to rapid vascularization to provide oxygen and nutrients to whole thickness of tissue
- Degrade at an appropriate rate to allow for replacement with cell-deposited ECM

Table 2.4. Commonly used synthetic polymers in tissue engineering

- Poly(lactic acid)
- Poly(glycolic acid)
- Poly(lactide-co-glycolide)
- Poly(caprolactone)
- Polyurethanes
- Poly(ethylene glycol)
- Poly(2-hydroxyethyl methacrylate)
- Poly(vinyl alchohol)
- Poly(acrylic acid)
- Poly(acrylamide)
- Poly(N-isopropylacrylamide)

Table 2.5. Commonly used natural polymers in tissue engineering

- Hyaluronic Acid
- Collagen
- Alginate
- Chitosan
- Silk

Table 2.6. Processing methods to create scaffold micro- and nanostructure

- Photolithography
- Laster etching
- Electron beam lithography
- Self assembly
- 3D printing
- Electrospinning

2.9. Figures

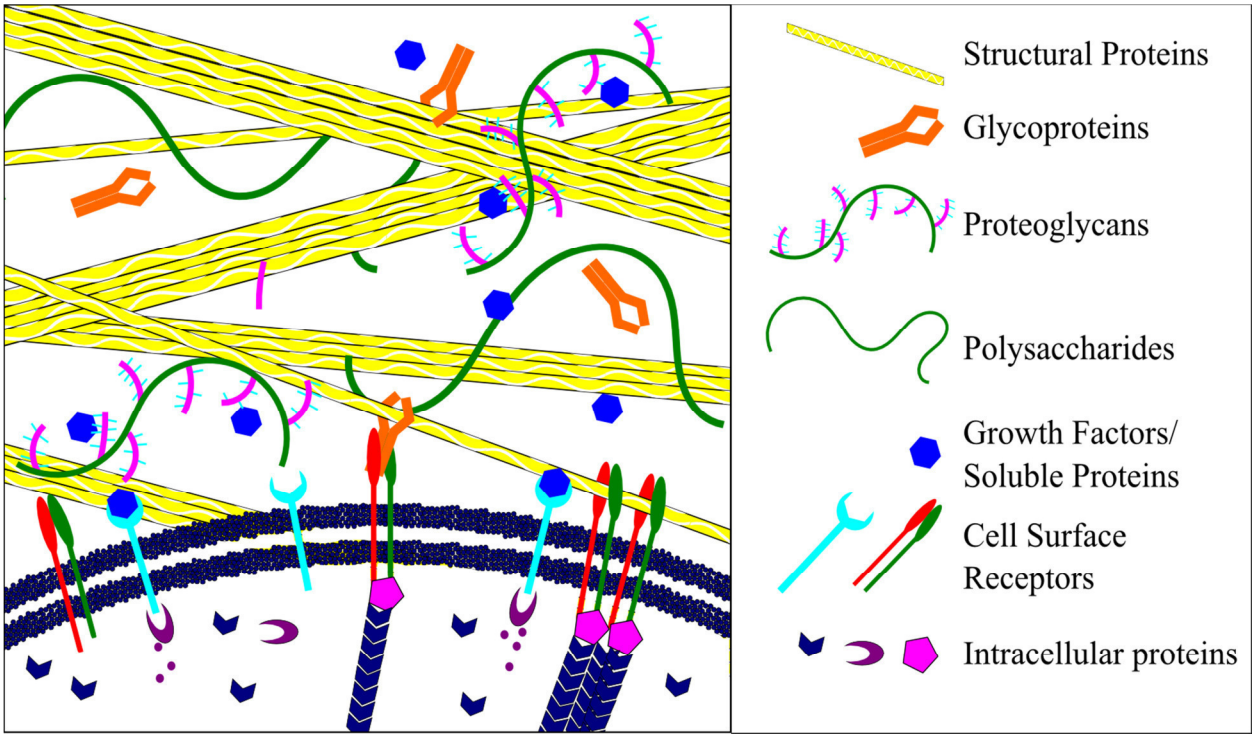

Figure 2.1. Diagram of the interaction between the cell surface and the ECM. The ECM consists of a mix of structural proteins, glycoproteins, proteoglycans, and polysaccharides. Cell surface receptors will bind to both ECM proteins and soluble proteins, which may be free in solution or bound to the ECM. These binding events cause signaling cascades within the cell, including the formation of stress fibers and rearrangement of the cytoskeleton, and provide chemical and mechanical communication between the interior and exterior of the cell.

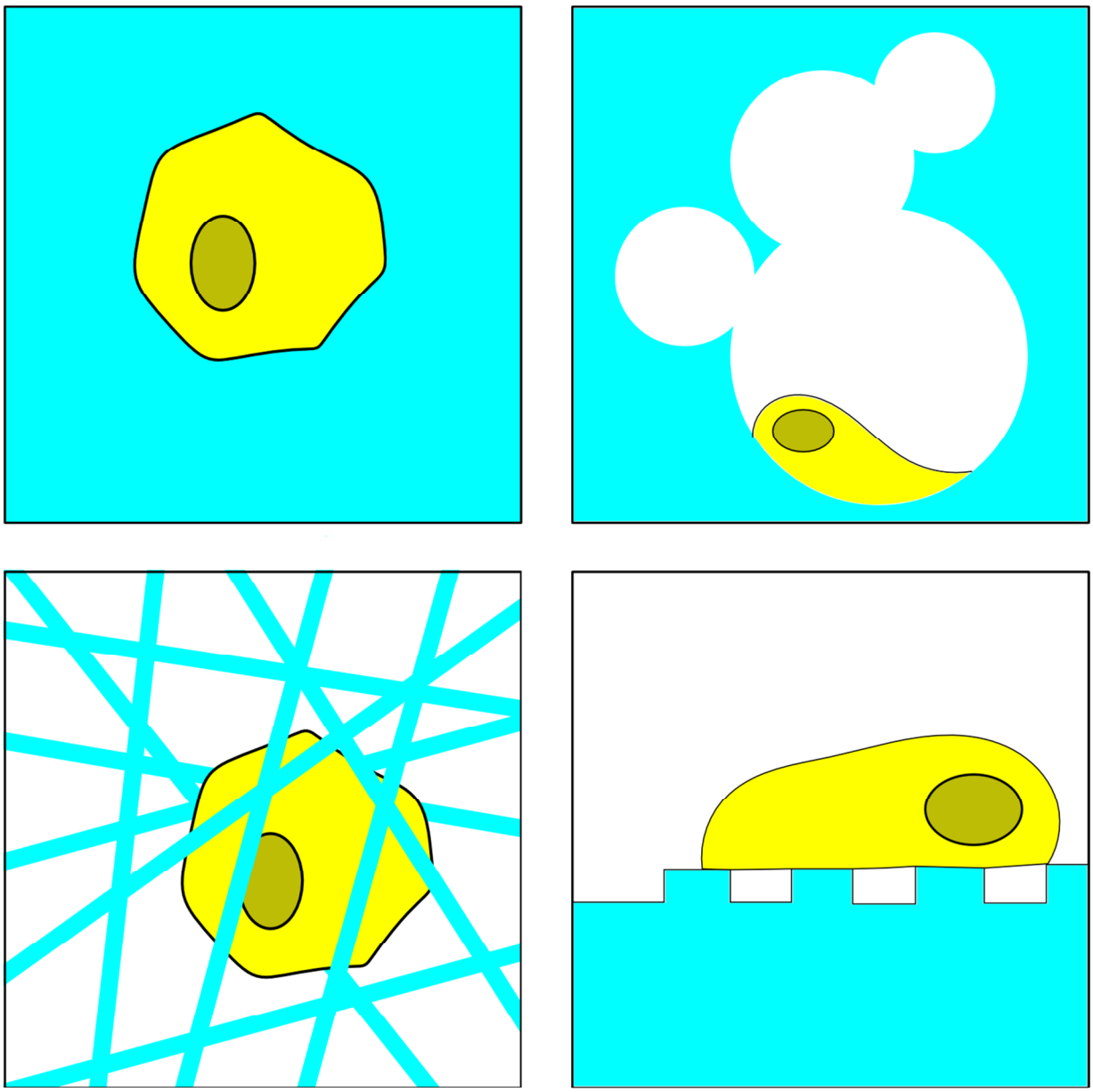

Figure 2.2. Material architecture plays an important role in cell-material interaction. Common microarchitectures for cell culture include bulk hydrogel materials with cells embedded (a), porous materials with encapsulated cells (b), fibrous materials with embedded cells (c), or patterned surfaces (d).

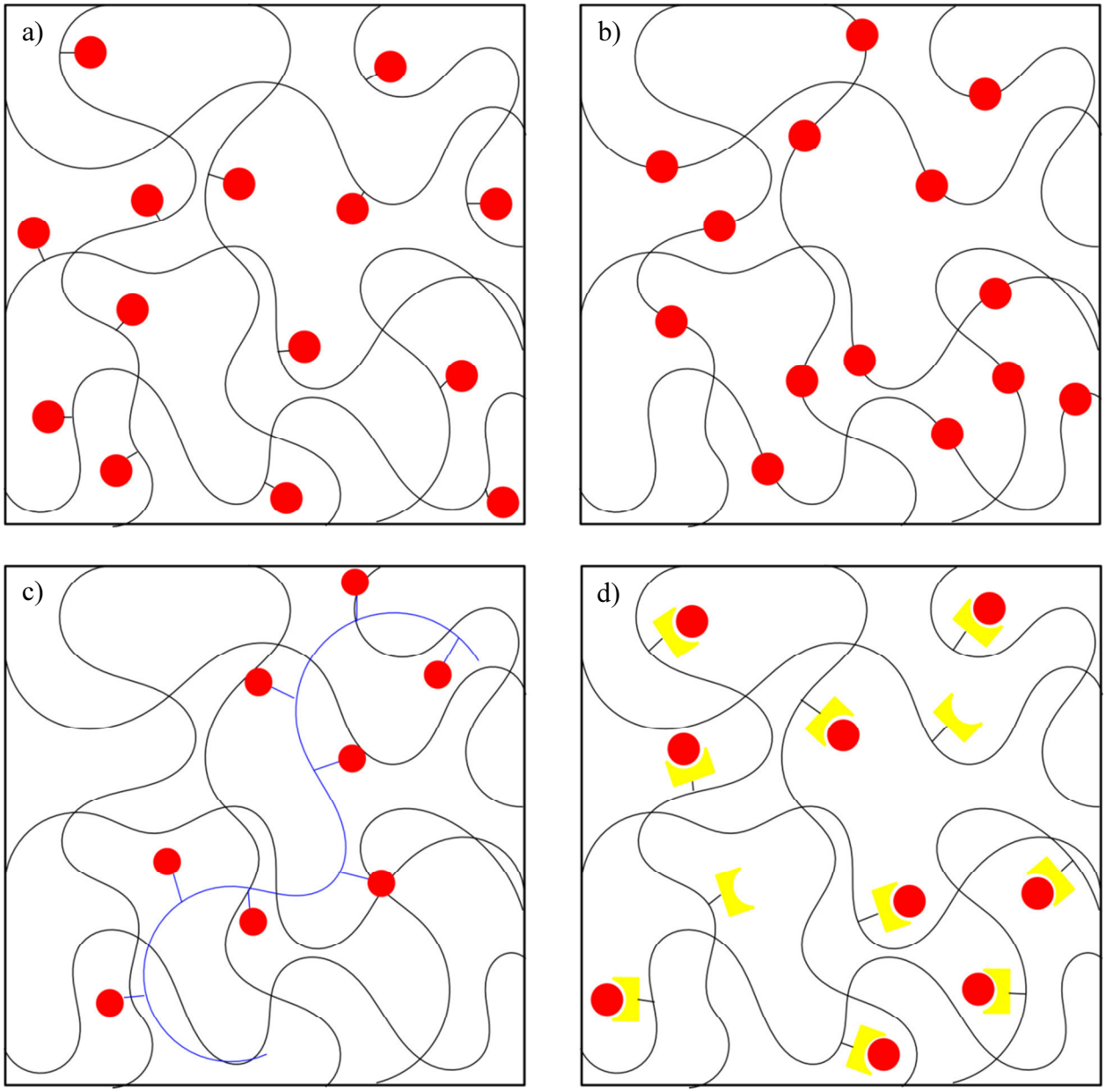

Figure 2.3. Methods of modifying hydrogel materials to impart specific bioactivity. Signal ligands, pictured as red circles, can be covalently attached to the hydrogel in a pendant fashion (a), incorporated into the polymer backbone itself (b), physically entrapped within the polymer matrix while attached to another macromolecule (c), or non-covalent association with specific binding locations that have been incorporated into to the hydrogel, pictured in yellow (d).

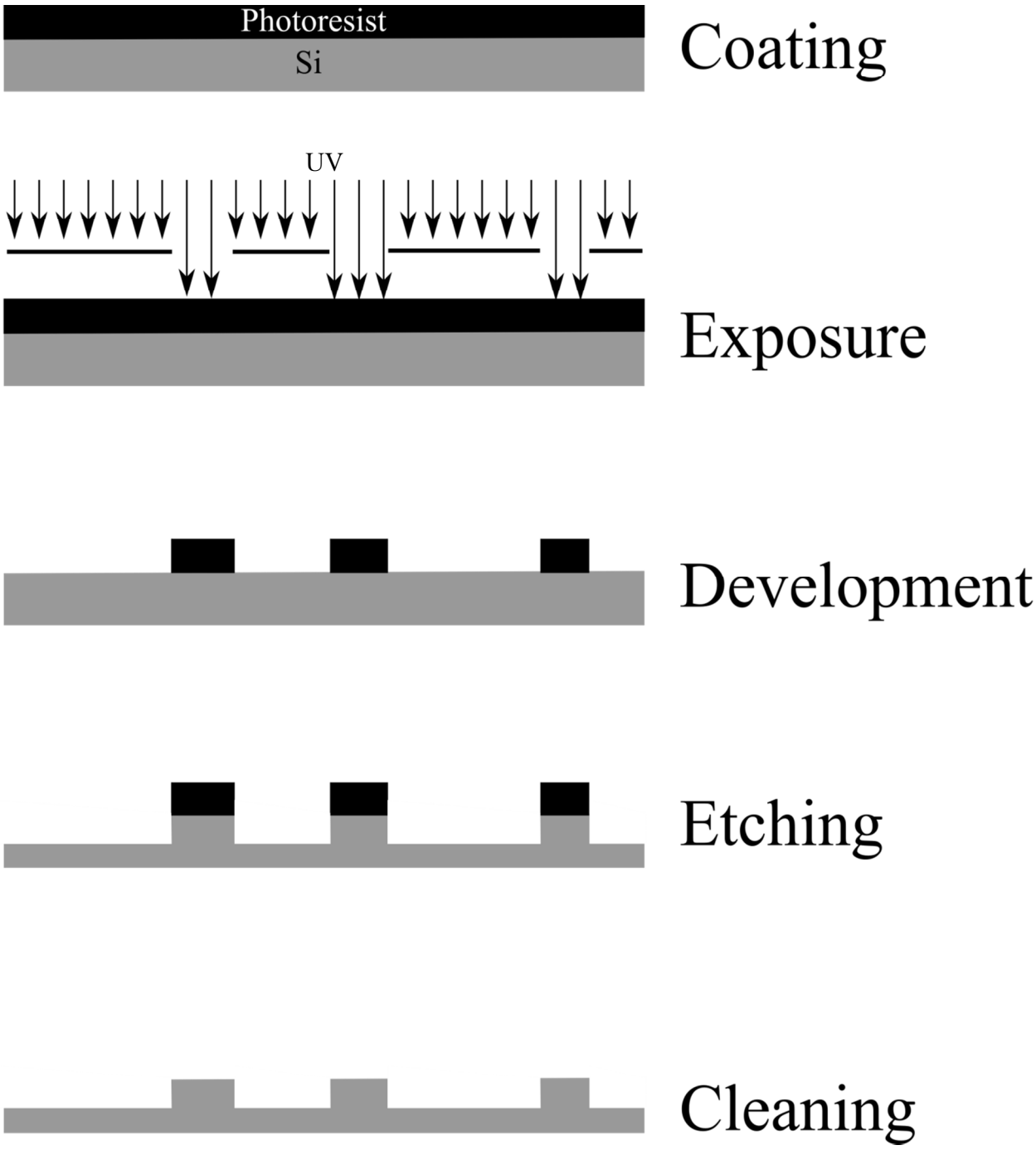

Figure 2.4. Process diagram of the photolithography process. The substrate is covered with a layer of photoresist. This photoresist in exposed to light through a mask. A developer is used to remove either photoresist that has been exposed to light, or that which has not, depending on the photoresist used (negative resist pictured above). The exposed substrate is etched, resulting in a patterned surface upon removal of the remaining photoresist.

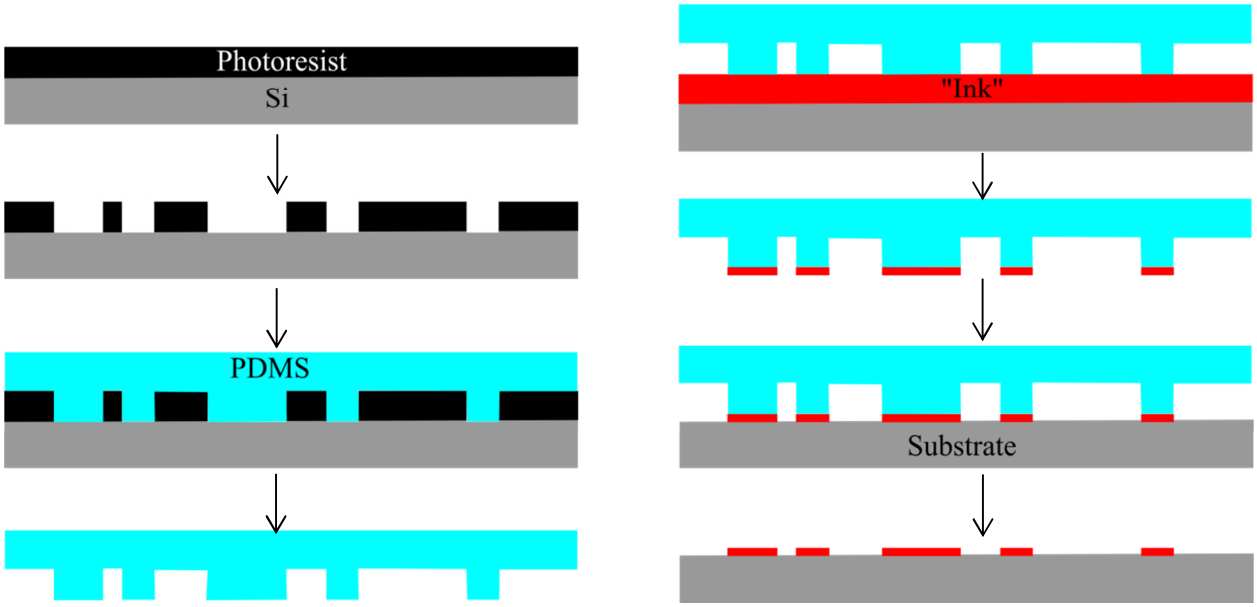

Figure 2.5. Process diagram of soft lithography technique for patterning surfaces, as seen in cross section. A PDMS master is created from a patterned silicon or photoresist on silicon surface. This master is covered in an “ink”, such as protein or polymer. The inked master is pressed onto the substrate like a stamp, resulting in a patterned surface.

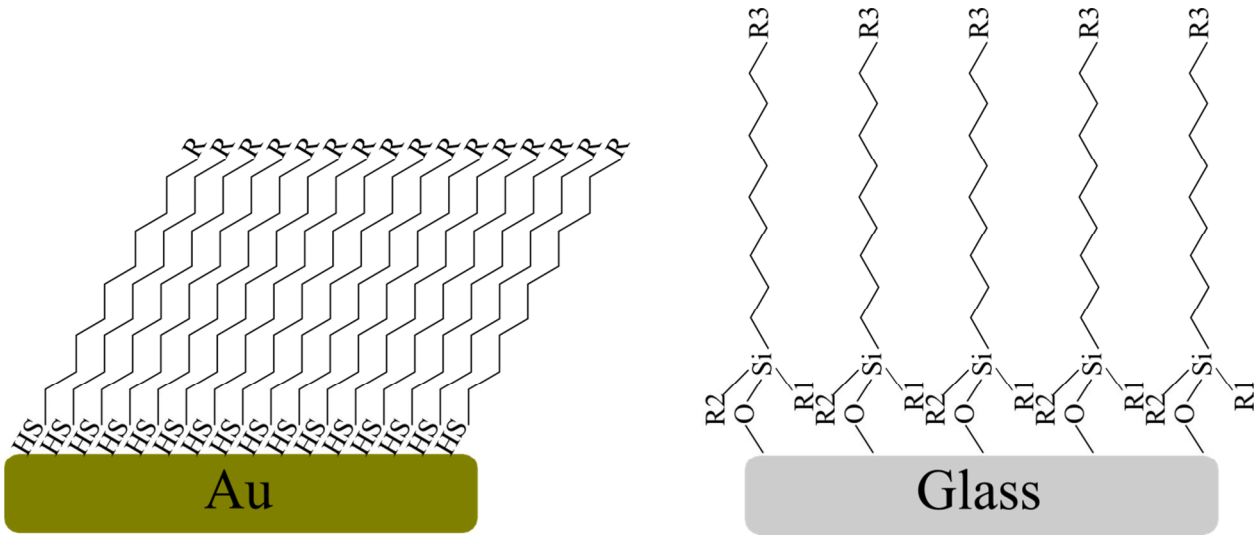

Figure 2.6. Functionalization of a substrate surface via two dimensional self-assembly of a) a thiol-terminated molecule on a gold surface and b) a silane-terminated molecule on a glass surface. The R groups on the terminus of the molecules can be engineered to promote a desired surface chemistry.

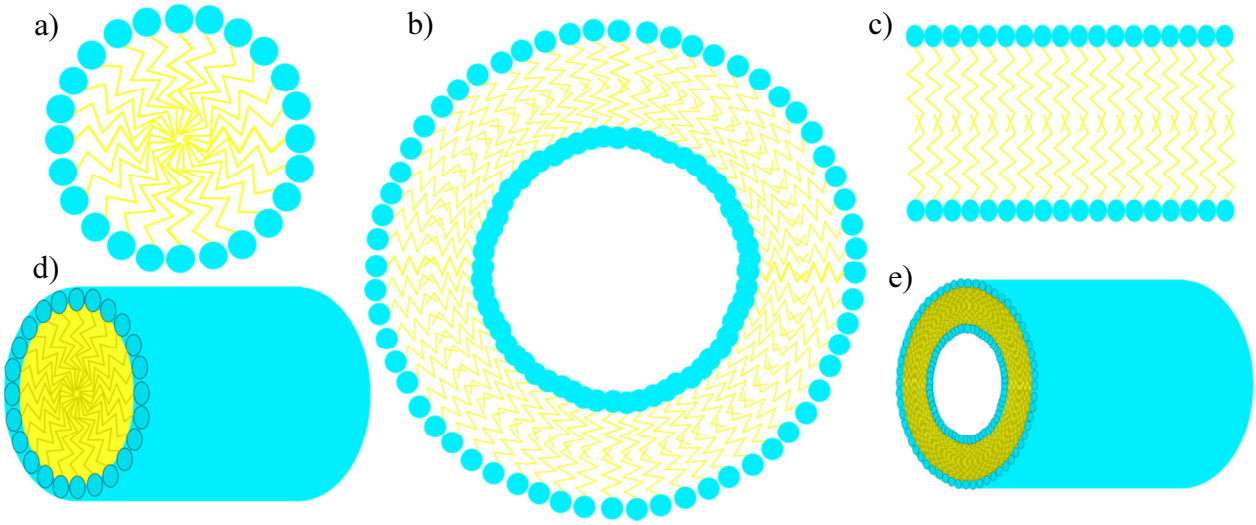

Figure 2.7. Self-assembled structures made from amphiphilic macromolecules, such as block copolymers. In these diagrams, hydrophilic polymer sections are colored blue, and hydrophobic sections are colored yellow. The polymers will self-assemble to isolate hydrophobic regions from the surrounding water. The structure formed will depend on parameters such as the length of the polymer blocks. Pictured structures are a) micelles, b) vesicles, c) bilayers, d) fibers, and e) tubes.

Chapter 3

Electrospun scaffolds for tissue engineering

3.1. Introduction to electrospinning

The process known as electrospinning has become an extensively used process for creating fibers with diameters in the nanometer to micron range. Electrospinning is a simple and cheap process to implement and is capable of large scale manufacturing of nanofibers. It has been implemented in a number of industries, including filtration[1], catalysis[2], and biomaterials[3,4,5]. One of the most attractive aspects of the process is its versatility. A large number of polymers have been electrospun, including biopolymers like collagen[6], silk[7], and hyaluronic acid[8], hydrophilic polymers such as poly(ethylene glycol)[9] and poly(2-hydroxyethyl methacrylate)[10], and hydrophobic polymers like poly(lactide-co-glycolide)[11] and poly(caprolactone)[12]. A variety of morphologies have been created using electrospinning, ranging from uniform circular fibers, to fibers with bead-like defects[13], to flat ribbon-like fibers[14]. The capability of electrospinning to produce fibers with a wide variety of diameters, and that can mimic the structure of the extracellular matrix, has made it a valuable tool in biomimetic tissue engineering.

3.2. The electrospinning process

The electrospinning process is simple to set up and use on the surface, belying incredibly complex and not fully understood underlying physics. A generalized electrospinning apparatus is depicted in Figure 3.1. A polymer solution is fed to the tip of a blunt needle, usually with the aid of a syringe pump, forming a small droplet. This droplet of solution in charged at high voltage, resulting in the accumulation of charge along the surface of the droplet. This charge buildup causes electrostatic repulsion which destabilizes the droplet, forming a cone morphology known as the Taylor cone[15]. A jet of charged solution emerges from the tip of the cone toward a target that has been either grounded or charged opposite the polymer solution. As it travels, the surface charge density causes the jet to become unstable and undergoes what is known as the "whipping instability", wherein the jet begins chaotically bending and whipping. The solvent in which the polymer has been dissolved evaporates as the solution whips and makes its way to the target, resulting in the deposition of solid polymer fibers. A representative SEM image of electrospun polymer fibers is shown in Figure 3.2. Other electrospinning configurations are possible, such as spinning from the surface of a polymer solution or a wetted wire, but the underlying principle is the same in all cases.

The physics of the electrospinning process are best described by the leaky dielectric model[16]. In a leaky dielectric, as opposed to a perfect conductor or dielectric, charges will build up on the surface of the material in response to an imposed electric field. This results in the development of tangential electrostatic forces on the material in addition to the tangential forces that would be seen in a perfect conductor or dielectric, which, together with the surface tension of the solution, deforms the surface into a Taylor cone. The balance between the surface properties and the conductivity of the solution are then of utmost importance in determining whether a polymer solution can be successfully electrospun. A more in depth description of the process, and the governing equations, can be found in other reviews[17].

3.3. Electrospinning process variables

Because of the complexity of the electrospinning process, there are a large number of variables which will alter the morphology of electrospun materials. These variables can be broken down into two categories: properties of the polymer solution, and processing parameters of the electrospinning equipment. The complex interconnectivity of these parameters is illustrated in Figure 3.3. These controllable parameters affect such properties as the surface charge density, solvent evaporation rate, and surface tension, which will ultimately dictate the diameter and morphology of the deposited fibers.

3.3.1. Solution parameters

The important controllable variables of the polymer solution itself are the choice of polymer, the choice of solvent, polymer molecular weight, polymer concentration, and any additives that may be included beyond the polymer. The choice of polymer should always be dictated by the desired final product, as the final product will consist primarily of dried polymer. The solvent chosen then must be compatible with the polymer. In addition, solvent choice will have an impact on properties such as solution conductivity, surface tension, and evaporation rate. The molecular weight of the polymer primarily affects the mechanical properties of the polymer solution, including the viscosity and relaxation time. The concentration of the polymer, in conjunction with the polymer molecular weight, will determine the number of entanglements per polymer chain, which has been implicated in the ability of the solution to be electrospun[18]. The concentration of polymer also plays an important role in the evaporation of the solvent, as the more polymer there is in the solution, the less solvent there is to evaporate before solid fibers are formed. Additives can be used in the solution to change its properties without changing the polymer component to improve its ability to be electrospun. Common examples include salts to increase solution conductivity and surfactants to lower surface tension.

3.3.2. Processing parameters

In addition to the properties of the polymer solution, the parameters of the electrospinning process itself have a large impact on the morphology of the final product. These parameters include the volumetric flow rate of solution to the needle tip, the diameter of the needle tip, the applied voltage, the distance from the needle tip to the collecting target, the configuration and rotational velocity of the collecting target, and ambient conditions such as the temperature and humidity. The feed rate of solution to the needle tip affects the mass balance in the Taylor cone as solution leaves through the jet, and the surface charge density of the droplet. If the flow rate is too high, more solution is added to the droplet than is removed through the electrospinning process, causing the droplet to grow and the surface charge density to lower until the droplet falls from the needle tip. If the flow rate is too low, the droplet is exhausted, resulting in unstable electrospinning from the surface of the needle itself, rather than from a droplet. The applied voltage, as would be expected, mainly affects the charge density on the polymer solution surface. Along with the distance between the needle tip and the collecting target, the voltage also affects the strength of the electric field produced. The distance between the tip and target will also dictate the amount of time that the solvent has to evaporate. The rate of evaporation depends on the polymer and solvent choice and polymer concentration, as well as the ambient conditions around the apparatus, such as temperature and humidity. High temperature and low humidity will

promote fast evaporation of solvent and solidification of the polymer jet. If the time of flight and evaporation kinetics of the polymer solution is not sufficient for complete drying, wet fibers could be deposited that will flow and bond with each other. The arrangement and alignment of the fibers can be altered by changing the geometry of the collecting target. For example, a rapidly rotating target can align the collected fibers, as can a parallel plate configuration where fibers are collected between two electrodes.

3.3.3. Parameter effects on fiber diameter

The most focused on quality of electrospun fibers is their diameter. Because of the complex interconnectivity of the various processing parameters, a large number of variables have a significant effect on the final fiber diameter. The strongest effects on fiber diameter are the diameter of the needle tip, the charge density, which is in turn affected by solution conductivity and applied voltage, distance from the needle tip to the collector, and the solution viscosity, which depends on solvent choice, polymer concentration and polymer molecular weight[19]. Weaker effects are seen from solvent vapor pressure, electric potential, humidity, and surface tension. Increases in needle diameter, polymer concentration, or surface tension will increase the final fiber diameter, while increases in tip to collector distance will decrease fiber diameter.

3.4. Electrospun materials for tissue engineering

A wide variety of polymers have been electrospun for use in tissue engineering applications. A summary of these polymers is shown in Table 4.1. They are broken down into three major categories based on their predominant component into hydrophobic polymer scaffolds, biomolecule scaffolds, and hydrogel scaffolds. The benefits and drawbacks of each type of scaffold material are outlined below.

3.4.1. Hydrophobic polymer scaffolds

Scaffolds made by electrospinning hydrophobic polymers, such as polyesters and polyurethanes, are the simplest to create, in part due to their diversity and versatility. Hydrophobic polymers are easily dissolved in organic solvents, which are ideal for electrospinning due to their volatility. Compared to water, most organic solvents will evaporate rapidly during the solution's flight from needle tip to collector. Because hydrophobic polymers can be synthesized under controlled conditions, their molecular weight and the distribution of that molecular weight can be tuned to ease the electrospinning process. The wide variety of available polymers allows for choice of properties such as mechanical modulus, hydrophobicity, and degradation rate. The major downside to using synthetic hydrophobic polymers is their lack of biological interaction and relevance. They lack any of the bidirectional signaling seen between the natural extracellular matrix and cells. Without specific measures taken to introduce biological signals, these materials serve as mostly inert support materials.

Electrospun hydrophobic polymers have been used for a vast number of tissue engineering applications. The most commonly used polymers are the closely related poly(lactic acid) and poly(glycolic acid), as well as their copolymers. These polymers have been electrospun for engineering of vascular grafts[20], cartilage[21], bone[22], neural tissue[23], cardiac tissue[3], skeletal muscle[24], and bladder[25].

3.4.2. Biomolecule scaffolds

Electrospun polymers and polysaccharides provide the necessary biological interaction between cells and the scaffolds without the need for additional modification. Though more limited than the library of synthetic polymers, there is a large number of biomolecules that can be electrospun, allowing for specific engineering of the cell-material interaction. Because of their innate biological significance, these materials found use in a variety of tissue engineering applications, including skeletal muscle[26], neural tissue[27], cardiac tissue[28,29], vascular grafts[30], cartilage[31], and as a wound dressing[32].

Electrospinning of biopolymers is much more difficult than synthetic polymers. The organic solvents used most commonly in electrospinning run the risk of denaturing or otherwise damaging proteins, and polysaccharides have limited solubility in organic solvents. Spinning from aqueous solution is possible, but more difficult. To ease the electrospinning process, a synthetic polymer is often used as a "carrier" molecule, but this addition imposes additional constraints on the solvents and parameters that can be used. In addition, with the exception of the most common proteins such as collagen, the price of materials may be prohibitive for high volume processing.

3.4.3. Hydrogel scaffolds

Hydrogel electrospinning is a recent invention, and so has not yet found widespread use. Hydrogels are incredibly difficult to electrospin. They have very limited solubility in organic solvents, requiring the use of aqueous solvents. However, the combination of water's low volatility and hydrogel material's affinity for water slows the drying process for the polymer jet, resulting in deposition of wet material rather than dry polymer fibers. Electrospinning of a crosslinked hydrogel is impossible due to the necessary polymer shearing in the process, necessitating the electrospinning of monomer or protopolymer and crosslinking after fiber formation.

The advantage of electrospinning hydrogels versus hydrophobic polymers or biopolymers is their combination of biomimicry and controllability. Unlike hydrophobic polymers, hydrogels have a tunable modulus, and can be made soft enough to mechanically mimic the extracellular matrix. They can be easily modified in multiple ways to present biologically relevant signals, such as binding peptides or growth factors. And unlike biopolymers, hydrogels provide a controlled, defined material platform, making them more scientifically relevant, as well as lowering the regulatory barrier. In this way, electrospun hydrogels combine many of the positive elements from synthetic polymers with those from biopolymers, and their use in tissue engineering will only increase as the process becomes better understood, and more applications are explored.

3.5. References

1. Gopal, R.; Kaur, S.; Ma, Z. W.; Chan, C.; Ramakrishna, S.; Matsuura, T., Electrospun nanofibrous filtration membrane. *J Membrane Sci* **2006,** *281* (1-2), 581-586.

2. Formo, E.; Lee, E.; Campbell, D.; Xia, Y. N., Functionalization of electrospun TiO2 nanofibers with Pt nanoparticles and nanowires for catalytic applications. *Nano Lett* **2008,** *8* (2), 668-672.

3. Zong, X. H.; Bien, H.; Chung, C. Y.; Yin, L. H.; Fang, D. F.; Hsiao, B. S.; Chu, B.; Entcheva, E., Electrospun fine-textured scaffolds for heart tissue constructs. *Biomaterials* **2005,** *26* (26), 5330-5338.

4. Li, C. M.; Vepari, C.; Jin, H. J.; Kim, H. J.; Kaplan, D. L., Electrospun silk-BMP-2 scaffolds for bone tissue engineering. *Biomaterials* **2006,** *27* (16), 3115-3124.

5. Yang, F.; Murugan, R.; Wang, S.; Ramakrishna, S., Electrospinning of nano/micro scale poly(L-lactic acid) aligned fibers and their potential in neural tissue engineering. *Biomaterials* **2005,** *26* (15), 2603-2610.

6. Dong, B.; Arnoult, O.; Smith, M. E.; Wnek, G. E., Electrospinning of Collagen Nanofiber Scaffolds from Benign Solvents. *Macromol Rapid Comm* **2009,** *30* (7), 539-542.

7. Min, B. M.; Lee, G.; Kim, S. H.; Nam, Y. S.; Lee, T. S.; Park, W. H., Electrospinning of silk fibroin nanofibers and its effect on the adhesion and spreading of normal human keratinocytes and fibroblasts in vitro. *Biomaterials* **2004,** *25* (7-8), 1289-1297.

8. Ji, Y.; Ghosh, K.; Shu, X. Z.; Li, B. Q.; Sokolov, J. C.; Prestwich, G. D.; Clark, R. A. F.; Rafailovich, M. H., Electrospun three-dimensional hyaluronic acid nanofibrous scaffolds. *Biomaterials* **2006,** *27* (20), 3782-3792.

9. Son, W. K.; Youk, J. H.; Lee, T. S.; Park, W. H., The effects of solution properties and polyelectrolyte on electrospinning of ultrafine poly(ethylene oxide) fibers. *Polymer* **2004,** *45* (9), 2959-2966.

10. Kim, S. H.; Nair, S.; Moore, E., Reactive electrospinning of cross-linked poly(2-hydroxyethyl methacrylate) nanofibers and elastic properties of individual hydrogel nanofibers in aqueous solutions. *Macromolecules* **2005,** *38* (9), 3719-3723.

11. Zhang, Y.; Lei, Y.; Chang, J.; Li, L.; He, B.; Gu, Z. W., Guidance of myoblast migration on aligned electrospun PLGA nanofibrous meshes. *Mater Lett* **2012,** *68*, 218-221.

12. Shin, M.; Ishii, O.; Sueda, T.; Vacanti, J. P., Contractile cardiac grafts using a novel nanofibrous mesh. *Biomaterials* **2004,** *25* (17), 3717-3723.

13. Qi, H. X.; Hu, P.; Xu, J.; Wang, A. J., Encapsulation of drug reservoirs in fibers by emulsion electrospinning: Morphology characterization and preliminary release assessment. *Biomacromolecules* **2006,** *7* (8), 2327-2330.

14. Koombhongse, S.; Liu, W. X.; Reneker, D. H., Flat polymer ribbons and other shapes by electrospinning. *J Polym Sci Pol Phys* **2001,** *39* (21), 2598-2606.

15. Taylor, G., Disintegration of Water Drops in an Electric Field. *Proc R Soc Lon Ser-A* **1964,** *280* (1382), 383-397.

16. Saville, D. A., Electrohydrodynamics: The Taylor-Melcher leaky dielectric model. *Annu Rev Fluid Mech* **1997,** *29*, 27-64.

17. Hohman, M. M.; Shin, M.; Rutledge, G.; Brenner, M. P., Electrospinning and electrically forced jets. I. Stability theory. *Phys Fluids* **2001,** *13* (8), 2201-2220.

18. Shenoy, S. L.; Bates, W. D.; Frisch, H. L.; Wnek, G. E., Role of chain entanglements on fiber formation during electrospinning of polymer solutions: good solvent, non-specific polymer-polymer interaction limit. *Polymer* **2005,** *46* (10), 3372-3384.

19. Thompson, C. J.; Chase, G. G.; Yarin, A. L.; Reneker, D. H., Effects of parameters on nanofiber diameter determined from electrospinning model. *Polymer* **2007,** *48* (23), 6913-6922.

20. Hashi, C. K.; Derugin, N.; Janairo, R. R. R.; Lee, R.; Schultz, D.; Lotz, J.; Li, S., Antithrombogenic Modification of Small-Diameter Microfibrous Vascular Grafts. *Arterioscl Throm Vas* **2010,** *30* (8), 1621-1627.

21. Chen, J. P.; Su, C. H., Surface modification of electrospun PLLA nanofibers by plasma treatment and cationized gelatin immobilization for cartilage tissue engineering. *Acta Biomater* **2011,** *7* (1), 234-243.

22. Zhou, C. J.; Shi, Q. F.; Guo, W. H.; Terrell, L.; Qureshi, A. T.; Hayes, D. J.; Wu, Q. L., Electrospun Bio-Nanocomposite Scaffolds for Bone Tissue Engineering by Cellulose Nanocrystals Reinforcing Maleic Anhydride Grafted PLA. *Acs Appl Mater Inter* **2013,** *5* (9), 3847-3854.

23. Koppes, A. N.; Zaccor, N. W.; Rivet, C. J.; Williams, L. A.; Piselli, J. M.; Gilbert, R. J.; Thompson, D. M., Neurite outgrowth on electrospun PLLA fibers is enhanced by exogenous electrical stimulation. *J Neural Eng* **2014,** *11* (4).

24. Aviss, K. J.; Gough, J. E.; Downes, S., Aligned Electrospun Polymer Fibres for Skeletal Muscle Regeneration. *Eur Cells Mater* **2010,** *19*, 193-204.

25. Shakhssalim, N.; Dehghan, M. M.; Moghadasali, R.; Soltani, M. H.; Shabani, I.; Soleimani, M., Bladder Tissue Engineering Using Biocompatible Nanofibrous Electrospun Constructs Feasibility and Safety Investigation. *Urol J* **2012,** *9* (1), 410-419.

26. Choi, J. S.; Lee, S. J.; Christ, G. J.; Atala, A.; Yoo, J. J., The influence of electrospun aligned poly(epsilon-caprolactone)/collagen nanofiber meshes on the formation of self-aligned skeletal muscle myotubes. *Biomaterials* **2008,** *29* (19), 2899-2906.

27. Ghasemi-Mobarakeh, L.; Prabhakaran, M. P.; Morshed, M.; Nasr-Esfahani, M. H.; Ramakrishna, S., Electrospun poly(epsilon-caprolactone)/gelatin nanofibrous scaffolds for nerve tissue engineering. *Biomaterials* **2008,** *29* (34), 4532-4539.

28. Kai, D.; Prabhakaran, M. P.; Jin, G. R.; Ramakrishna, S., Guided orientation of cardiomyocytes on electrospun aligned nanofibers for cardiac tissue engineering. *J Biomed Mater Res B* **2011,** *98B* (2), 379-386.

29. Dang, J. M.; Leong, K. W., Myogenic induction of aligned mesenchymal stem cell sheets by culture on thermally responsive electrospun nanofibers. *Adv Mater* **2007,** *19* (19), 2775-+.

30. Cattaneo, I.; Figliuzzi, M.; Azzollini, N.; Catto, V.; Fare, S.; Tanzi, M. C.; Alessandrino, A.; Freddi, G.; Remuzzi, A., In vivo regeneration of elastic lamina on fibroin biodegradable vascular scaffold. *Int J Artif Organs* **2013,** *36* (3), 166-174.

31. Kim, I. L.; Khetan, S.; Baker, B. M.; Chen, C. S.; Burdick, J. A., Fibrous hyaluronic acid hydrogels that direct MSC chondrogenesis through mechanical and adhesive cues. *Biomaterials* **2013,** *34* (22), 5571-5580.

32. Han, I.; Shim, K. J.; Kim, J. Y.; Im, S. U.; Sung, Y. K.; Kim, M.; Kang, I. K.; Kim, J. C., Effect of poly(3-hydroxybutyrate-co-3-hydroxyvalerate) nanofiber matrices cocultured with hair follicular epithelial and dermal cells for biological wound dressing. *Artif Organs* **2007,** *31* (11), 801-808.

33. de Valence, S.; Tille, J. C.; Mugnai, D.; Mrowczynski, W.; Gurny, R.; Moller, M.; Walpoth, B. H., Long term performance of polycaprolactone vascular grafts in a rat abdominal aorta replacement model. *Biomaterials* **2012,** *33* (1), 38-47.

34. Soletti, L.; Nieponice, A.; Hong, Y.; Ye, S. H.; Stankus, J. J.; Wagner, W. R.; Vorp, D. A., In vivo performance of a phospholipid-coated bioerodable elastomeric graft for small-diameter vascular applications. *J Biomed Mater Res A* **2011,** *96A* (2), 436-448.

35. Rockwood, D. N.; Akins, R. E.; Parrag, I. C.; Woodhouse, K. A.; Rabolt, J. F., Culture on electrospun polyurethane scaffolds decreases atrial natriuretic peptide expression by cardiomyocytes in vitro. *Biomaterials* **2008,** *29* (36), 4783-4791.

36. Orlova, Y.; Magome, N.; Liu, L.; Chen, Y.; Agladze, K., Electrospun nanofibers as a tool for architecture control in engineered cardiac tissue. *Biomaterials* **2011,** *32* (24), 5615-5624.

37. Yang, X.; Ogbolu, K. R.; Wang, H., Multifunctional nanofibrous scaffold for tissue engineering. *J Exp Nanosci* **2008,** *3* (4), 329-345.

38. Schultz, K. M.; Campo-Deano, L.; Baldwin, A. D.; Kiick, K. L.; Clasen, C.; Furst, E. M., Electrospinning covalently cross-linking biocompatible hydrogelators. *Polymer* **2013,** *54* (1), 363-371.

39. Kyu-Oh Kim, Y. A., Wei Kai, Byoung-Sukh Kim, Ick-Soo Kim, Cells attachment property of PVA hydrogel nanofibers incorporating hyaluronic acid for tissue engineering. *Journal of Biomaterials and Nanobiotechnology* **2011,** *2*, 353-360.

40. Fernandes, J. G.; Correia, D. M.; Botelho, G.; Padrao, J.; Dourado, F.; Ribeiro, C.; Lanceros-Mendez, S.; Sencadas, V., PHB-PEO electrospun fiber membranes containing chlorhexidine for drug delivery applications. *Polym Test* **2014,** *34*, 64-71.

3.6. Tables

Table 3.1. Summary of recent uses of electrospinning in generating scaffolds for tissue engineering.

Predominant Component	**Polymer**	**Average Fiber Diameter (nm)**	**Application**
Hydrophobic polymers	PCL	2200	Vascular graft[33]
	PCL	250	Cardiac[12]
	PLLA	2000	Vascular graft[20]
	PLLA	222	Cartilage[21]
	PLLA	361	Bone[22]
	PLLA	2170	Neural[23]
	Polyurethane	1000	Vascular graft[34]
	Polyurethane	1800	Cardiac[35]
	PLLA/PLGA	1000	Cardiac[3]
	PLGA/PCL	---	Bladder[25]
	PMGI	400-1200	Cardiac[36]
Biomolecules	Collagen/PCL	200-500	General tissue engineering[37]
	Collagen/PCL	300	Skeletal muscle[26]
	Gelatin/PCL	113	Neural[27]
	Gelatin/PCL	269	Cardiac[28]
	Gelatin/PHBV	200-300	Wound dressing[32]
	HBC	463	Cardiac[29]
	Silk	---	Vascular graft[30]
	Hyaluronic acid	744	Cartilage[31]
Hydrogels	PEG	280-420	General tissue engineering[38]
	PVA	430	General tissue engineering[39]
	PHB/PEG	1500	Drug Delivery[40]

3.9. Figures

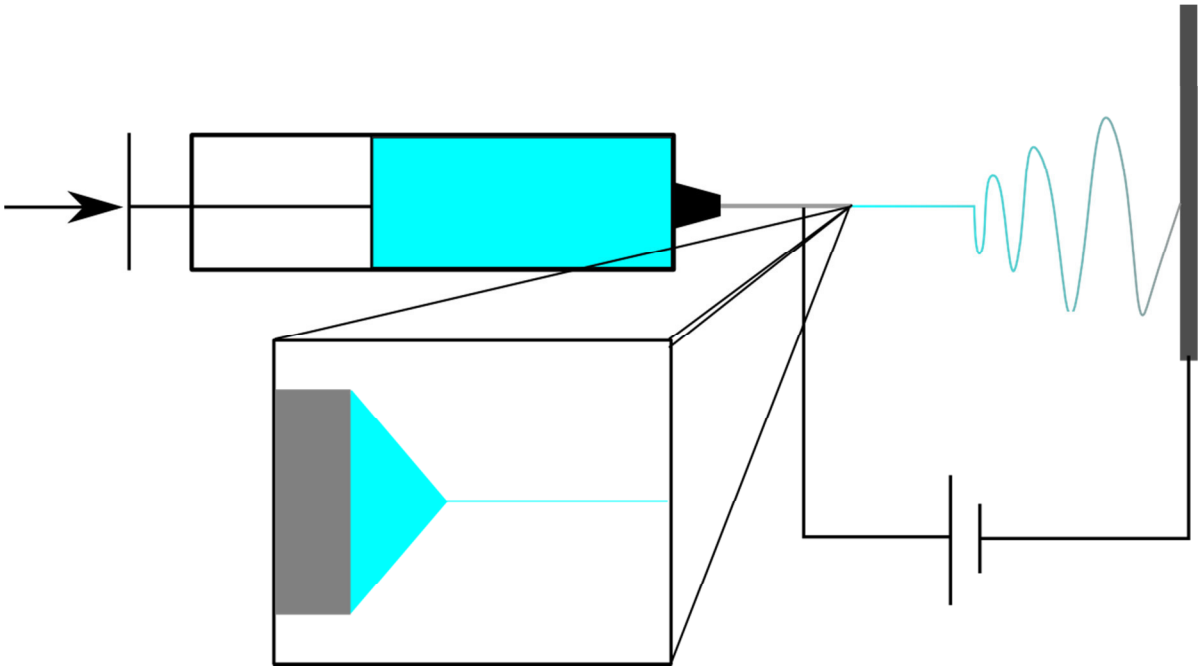

Figure 3.1. Generalized schematic of the electrospinning apparatus. As polymer solution is fed to the needle tip, it is charged at high voltage. The jet emerges, undergoing a whipping instability and drying en route to the target. Inset: the Taylor cone formation at the tip of the needle, from which the jet emerges.

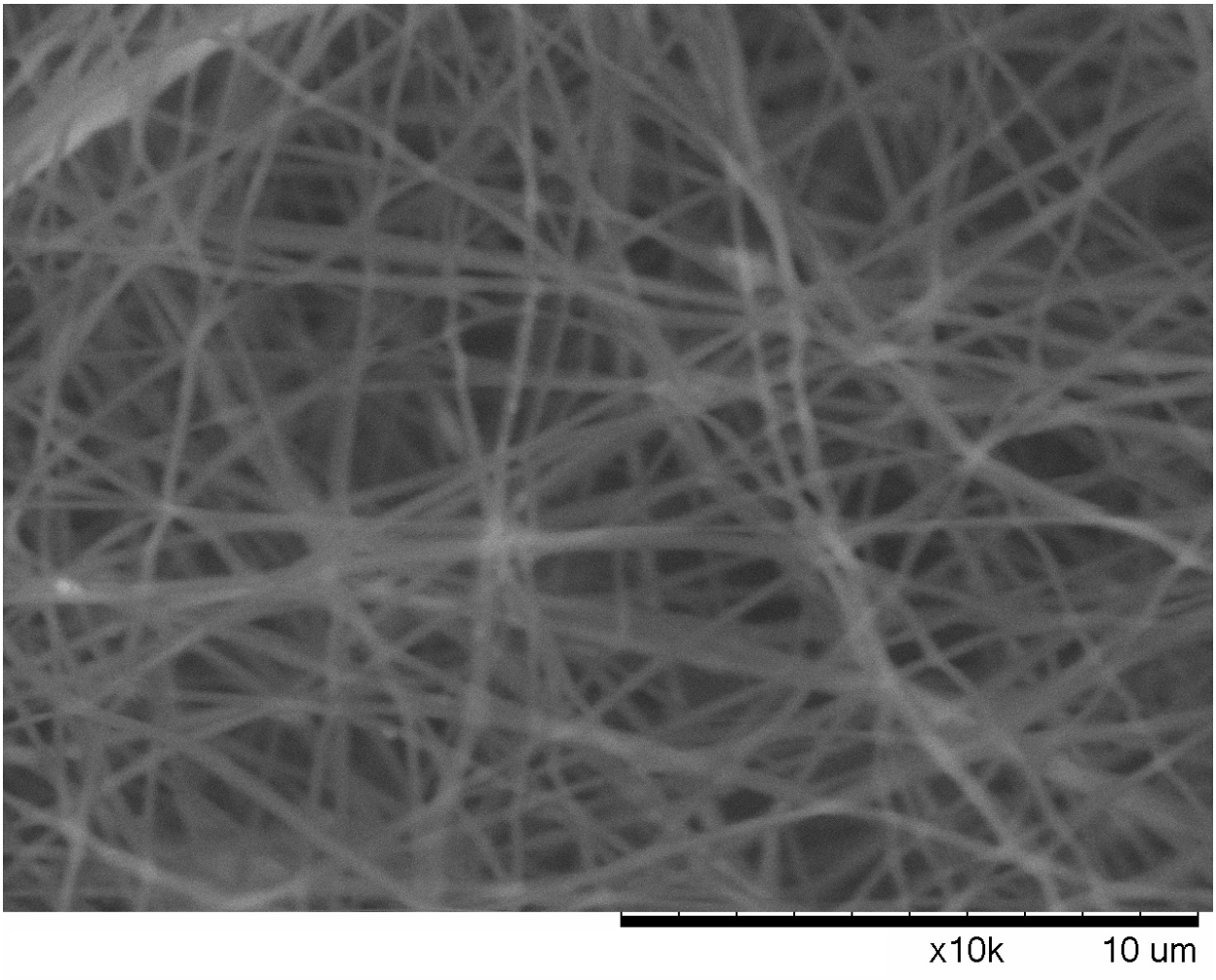

Figure 3.2. SEM image of electrospun polymer nanofibers.

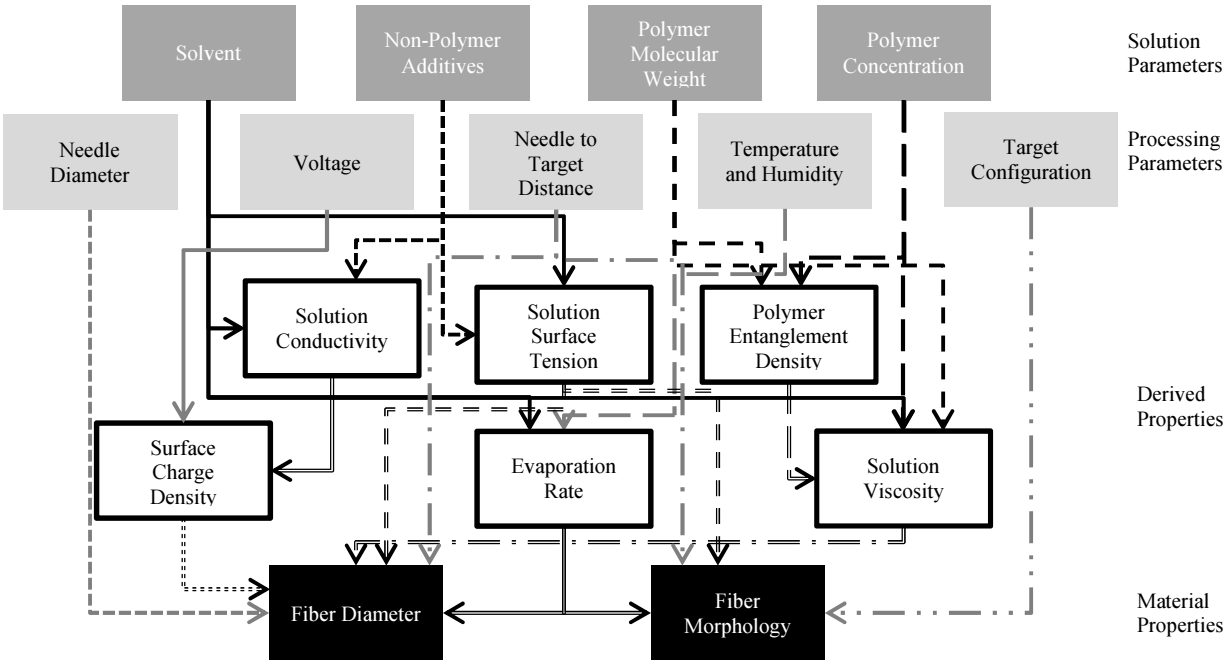

Figure 3.3. Flow diagram demonstrating how the various solution and processing parameters will affect the diameter and morphology of the resulting electrospun fibers.

Chapter 4

Synthesis and characterization of multivalent peptide-hyaluronic acid conjugates

4.1. Abstract

Complex composite materials of conjugated biomolecules are becoming increasingly important in the field of biomaterials and tissue regeneration. Multivalent bioconjugates have been shown to have many favorable characteristics over soluble signals, including improved localization, prolonged retention in tissue, and increased potency. However, due to their complicated structure, they are often poorly or incompletely characterized. In this study, as a model study I synthesized a multivalent conjugate of an RGD-containing peptide grafted to hyaluronic acid, and characterized it using in-line size-exclusion chromatography, static multi-angle light scattering, UV absorption, and differential refractive index (SEC-MALS-UV-RI) measurements. Using this technique, I was able to fully characterize the molecular weight, valency, and reaction efficiency in an absolute manner without use of a standard. Extended use and further refinement of this technique will improve the understanding and design of engineered biomacromolecules.

4.2. Introduction

The field of polymer-protein and polymer-peptide bioconjugation has become increasingly prevalent in the realms of drug delivery[2,3,4], surface modification[5,6,], imaging[7,8], and *ex vivo* tissue scaffolding[9,10,11]. One of the major advantages of using these techniques is the ability to modulate the function of the peptide or protein by the addition of a synthetic or natural polymer. This can cause changes in the circulation time of the protein in the bloodstream[12,13], the residency time of injected therapeutics in the desired location[14], or the potency of the protein binding and signaling[15]. Coupling small molecules or peptides to larger structural molecules allows for the integration of biological signals to otherwise inert or low functionality scaffolds[16,17].

However, to fully explore the use of these bioconjugate materials, the materials themselves must be characterized and understood. By definition, protein-polymer or peptide-polymer bioconjugates are more complex than their constituent parts and simple measurements such as protein fraction or molecular weight are no longer sufficient for understanding their behavior. In addition to these properties, bioconjugate valency[15,18,19] and degree of substitution are of key importance to understanding and controlling their function. Multivalency of bioconjugates has been shown to increase the signal potency over monovalent or free signals due to their increased localization and clustering effects on membrane bound receptors[20]. The increased potency of multivalent signaling compared to monovalent or free signals offers the possibility of many improvements in therapy, including reducing cost and waste of drugs. Multivalent bioconjugate materials also allows for the possibility of colocalizing multiple different signals on the same molecule to provide a more complex and biomimetic environment as a tissue scaffold.

The process of properly characterizing these complex molecules is still evolving. Many techniques provide partial or incomplete information and may be misleading unless many are used simultaneously[21]. Protein quantification methods such as ultraviolet light absorbance or

bicinchoninic acid assay (i.e., BCA) can estimate the total amount of protein or peptide in the sample, but cannot describe the structure or valency of the conjugate without separate information about the molecular weight distribution. Techniques such as Fourier transform infrared spectroscopy[22] or nuclear magnetic resonance[23] can provide average molecular weight information, but not distribution, and require end group identification or tagging. Molecular weight distributions can be measured using chromatography[24], but require comparisons to standards with similar chemistry.

However, the coupling of chromatography with static light scattering can provide an absolute measure of molecular weight distribution and can be combined in-line with other techniques to provide complete analysis of complex bioconjugates. To this end we have developed a technique that can fully characterize the distribution of molecular mass and valency of a bioconjugate molecule. Three detectors were used in series in an automated process. The sample was separated by size exclusion chromatography[25,26]. Both an ultraviolet light absorbance (UV) and a differential refractometer (RI) monitored the concentration of the sample. Using both detectors, the concentration of a mixed sample can be accurately determined, as well as their relative abundance. Combining this concentration detection with multi-angle light scattering (MALS) allows for the absolute measurement of molecular weight. Using the molecular weight and the protein fraction measured by this method, the valency of the bioconjugates can be calculated.

4.3. Materials and methods

Hyaluronic acid sodium salts (**HyA**) of 600 kDa molecular weight were obtained from Genzyme. All chemicals used in the conjugation reaction, including 1-ethyl-3-(3-dimethylaminoproyl)carbodiimide hydrochloride (**EDC**), N-hydroxysulfosuccinimide (**sulfoNHS**) and 3,3'-N-(ε-maleimidocaproic acid)hydrazide trifluoroacetic acid (**EMCH**), tris(2-carboxyethyl) phosphine (**TCEP**), and the buffers phosphate buffered saline (**PBS**) and 2-(N-morpholino)ethanesulfonic acid (**MES**) were purchased from Thermo Scientific. SnakeSkin dialysis tubing with 10k molecular weight cutoff was also purchased from Thermo Scientific. The peptide

-RGD(15) [Ac-CGGNGEPRGDTYRAY-NH_2] was synthesized by American Peptide as previously described[27].

4.3.1. Activation of hyaluronic acid

In preparation for conjugation of a cysteine-terminated peptide, hyaluronic acid was activated by the addition of a maleimide residue to the carboxylic acid of the hyaluronic acid chain. First, HyA was dissolved in MES buffer. To ensure complete homogenization of the solution, this was left gently stirring overnight at 60 rpm. EDC, sulfoNHS and EMCH were dissolved in MES buffer and added to the HyA solution. The final concentrations for the reagents were 5 mg/mL HyA, 10 mg/mL EDC, 2.8 mg/mL sulfoNHS, and 1.2 mg/mL EMCH. The reaction was allowed to proceed for two hours in the dark with gentle stirring. The product was then purified through dialysis in a 10k MWCO dialysis tube against PBS. Dialysis lasted for 24h in 2L of buffer, with fresh buffer added at the 0h, 2h, and 4h time points.

4.3.2. Conjugation of peptide to activated hyaluronic acid

After dialysis, the activated hyaluronic acid was reacted with the cysteine-terminated RGD-containing peptide bsp-RGD(15). The peptide was reduced in a solution of 5.7 mg/mL TCEP with 3 mg/mL NaOH in order to disrupt any disulfide bonds that had formed between the peptides. This solution was then added to the activated HyA and allowed to react overnight in the dark at 4^{o}C. The amount of peptide added varied from 0.08 mg peptide per mg HyA to 0.32 mg peptide per mg HyA to achieve a range of final conjugate valencies.

Once the reaction was complete, the peptide-HyA conjugates were purified via dialysis in a 10k MWCO dialysis tube against water. The dialysis was kept at 4^{o}C and lasted for 24h, with fresh water added at the 0h, 2h, and 4h time points. After dialysis, the product was lyophilized and kept at -20^{o}C until used.

4.3.3. SEC-MALS analysis of peptide-hyaluronic acid conjugates

The final conjugate molecular weight, peptide mass fraction and valency were measured using an in-line SEC-MALS-UV-RI system, consisting of an Agilent 1100 HPLC system, including degasser, quaternary pump, autosampler, column, and UV diode array detector, in-line with a HELEOS II multi-angle light scatterer and a T-rEX differential refractometer, both from Wyatt Technology. The sample was dissolved at a concentration of 1 mg/mL and a sample volume of 100μL was injected. Separation of the conjugates was achieved with a Shodex OHpak SB-804 HQ column. UV absorbance was measured at a wavelength of 280 nm. Multi-angle light scattering was measured with 660 nm laser light and 18 photodiode detectors. Differential refractive index was measured at a wavelength of 690 nm. Data analysis was performed using ASTRA VI software from Wyatt. Normalization, peak alignment and band broadening was performed using a 100μL injection of 1 mg/mL bovine serum albumin (BSA).

Specific differential refractive index increments and UV absorption coefficients of the peptides and of hyaluronic acid were verified using off-line injection of known solution concentrations. Serial dilutions of each were injected using a syringe pump directly into the detector, which was allowed to reach equilibrium before injection of the next concentration. A linear regression was performed on the resulting data to calculate either the UV absorption coefficient or the specific refractive index increment, as appropriate.

4.4. Results and discussion

4.4.1. Determination of specific refractive index increment and UV extinction coefficient of material components

The measured constants for the components and intermediates in the conjugation reaction are shown in Table 4.1. For the peptide bsp-RGD(15), the measured specific refractive index increment of 0.185 mL g^{-1} was in line with that reported in the literature[28]. The measured extinction coefficient of 1.84 at 280 nm was also in agreement with available theoretical calculators (ExPASy). The constants measured for HyA, however, differed from those reported in the literature[29]. The specific refractive index increment of HyA has been reported to be between 0.160 and 0.180 in aqueous buffer, with an average value of 0.167. Here, we have

measured it to be 0.160. While this represents only a 4.2% change in the measured value from the average literature value, the constant dn/dc is a significant determinant in the equation to calculate molecular weight, which is squared in the equation and would lead to an 8.2% error in calculated molecular weight. The UV absorbance of HyA at 280 nm was too low to be accurately measured using this method, so a value of 0.022 was used, as had been measured previously using a UV spectrophotometer[1].

Activation of the HyA with EMCH caused significant changes to its measured constants. EMCH does not absorb UV strongly at 280 nm, so there was no observable increase in the measured extinction coefficient. Because of this, the same value of 0.022 as was measured for unmodified HyA was used in calculations. The specific refractive index increment, however, was significantly lowered from 0.160 to 0.144. This can be understood by analyzing the polarizability of the two components of the activated HyA. Molecules with a higher polarizability will more strongly interact with photons, resulting in a higher refractive index and thus a higher specific refractive index increment. The majority of the EMCH molecule is a linear hydrocarbon, which is significantly less polarizable than the component saccharide units of HyA. Thus, as EMCH residues are added to the HyA chain, the molecule becomes relatively less polarizable and the specific refractive index increment will drop.

4.4.2. SEC-MALS-UV-RI analysis of conjugates

Hyaluronic acid (HyA) was coupled to a cysteine terminated Arg-Gly-Asp (RGD)-containing cell-binding peptide derived from bone sialoprotein, bsp-RGD(15)[30] via carbodiimide and maleimide chemistry. A schematic of the conjugation reaction is shown in Figure 4.1. The peptide bsp-RGD(15) was chosen, as the Arg-Gly-Asp (RGD) sequence has been shown to improve the adhesion and function of myriad cell types, ranging from osteoblasts to cardiomyocytes[31]. The resulting peptide-polysaccharide conjugate presents pendant ligands in a multivalent fashion. Multivalent presentation of ligands has been shown to increase their potency compared to soluble peptide or protein[15]. By utilizing a multivalent conjugate embedded into the fiber, a smaller amount of peptide is necessary to elicit the same response from cells.

The conjugates provided a strong signal in all three detectors (light scattering, differential refractive index, and UV absorbance), indicating that the conjugation reaction was successful. An example chromatogram showing these three signals is shown in Figure 4.2. The chromatograms are typical of a mildly polydisperse sample, as the peaks from the detectors for concentration, namely the UV absorbance and differential refractometer, are offset from and have a different shape than the light scattering peak. This is due to the separation of the conjugates based on size by the SEC column, with larger molecules eluting into the detectors first. This separation of the conjugates is shown in Figure 4.3. As the light scattering signal is dependent on both the sample concentration and its molecular weight, the light scattering signal will peak before the concentration signal. The calculated polydispersity of the conjugates was 1.24.

The final multivalent conjugate was found to have a weight average molecular weight of 605 kDa. This is broken down into 570 kDa of HyA and 35 kDa peptide. This corresponds to 21.2 peptides per backbone molecule on average. Looking at the distribution of molecular weights in more detail, the HyA backbone molecular weight varied from 350 kDa to 2 Mda, with a peak at 536 kDa. The peptide “molecular weight”, representing the total mass of peptide

attached to a single HyA chain rather than the weight of the peptide itself, had a wider range, varying from 17.2 kDa to 108 kDa, with a peak at 28.5 kDa. These values correspond to conjugation ratios of 10.4:1, 65.2:2, and 17.2:1, respectively. These distributions are shown in Figure 4.4. Though the extreme molecular weights are disparate, the distribution itself is relatively narrow, with a 1.47 "polydispersity" of conjugation ratios.

Despite the wide range of conjugation ratios measured, the efficiency of the conjugation per reaction site was consistent. The range of peptide weight fraction, as shown in Figure 4.5, varied from 4.7% to 5.3%, indicating the variation seen in conjugation ratio was primarily due to the variation in hyaluronic acid molecular weight, not in conjugation efficiency.

4.5 Conclusions

A cell-adhesive RGD-containing peptide was conjugated to hyaluronic acid in a multivalent fashion. This material architecture has been shown to have many benefits over monomeric, soluble peptide. These conjugates were characterized using an in-line SEC-MALS-UV-RI detection method. This technique is uniquely capable of complete and absolute characterization of multivalent bioconjugates using a minimal amount of sample. Other than molecular weight, peptide fraction and valency, this technique can be used to characterize physical characteristics of the conjugates, such as radius of gyration and shape. Improved characterization of these complex molecules will lead to a greater understanding of cell-ligand interactions, especially in terms of multivalency, receptor clustering, and receptor-ligand dynamics. Because of the efficiency of this method, both in terms of time and material required, it is useful both in characterization of novel materials in research where the amount of sample may be limited, as well as in quality control of commercial materials, where high throughput in necessary.

4.6. Acknowledgements

The authors would like to thank Eda Altiok for her assistance in obtaining SEC-MALS-UV-RI data.

4.7. References

1. Pollock, J. F.; Ashton, R. S.; Rode, N. A.; Schaffer, D. V.; Healy, K. E., Molecular Characterization of Multivalent Bioconjugates by Size-Exclusion Chromatography with Multiangle Laser Light Scattering. *Bioconjugate Chem* **2012,** *23* (9), 1794-1801.

2. Veronese, F. M.; Pasut, G., PEGylation, successful approach to drug delivery. *Drug Discov Today* **2005,** *10* (21), 1451-1458.

3. Kratz, F.; Muller, I. A.; Ryppa, C.; Warnecke, A., Prodrug strategies in anticancer chemotherapy. *Chemmedchem* **2008,** *3* (1), 20-53.

4. Larson, N.; Ghandehari, H., Polymeric Conjugates for Drug Delivery. *Chem Mater* **2012,** *24* (5), 840-853.

5. Ho, M. H.; Wang, D. M.; Hsieh, H. J.; Liu, H. C.; Hsien, T. Y.; Lai, J. Y.; Hou, L. T., Preparation and characterization of RGD-immobilized chitosan scaffolds. *Biomaterials* **2005,** *26* (16), 3197-3206.

6. Ito, Y., Covalently immobilized biosignal molecule materials for tissue engineering. *Soft Matter* **2008,** *4* (1), 46-56.

7. Sehgal, I.; Li, H. R.; Ongarora, B.; Devillier, D.; Vicente, M. G. H., Synthesis and biological investigations of a ZnPc-antiCEA bioconjugate for imaging of colorectal cancer. *J Porphyr Phthalocya* **2013,** *17* (1-2), 150-156.

8. Su, X.; Kuang, L.; Battle, C.; Shaner, T.; Mitchell, B. S.; Fink, M. J.; Jayawickramarajah, J., Mild Two-Step Method to Construct DNA-Conjugated Silicon Nanoparticles: Scaffolds for the Detection of MicroRNA-21. *Bioconjug Chem* **2014**.

9. Elbert, D. L.; Hubbell, J. A., Conjugate addition reactions combined with free-radical cross-linking for the design of materials for tissue engineering. *Biomacromolecules* **2001,** *2* (2), 430-441.

10. Drumheller, P. D.; Elbert, D. L.; Hubbell, J. A., Multifunctional Poly(Ethylene Glycol) Semiinterpenetrating Polymer Networks as Highly Selective Adhesive Substrates for Bioadhesive Peptide Grafting. *Biotechnol Bioeng* **1994,** *43* (8), 772-780.

11. Stile, R. A.; Healy, K. E., Thermo-responsive peptide-modified hydrogels for tissue regeneration. *Biomacromolecules* **2001,** *2* (1), 185-194.

12. Murphy, A. J.; Funt, S.; Gorman, D.; Tall, A. R.; Wang, N., Pegylation of High-Density Lipoprotein Decreases Plasma Clearance and Enhances Antiatherogenic Activity. *Circ Res* **2013,** *113* (1), e1-e9.

13. Lankveld, D. P. K.; Rayavarapu, R. G.; Krystek, P.; Oomen, A. G.; Verharen, H. W.; van Leeuwen, T. G.; De Jong, W. H.; Manohar, S., Blood clearance and tissue distribution of PEGylated and non-PEGylated gold nanorods after intravenous administration in rats. *Nanomedicine-Uk* **2011,** *6* (2), 339-349.

14. Bhattarai, N.; Gunn, J.; Zhang, M. Q., Chitosan-based hydrogels for controlled, localized drug delivery. *Adv Drug Deliver Rev* **2010,** *62* (1), 83-99.

15. Wall, S. T.; Saha, K.; Ashton, R. S.; Kam, K. R.; Schaffer, D. V.; Healy, K. E., Multivalency of Sonic hedgehog conjugated to linear polymer chains modulates protein potency. *Bioconjugate Chem* **2008,** *19* (4), 806-812.

16. Xu, X.; Jha, A. K.; Duncan, R. L.; Jia, X. Q., Heparin-decorated, hyaluronic acid-based hydrogel particles for the controlled release of bone morphogenetic protein 2. *Acta Biomater* **2011,** *7* (8), 3050-3059.

17. Lam, J.; Truong, N. F.; Segura, T., Design of cell-matrix interactions in hyaluronic acid hydrogel scaffolds. *Acta Biomater* **2014,** *10* (4), 1571-1580.

18. Sacchettini, J. C.; Baum, L. G.; Brewer, C. F., Multivalent protein-carbohydrate interactions. A new paradigm for supermolecular assembly and signal transduction. *Biochemistry-Us* **2001,** *40* (10), 3009-3015.

19. Kiessling, L. L.; Gestwicki, J. E.; Strong, L. E., Synthetic multivalent ligands in the exploration of cell-surface interactions. *Curr Opin Chem Biol* **2000,** *4* (6), 696-703.

20. Schamel, W. W. A.; Reth, M., Clustering Models. *Adv Exp Med Biol* **2008,** *640*, 64-73.

21. Bi, X. D.; Shi, X. Y.; Baker, J. R., Synthesis, characterization and stability of a luteinizing hormone-releasing hormone (LHRH)-functionalized poly(amidoamine) dendrimer conjugate. *J Biomat Sci-Polym E* **2008,** *19* (1), 131-142.

22. Mi, F. L., Synthesis and characterization of a novel chitosan-gelatin bioconjugate with fluorescence emission. *Biomacromolecules* **2005,** *6* (2), 975-987.

23. Oh, E. J.; Park, K.; Choi, J. S.; Joo, C. K.; Hahn, S. K., Synthesis, characterization, and preliminary assessment of anti-Flt1 peptide-hyaluronate conjugate for the treatment of corneal neovascularization. *Biomaterials* **2009,** *30* (30), 6026-6034.

24. Sasaki, Y.; Uzuki, M.; Nohmi, K.; Kitagawa, H.; Kamataki, A.; Komagamine, M.; Murakami, K.; Sawai, T., Quantitative measurement of serum hyaluronic acid molecular weight in rheumatoid arthritis patients and the role of hyaluronidase. *Int J Rheum Dis* **2011,** *14* (4), 313-319.

25. Wen, J.; Arakawa, T.; Philo, J. S., Size-exclusion chromatography with on-line light-scattering, absorbance, and refractive index detectors for studying proteins and their interactions. *Anal Biochem* **1996,** *240* (2), 155-166.

26. Kendrick, B. S.; Kerwin, B. A.; Chang, B. S.; Philo, J. S., Online size-exclusion high-performance liquid chromatography light scattering and differential refractometry methods to determine degree of polymer conjugation to proteins and protein-protein or protein-ligand association states. *Anal Biochem* **2001,** *299* (2), 136-146.

27. Harbers, G. M.; Healy, K. E., The effect of ligand type and density on osteoblast adhesion, proliferation, and matrix mineralization. *J Biomed Mater Res A* **2005,** *75A* (4), 855-869.

28. Zhao, H. Y.; Brown, P. H.; Schuckt, P., On the Distribution of Protein Refractive Index Increments. *Biophys J* **2011,** *100* (9), 2309-2317.

29. Balazs, E. A.; Watson, D.; Duff, I. F.; Roseman, S., Hyaluronic Acid in Synovial Fluid .I. Molecular Parameters of Hyaluronic Acid in Normal and Arthritic Human Fluids. *Arthritis Rheum* **1967,** *10* (4), 357-&.

30. Rezania, A.; Healy, K. E., The effect of peptide surface density on mineralization of a matrix deposited by osteogenic cells. *J Biomed Mater Res* **2000,** *52* (4), 595-600.

31. Shachar, M.; Tsur-Gang, O.; Dvir, T.; Leor, J.; Cohen, S., The effect of immobilized RGD peptide in alginate scaffolds on cardiac tissue engineering. *Acta Biomater* **2011,** *7* (1), 152-162.

4.8. Tables

Table 4.1. Measured constants of bioconjugate components. Starred values were too low to measure directly on the SEC-MALS-UV-RI system and are taken from previous studies, where they were measured using a spectrophotometer[1].

Component	Specific Refractive Index Increment dn/dc (mL g^{-1})	UV Extinction Coefficient (mL mg^{-1} cm^{-1})	Molecular Weight
Hyaluronic Acid	0.160	0.022*	600 kDa (initial)
Activated Hyaluronic Acid	0.144	0.022*	600 kDa (initial)
bsp-RGD(15)	0.185	1.84	1,657 Da

4.9. Figures

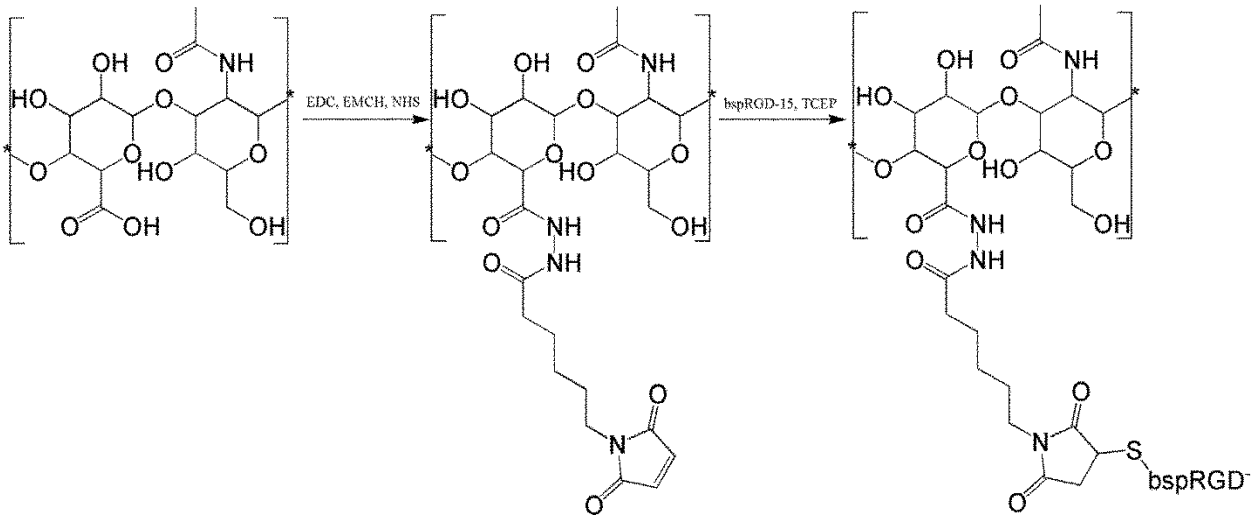

Figure 4.1. Conjugation scheme of bsp-RGD(15) peptide to hyaluronic acid.

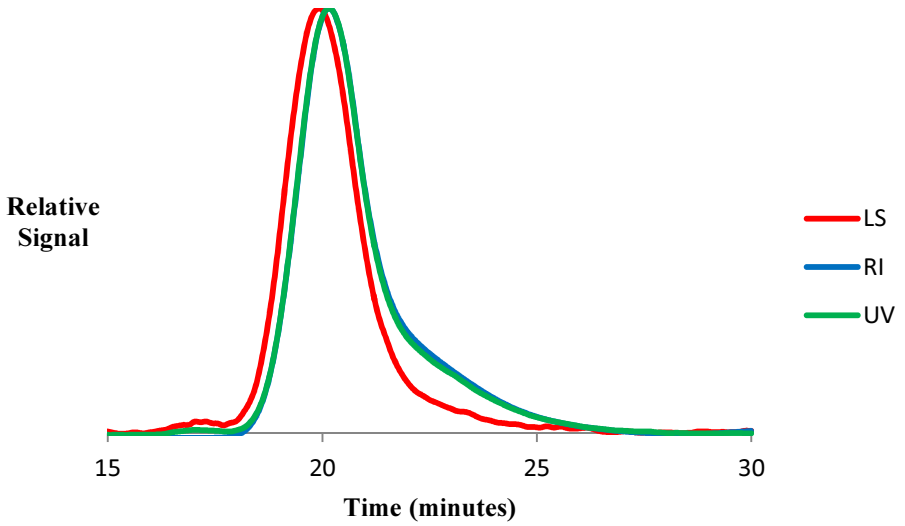

Figure 4.2. Example chromatogram for SEC-MALS-UV-RI analysis of peptide-HyA conjugates. The light scattering signal is presented in red, the differential refractive index in blue, and the UV absorbance in green. For illustrative purposes, the intensity of the signals has been normalized.

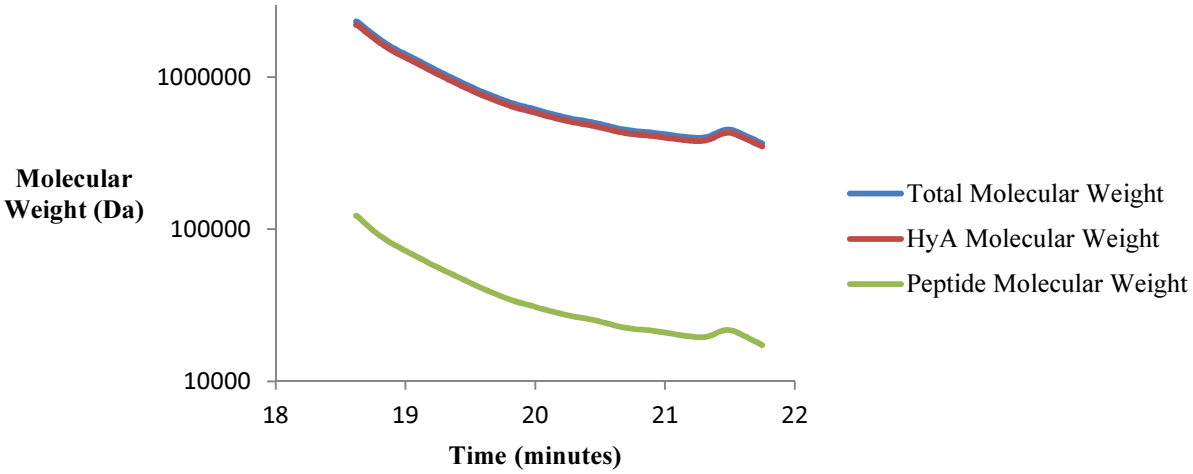

Figure 4.3. Measured molecular weight of conjugates with SEC-MALS analysis as a function of elution time.

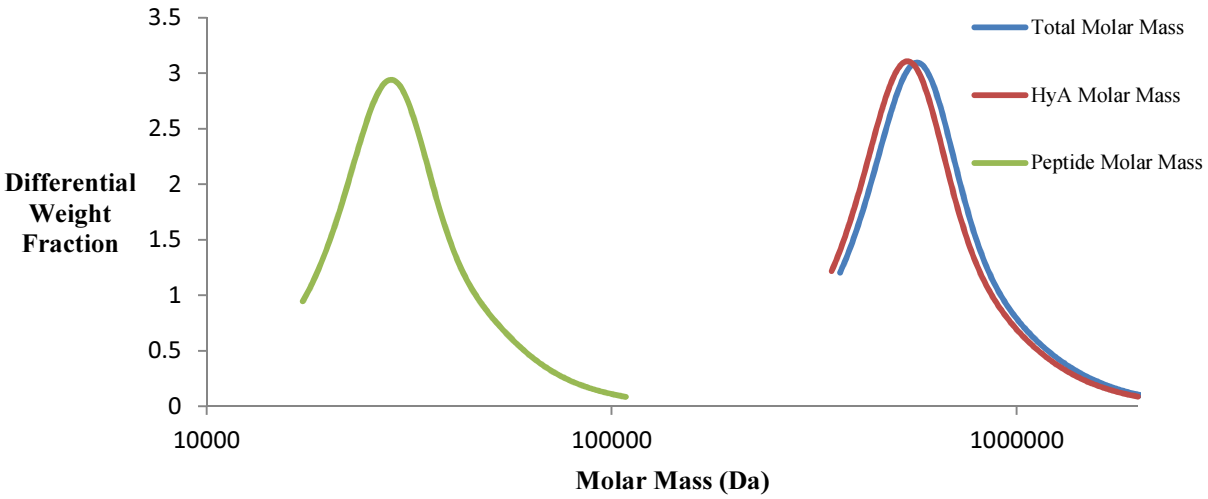

Figure 4.4. Differential weight fraction of peptide-HyA conjugates as measured by SEC-MALS.

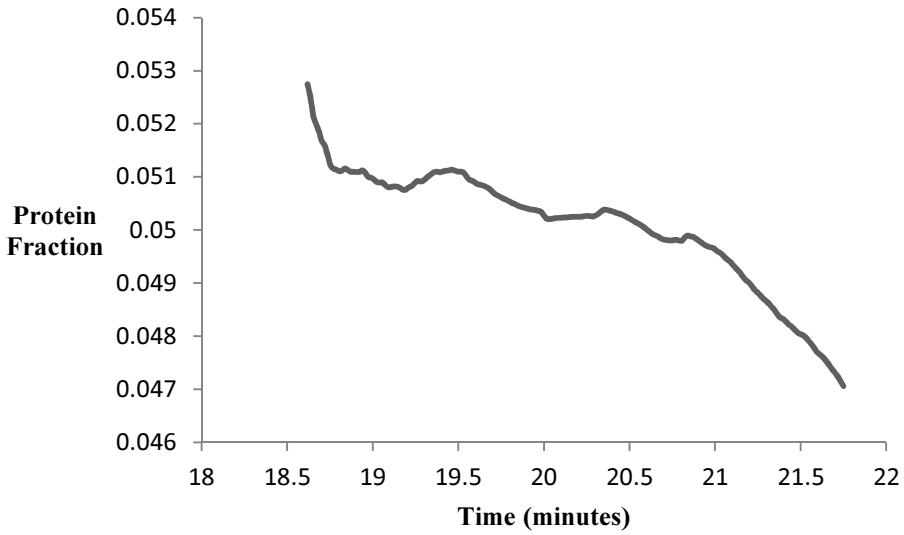

Figure 4.5. Protein fraction of peptide-HyA conjugates as a function of elution time.

Chapter 5

Electrospinning and structural characterization of semi-interpenetrating hydrogel networks (sIPNs) containing multivalent conjugates of peptides on hyaluronic acid

5.1. Abstract

When designing a material for use as an *ex vivo* tissue scaffold, it is important to take into account the chemical, mechanical and topographical signals that the material will be providing to the cells. Traditional hydrogel materials are capable of providing a controlled chemical and mechanical environment, but lack control over nanotopography. In this study, electrospinning was used to generate a hydrogel with controlled nanofibrous topography, to recapitulate the natural structure of the extracellular matrix (**ECM**). Processing parameters were explored to ensure the generation of defect-free electrospun fibers. Scanning electron microscopy was used to assess the morphology of the fibers and to quantify their diameters and orientation. By controlling the concentration of poly(ethylene glycol) diacrylate (**pEGDA**) present in the electrospinning solution, the distribution of diameters in the electrospun material was made to resemble that of collagen fibers in the native ECM. These fibers were aligned through the use of a rapidly rotating barrel or disk as the electrospinning collector. In this way, alignment of over 80% of the fibers to a 10^{o} window was achieved. Use of this method for the generation of nanotopographically controlled hydrogels will provide a customizable platform for use as a tissue scaffold for both *in vitro* and *in vivo* applications.

5.2. Introduction

Tissue scaffolds *in vitro* or *in vivo* must recapitulate as many of the signals the natural extracellular matrix provides to cells as is possible. In particular, biochemical signals such as cell-binding proteins or growth factors, mechanical signals such as material stiffness and viscoelastic response, and topographical signals such as material nanoscale organization must be addressed[1].

Myriad materials have been investigated as possible scaffolds for tissue engineering. Hydrogels in particular have proven to be effective[2]. Naturally derived hydrogels such as collagen or hyaluronic acid (**HyA**) readily recapitulate the chemical environment of the native ECM[3,4]. However, these natural materials suffer from problems with batch to batch variability, sourcing, and sterility[5]. Synthetic hydrogels such as polyethylene glycol or N-isopropyl acrylamide avoid many of these problems, providing repeatable and controllable systems. These gels, however, require additional modification to provide the necessary chemical and biological cues to cells. In-situ crosslinking of these hydrogels allows for three-dimensional encapsulation of cells[6], as well as injectable delivery[7]. However, there is little control over the nanostructure of hydrogel materials, limiting their use for anisotropic tissue applications.

In the body, collagen fibers in the extracellular matrix have a distribution of diameters ranging from 500 nm to 3 μm[8]. These are built of smaller collagen fibrils with diameters in the range of 10-300 nm. Nanoscale topographical cues can cause a variety of changes in cell behavior as well, influencing cellular adhesion[9], altering protein expression and differentiation[10], and causing cytoskeletal alignment[11]. Special attention must be paid to the physical cues when designing scaffolds for tissues with structural or mechanical roles.

Electrospinning has emerged as a versatile, inexpensive, and scalable method to create materials that that provide nanostructural control over tissue scaffold materials[12,13,14]. The technique involves the charging of a polymer solution at high voltage. The accumulation of charge at the solution surface results in the formation of a Taylor cone and the ejection of a jet of material toward a grounded or oppositely charged target. Over the flight of this jet, the solvent evaporates, resulting in the deposition of solid polymer nanofibers. This process is diagrammed in Figure 5.1. The number of polymers that have been successfully electrospun for use in tissue engineering or regenerative medicine applications is currently limited. The most widely used are polyesters and polyurethanes[15]. Matrices consisting of either aligned or non-aligned fibers with nanoscale diameters for use as cell scaffolds have been created for the regeneration of several tissue types, including neural[16], vascular[17], ligament[18], bone[19], muscular[20], and cardiac tissues[21,22]. Although these electrospun materials provide physical support and topographical cues to cells, they do not faithfully recreate the chemical and biological extracellular environment deemed necessary for optimal cell-materials interactions and tissue regeneration.

Natural materials such as collagen[23,24], gelatin[11,25] and elastin[26] have also been used in electrospinning systems as one strategy of providing relevant chemical signals to cells. . This approach is restricted to a limited set of biomolecules that are compatible with the electrospinning methodology. Electrospinning generally uses organic solvents, which run the risk of damaging or denaturing proteins. Aqueous electrospinning is possible, but many proteins have limited solubility well below that necessary for electrospinning, necessitating the use of a secondary synthetic polymer acting as a carrier[27,28]. The high electric fields and large shear stress experienced by polymers during the electrospinning process also run the risk of altering protein morphology and thus function[24]. For this study we have chosen HyA, as it provides an easily modifiable backbone from which to present pendant biological motifs like peptides, and will not cause an unwanted immune response[29]. However, HyA on its own is difficult to electrospin due to its high viscosity and surface tension[30], so a high molecular weight poly(ethylene glycol) (**pEG**) carrier polymer was required to achieve electrospinning of HyA.

In order to fully realize the potential of electrospun materials as tissue scaffolds, it is necessary to devise a method of tuning the biological signaling component independently of the electrospinning process. To accomplish this, we have created a material combining the use of electrospinning to control the morphology of the material with multivalent peptide conjugates embedded in the electrospun fibers to control their biochemical environment. The use of multivalent conjugates provides four significant improvements over previously developed materials: control over the biological signals presented to cells in an electrospun matrix; improved peptide potency through multivalent interactions with cell surface receptors[31]; control over the amount of peptide presented independent of substrate modulus; and, the capacity to present multiple peptides simultaneously.

5.3. Materials and methods

Hyaluronic acid sodium salts (HyA) of 600 kDa molecular weight were obtained from Genzyme. Various polyethylene glycol (pEG) polymers of 200 kDa, 400 kDa, 600 kDa, 1 MDa, and 2MDa molecular weight were purchased from Sigma-Aldrich. Polyethylene glycol diacrylate (pEGDA) of 200 Da molecular weight was obtained from Polysciences. The photoinitiator Irgacure 2959 was purchased from BASF.

5.3.1. Preparation of electrospinning solutions

For the generation of the electrospinning phase diagram, aqueous solutions of polyethylene glycol (pEG) of differing molecular weights and concentrations were mixed and allowed to sit for 48 hours at room temperature to achieve full homogenization. 200 kDa, 400 kDa, 600 kDa, 1 MDa and 2 MDa PEG were prepared at concentrations of 10-20 wt%, 5-12 wt%, 3-8 wt%, 1.5-6 wt% and 1-3.25 wt% respectively. To examine the effect of hyaluronic acid on the phase diagram, 0.5 wt% 600 kDa HyA was added to solutions containing 200 kDa pEG at 4-10 wt%, 600 kDa pEG at 1-4 wt% and 1 MDa pEG at 0.75-3.75 wt%.

For all other analysis, an aqueous solution containing 1 MDa pEG at 3 wt%, 0.5 wt% 600 kDa peptide conjugated HyA, 1-5 v% pEGDA and 3 mg/mL Irgacure 2959 was mixed and allowed to sit at room temperature for 48 hours to achieve full homogenization.

5.3.2. Electrospinning of hydrogels

The electrospinning process was carried out on a custom electrospinning apparatus. The solutions were loaded into a 3 mL plastic syringe (Becton-Dickinson). These solutions were delivered to a 22g needle through a length of 1/16" inner diameter polyvinyl chloride tubing (McMaster Carr) by a syringe pump (Chemyx) at 0.1 mL/h. A rotating barrel or disk was used as a collector (NaBond). For unaligned fibers, a 20 mm diameter mandrel rotating at 1000 rpm was used at the target. For aligned fibers, either a 75 mm diameter barrel or 140 mm diameter disk rotating at 5000 rpm was used as the collector. These three electrospinning targets are pictured in Figure 5.2. The needle was charged to +10.5 kV, and the collector was charged to -1.5 kV using a high voltage power supply (Gamma High Voltage).

After electrospinning, the fibers were exposed to 365 nm UV light at 7 mW/cm^2 for 90 s to initiate crosslinking. Uncrosslinked or suboptimally crosslinked fibers immediately dissolved when exposed to aqueous media, but crosslinked fibers were stable for extended periods, as shown in Figure 5.3. After fabrication, the materials were stored at -20^{o}C until used.

5.3.3. Construction of electrospinning phase diagram

The electrospun fibers were imaged using a TM-1000 tabletop scanning electron microscope (Hitachi) with an accelerating voltage of 15 kV. For construction of the phase diagram, each image was visually classified as having the "beads", "beads on a string", or "fiber" morphology. Samples consisting of isolated spherical or near spherical polymer particles with diameters in the micron range were labeled as "beads". Samples in which these particles were connected by thinner fibers with diameters of hundreds of nanometers were designated as "beads on a string". Samples showing defect-free fibers with no bead formation were labeled as "fibers". For a given molecular weight of pEG, the highest concentration at which "beads" were found and the lowest molecular weight at which "fibers" were found were used as the boundaries for the phase transitions.

5.3.4. Analysis of electrospun fiber morphology

The morphology of the electrospun fibers was assessed using a TM-1000 tabletop scanning electron microscope (Hitachi). For each condition, two electrospun samples were fabricated. Three regions of each electrospun mat were chosen at random and imaged at various

magnifications at three different locations. From these images, fibers were chosen at random and the diameter of these fibers was measured manually in ImageJ (NIH). A total of one hundred fibers were measured for each condition to determine the distribution of diameters present in the material.

The OrientationJ plugin for ImageJ (Biomedical Image Group, EPFL) was used to quantify the degree of fiber alignment. Three SEM images each from unaligned fiber mats, mats aligned with the spinning barrel, and mats from the spinning disk were analyzed. The total distributions for these conditions were summated, defining the angle of highest predominance as 0^o in for each individual image.

5.4. Results and discussion

5.4.1. Electrospinning phase diagram of poly(ethylene glycol)/hyaluronic acid solutions

At low concentrations and molecular weights, polymer beads were deposited rather than fibers. As the polymer molecular weight and concentration were increased, the morphology progressed from beads to beads on a string and finally to well-formed fibers (Figure 5.4a). The transitions between these three morphologies were abrupt and well defined, which enabled the construction of a phase diagram mapping the transition concentrations and molecular weights (Figure 5.4b). A power curve was fit to these points to create the apparent boundary between phases.

The physics behind the transitions between the phases is complex and relies on many different parameters, such as solution surface tension, needle to target distance, and polymer concentration. As the polymer solution travels from the needle to the target, the solvent evaporates, depositing dry material. During this process, electrostatic repulsion drives the formation of thin fibers, while surface tension favors the formation of spherical droplets. Given enough time between the ejection of material from the needle and the full solidification of the fiber, the material will tend to form beads. High surface tension will drive bead formation more strongly, and a longer needle to target distance will allow more time for the process to take place. A low polymer concentration requires the evaporation of more solvent, increasing the time needed for full solidification of the fibers and increasing bead formation. In this way, phase diagrams for electrospinning are highly dependent on the configuration of the apparatus and processing and solution parameters, and therefore are not a fundamental thermodynamic or materials property.

For a fixed tip-target distance the addition of 0.5 wt% HyA decreased the concentration necessary to achieve fiber formation in all conditions (Figure 5.4c). This change in electrospinning properties was due to effects of the polar high molecular weight HyA on solution conductivity, surface tension, and viscosity, even at low concentrations. In particular, small amounts of HyA are capable of lowering the surface tension of deionized water, forming smaller fibers and reducing bead formation[32].

These phase diagrams were used to choose polymer concentrations and apparatus configurations to generate nanofiber scaffolds for cell culture that included the multivalent peptide HyA in the system. In order to maximize the presence of the bioactive HyA in the fibers

relative to the biologically inert pEG, a minimal concentration of pEG capable of spinning well-formed fibers(i.e., 3 wt% 1 MDa PEG) was chosen.

5.4.2. Distribution of fiber diameters

For electrospinning conditions tested within the "fiber" region of the phase diagram, no significant change in fiber morphology or diameter was seen with changes in polymer concentration or molecular weight. Analysis of the fiber diameters showed a distribution with an average diameter of 306.2±70.5 nm when no pEGDA was present. The distribution of fiber diameters is shown in Figure 5.5.

Upon addition of pEGDA to the electrospinning solution, two significant changes to the resulting fiber morphology were observed. First, the average fiber diameter increased with increasing amounts of pEGDA. Second, the width of the distribution of diameters increased with increasing pEGDA concentration. For 1 v% pEGDA, the average fiber diameter was 336±134 nm, and for 5 v% pEGDA the average diameter was 538±262 nm. This difference in fiber diameters is shown in Figure 5.6. Fiber diameters were measured in the dry state. The hydrogel fibers are expected to swell when placed in an aqueous environment, but not to a large degree due to the small mesh size in the pEGDA matrix.

The increase in the diameter of the electrospun fibers can be accounted for by considering the pEGDA as an additional, non-evaporative inclusion in the electrospinning process. The fraction of material in the original solution that remains within the fibers during the electrospinning process is increased. In order to accommodate this extra material, the final diameter of the fiber increases. The additional widening of the distribution can be accounted for by the fact that the pEGDA is not solid at room temperature, which can result in flowing and fusion of the fibers before they can be crosslinked, creating thicker and less uniform fibers.

5.4.3. Degree of alignment of electrospun fibers

A surface speed of 10 m/s has been reported to be sufficient to induce significant alignment of electrospun fibers via rotation of the target[33]. Three target speeds and diameters were tested: a 20 mm mandrel rotating at 1000 rpm, a 76 mm barrel rotating at 5000 rpm, and a 140 mm disk rotating at 5000 rpm. These three conditions represent a target surface rotational speed of 1 m/s, 19.9 m/s, and 36.6 m/s, and will be referred to as "unaligned", "barrel", and "disk", respectively.

Fibers spun under the "unaligned" conditions showed a small amount of alignment over a theoretical completely unaligned material, in which you would expect 5.6%, 11.1%, and 16.7% of the fibers to be aligned within a 5^{o}, 10^{o}, and 15^{o} window of the predominant axis, respectively. For the "unaligned" conditions, 10.3%, 18.9%, and 27.1% were found to be aligned within these three windows. This small amount of alignment can be accounted for in two ways. First, the slow rotation of the mandrel can be expected to provide minimal alignment of the fibers. Second, the sampling and measuring process magnifies small anisotropies in the distribution of alignments. To generate a large enough sample size, several samples were imaged. As maintaining a baseline alignment of the sample during imaging was difficult, the predominant angle present in any given image was defined as 0^{o}. Thus, the measured alignment in these samples will err toward

increasing the degree of fiber alignment. For highly aligned samples in which a predominant angle is easily identifiable, this effect is minimal.

Fibers spun under both the "barrel" and "blade" conditions showed a much higher degree of alignment, compared to the "unaligned" fibers. A representative set of SEM and false color images demonstrating the induction of alignment is shown in Figure 5.7. The quantitative distribution of fiber diameters is shown in Figure 5.8. For the "barrel" condition, 52.4%, 82.7%, and 94.3% of the fibers were oriented within 5^{o}, 10^{o}, and 15^{o} of the main axis, respectively. For the "disk" configuration, these numbers were further increased to 60.8%, 86.4%, and 95%, respectively. These values are presented in Table 5.1.

5.5. Conclusions

We created a novel nanofiber material via specific biological activity programmed into electrospun hydrogel fibers. This material is capable of mimicking the mechanical and topographical environment of the native ECM. By tailoring the electrospinning processing parameters, we can generate defect-free hydrogel nanofibers that are embedded with a multivalent peptide-hyaluronic acid conjugate. Exposure of the electrospun material to UV illumination post-spinning initiates photocrosslinking in the dry state, rendering the fibers insoluble and preserving their structure when submerged in aqueous media. The distribution of diameters present in the electrospun mats is within the range of diameters seen in the fibers in the natural extracellular matrix and can be altered by changing the concentration of poly(ethylene glycol) diacrylate in the electrospinning solution. By controlling the surface speed of the rotating target used, alignment of the hydrogel fibers can be achieved, further mimicking the microstructure seen in anisotropic tissues *in vivo*. This processing methodology provides a strong base from which tissue- and cell type-specific scaffolds can be generated by controlling the identity and quantity of peptide presented by a topographically controlled hydrogel material.

5.6. Acknowledgements

The authors would like to thank Riley Reese and Albert Lin for their work in elucidating the electrospinning phase diagram of the pEG and pEG-HyA systems, and the mechanisms at work therein.

5.7. References

1. Singelyn, J. M.; DeQuach, J. A.; Seif-Naraghi, S. B.; Littlefield, R. B.; Schup-Magoffin, P. J.; Christman, K. L., Naturally derived myocardial matrix as an injectable scaffold for cardiac tissue engineering. *Biomaterials* **2009,** *30* (29), 5409-5416.

2. Zhu, J. M., Bioactive modification of poly(ethylene glycol) hydrogels for tissue engineering. *Biomaterials* **2010,** *31* (17), 4639-4656.

3. Parenteau-Bareil, R.; Gauvin, R.; Berthod, F., Collagen-Based Biomaterials for Tissue Engineering Applications. *Materials* **2010,** *3* (3), 1863-1887.

4. Kim, I. L.; Mauck, R. L.; Burdick, J. A., Hydrogel design for cartilage tissue engineering: A case study with hyaluronic acid. *Biomaterials* **2011,** *32* (34), 8771-8782.

5. Kim, B. S.; Mooney, D. J., Development of biocompatible synthetic extracellular matrices for tissue engineering. *Trends Biotechnol* **1998,** *16* (5), 224-230.

6. Klouda, L.; Perkins, K. R.; Watson, B. M.; Hacker, M. C.; Bryant, S. J.; Raphael, R. M.; Kasper, F. K.; Mikos, A. G., Thermoresponsive, in situ cross-linkable hydrogels based on N-isopropylacrylamide: Fabrication, characterization and mesenchymal stem cell encapsulation. *Acta Biomater* **2011,** *7* (4), 1460-1467.

7. Wu, J.; Zeng, F. Q.; Huang, X. P.; Chung, J. C. Y.; Konecny, F.; Weisel, R. D.; Li, R. K., Infarct stabilization and cardiac repair with a VEGF-conjugated, injectable hydrogel. *Biomaterials* **2011,** *32* (2), 579-586.

8. Temenoff, J. S.; Mikos, A. G., *Biomaterials : the Intersection of biology and materials science*. Pearson/Prentice Hall: Upper Saddle River, N.J., 2008; p xxiv, 478 p.

9. Koo, L. Y.; Irvine, D. J.; Mayes, A. M.; Lauffenburger, D. A.; Griffith, L. G., Co-regulation of cell adhesion by nanoscale RGD organization and mechanical stimulus. *J Cell Sci* **2002,** *115* (7), 1423-1433.

10. Dalby, M. J.; Gadegaard, N.; Tare, R.; Andar, A.; Riehle, M. O.; Herzyk, P.; Wilkinson, C. D. W.; Oreffo, R. O. C., The control of human mesenchymal cell differentiation using nanoscale symmetry and disorder. *Nat Mater* **2007,** *6* (12), 997-1003.

11. Kai, D.; Prabhakaran, M. P.; Jin, G. R.; Ramakrishna, S., Guided orientation of cardiomyocytes on electrospun aligned nanofibers for cardiac tissue engineering. *J Biomed Mater Res B* **2011,** *98B* (2), 379-386.

12. Orlova, Y.; Magome, N.; Liu, L.; Chen, Y.; Agladze, K., Electrospun nanofibers as a tool for architecture control in engineered cardiac tissue. *Biomaterials* **2011,** *32* (24), 5615-5624.

13. Heydarkhan-Hagvall, S.; Schenke-Layland, K.; Dhanasopon, A. P.; Rofail, F.; Smith, H.; Wu, B. M.; Shemin, R.; Beygui, R. E.; MacLellan, W. R., Three-dimensional electrospun ECM-based hybrid scaffolds for cardiovascular tissue engineering. *Biomaterials* **2008,** *29* (19), 2907-2914.

14. Vasita, R.; Katti, D. S., Nanofibers and their applications in tissue engineering. *Int J Nanomed* **2006,** *1* (1), 15-30.

15. Chen, Q. Z.; Ishii, H.; Thouas, G. A.; Lyon, A. R.; Wright, J. S.; Blaker, J. J.; Chrzanowski, W.; Boccaccini, A. R.; Ali, N. N.; Knowles, J. C.; Harding, S. E., An elastomeric patch derived from poly(glycerol sebacate) for delivery of embryonic stem cells to the heart. *Biomaterials* **2010,** *31* (14), 3885-3893.

16. Yang, F.; Murugan, R.; Wang, S.; Ramakrishna, S., Electrospinning of nano/micro scale poly(L-lactic acid) aligned fibers and their potential in neural tissue engineering. *Biomaterials* **2005,** *26* (15), 2603-2610.

17. Stitzel, J.; Liu, L.; Lee, S. J.; Komura, M.; Berry, J.; Soker, S.; Lim, G.; Van Dyke, M.; Czerw, R.; Yoo, J. J.; Atala, A., Controlled fabrication of a biological vascular substitute. *Biomaterials* **2006,** *27* (7), 1088-1094.

18. Sahoo, S.; Toh, S. L.; Goh, J. C. H., A bFGF-releasing silk/PLGA-based biohybrid scaffold for ligament/tendon tissue engineering using mesenchymal progenitor cells. *Biomaterials* **2010,** *31* (11), 2990-2998.

19. Yoshimoto, H.; Shin, Y. M.; Terai, H.; Vacanti, J. P., A biodegradable nanofiber scaffold by electrospinning and its potential for bone tissue engineering. *Biomaterials* **2003,** *24* (12), 2077-2082.

20. Riboldi, S. A.; Sampaolesi, M.; Neuenschwander, P.; Cossu, G.; Mantero, S., Electrospun degradable polyesterurethane membranes: potential scaffolds for skeletal muscle tissue engineering. *Biomaterials* **2005,** *26* (22), 4606-4615.

21. Shin, M.; Ishii, O.; Sueda, T.; Vacanti, J. P., Contractile cardiac grafts using a novel nanofibrous mesh. *Biomaterials* **2004,** *25* (17), 3717-3723.

22. Zong, X. H.; Bien, H.; Chung, C. Y.; Yin, L. H.; Fang, D. F.; Hsiao, B. S.; Chu, B.; Entcheva, E., Electrospun fine-textured scaffolds for heart tissue constructs. *Biomaterials* **2005,** *26* (26), 5330-5338.

23. Matthews, J. A.; Wnek, G. E.; Simpson, D. G.; Bowlin, G. L., Electrospinning of collagen nanofibers. *Biomacromolecules* **2002,** *3* (2), 232-238.

24. Dong, B.; Arnoult, O.; Smith, M. E.; Wnek, G. E., Electrospinning of Collagen Nanofiber Scaffolds from Benign Solvents. *Macromol Rapid Comm* **2009,** *30* (7), 539-542.

25. Huang, Z. M.; Zhang, Y. Z.; Ramakrishna, S.; Lim, C. T., Electrospinning and mechanical characterization of gelatin nanofibers. *Polymer* **2004,** *45* (15), 5361-5368.

26. Buttafoco, L.; Kolkman, N. G.; Engbers-Buijtenhuijs, P.; Poot, A. A.; Dijkstra, P. J.; Vermes, I.; Feijen, J., Electrospinning of collagen and elastin for tissue engineering applications. *Biomaterials* **2006,** *27* (5), 724-734.

27. Ji, Y.; Ghosh, K.; Li, B. Q.; Sokolov, J. C.; Clark, R. A. F.; Rafailovich, M. H., Dual-syringe reactive electrospinning of cross-linked hyaluronic acid hydrogel nanofibers for tissue engineering applications. *Macromol Biosci* **2006,** *6* (10), 811-817.

28. Li, L. H.; Qian, Y. N.; Jiang, C.; Lv, Y. G.; Liu, W. Q.; Zhong, L.; Cai, K. Y.; Li, S.; Yang, L., The use of hyaluronan to regulate protein adsorption and cell infiltration in nanofibrous scaffolds. *Biomaterials* **2012,** *33* (12), 3428-3445.

29. Bulpitt, P.; Aeschlimann, D., New strategy for chemical modification of hyaluronic acid: Preparation of functionalized derivatives and their use in the formation of novel biocompatible hydrogels. *J Biomed Mater Res* **1999,** *47* (2), 152-169.

30. Ji, Y.; Ghosh, K.; Shu, X. Z.; Li, B. Q.; Sokolov, J. C.; Prestwich, G. D.; Clark, R. A. F.; Rafailovich, M. H., Electrospun three-dimensional hyaluronic acid nanofibrous scaffolds. *Biomaterials* **2006,** *27* (20), 3782-3792.

31. Wall, S. T.; Saha, K.; Ashton, R. S.; Kam, K. R.; Schaffer, D. V.; Healy, K. E., Multivalency of Sonic hedgehog conjugated to linear polymer chains modulates protein potency. *Bioconjugate Chem* **2008,** *19* (4), 806-812.

32. Covici, S.; Fadel, J. R.; Mayanil, C. S. K.; Ritch, R.; Knepper, P. A., Surface-Tension Properties of Hyaluronic-Acid. *Invest Ophth Vis Sci* **1993,** *34* (4), 1202-1202.

33. Rockwood, D. N.; Akins, R. E.; Parrag, I. C.; Woodhouse, K. A.; Rabolt, J. F., Culture on electrospun polyurethane scaffolds decreases atrial natriuretic peptide expression by cardiomyocytes in vitro. *Biomaterials* **2008,** *29* (36), 4783-4791.

5.8. Tables

Table 5.1. Percentage of fibers aligned within a given angle of the predominant angle of alignment. The theoretical unaligned values represent an equal chance of a fiber lying on any axis. The small degree of alignment seen in experimentally unaligned samples can be attributed to a moderate rotational speed of the target, as well as a methodology that maximizes the degree of alignment measured.

Half-angle of alignment	Theoretical Unaligned	Experimental Unaligned	76 mm barrel	120 mm disk
5^{o}	5.5%	10.3%	52.4%	60.8%
10^{o}	11.1%	18.9%	82.7%	86.4%
15^{o}	16.7%	27.1%	94.3%	95.0%

5.9. Figures

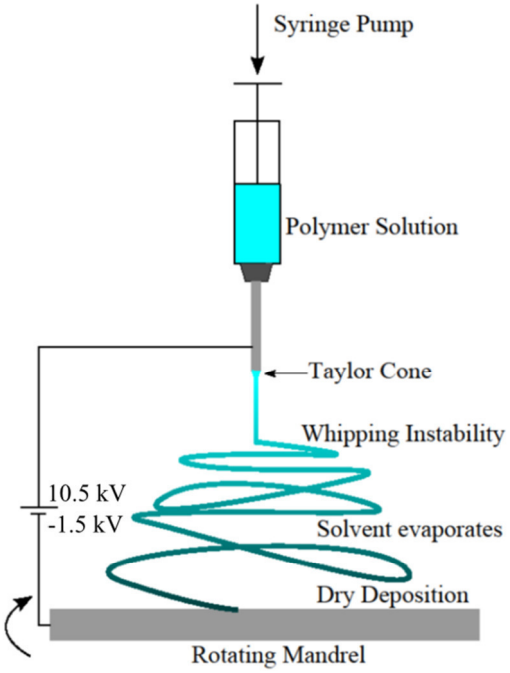

Figure 5.1. Diagram of the electrospinning procedure. Polymer solution is delivered to a charged needle tip at a steady rate by a syringe pump. The electrostatic charge causes the deformation of the droplet into a cone and the ejection of a jet of polymer solution, which accelerates toward an oppositely charged target. As the jet travels, the solvent evaporates, resulting in the deposition of dry polymer fibers.

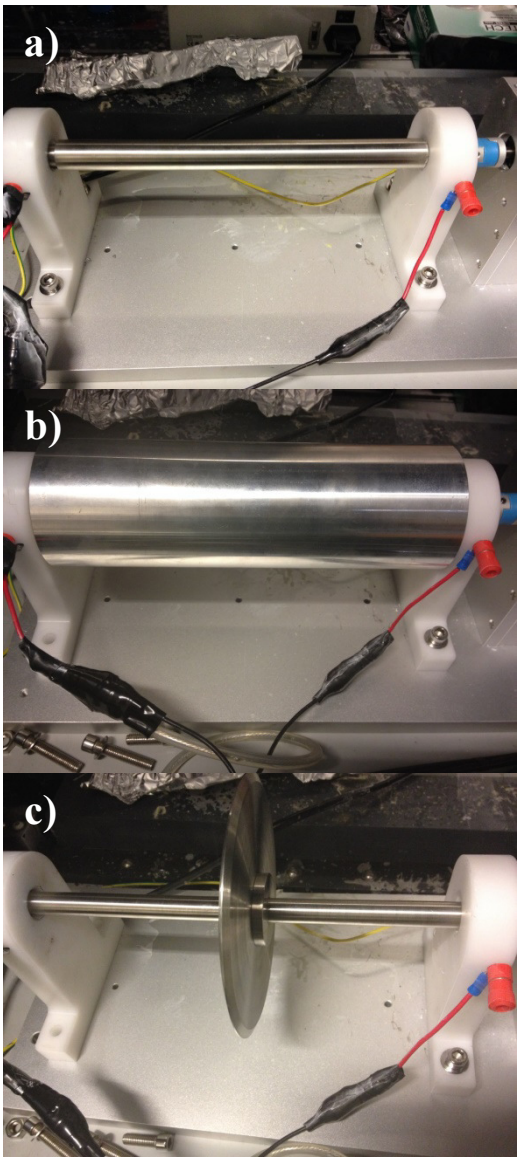

Figure 5.2. Photographs of the electrospinning targets. a) 20 mm diameter mandrel. b) 75 mm diameter barrel. c) 140 mm diameter disk.

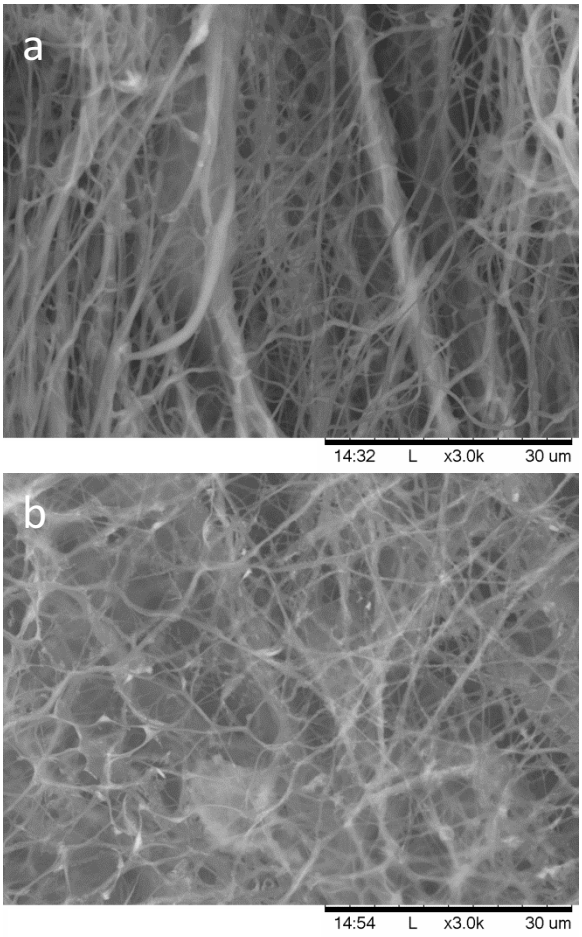

Figure 5.3. Images of crosslinked electrospun fibers a) as spun and b) after 24h in PBS at room temperature. Without UV photoinitiation of crosslinking, fibers dissolve near instantaneously when exposed to aqueous solvents.

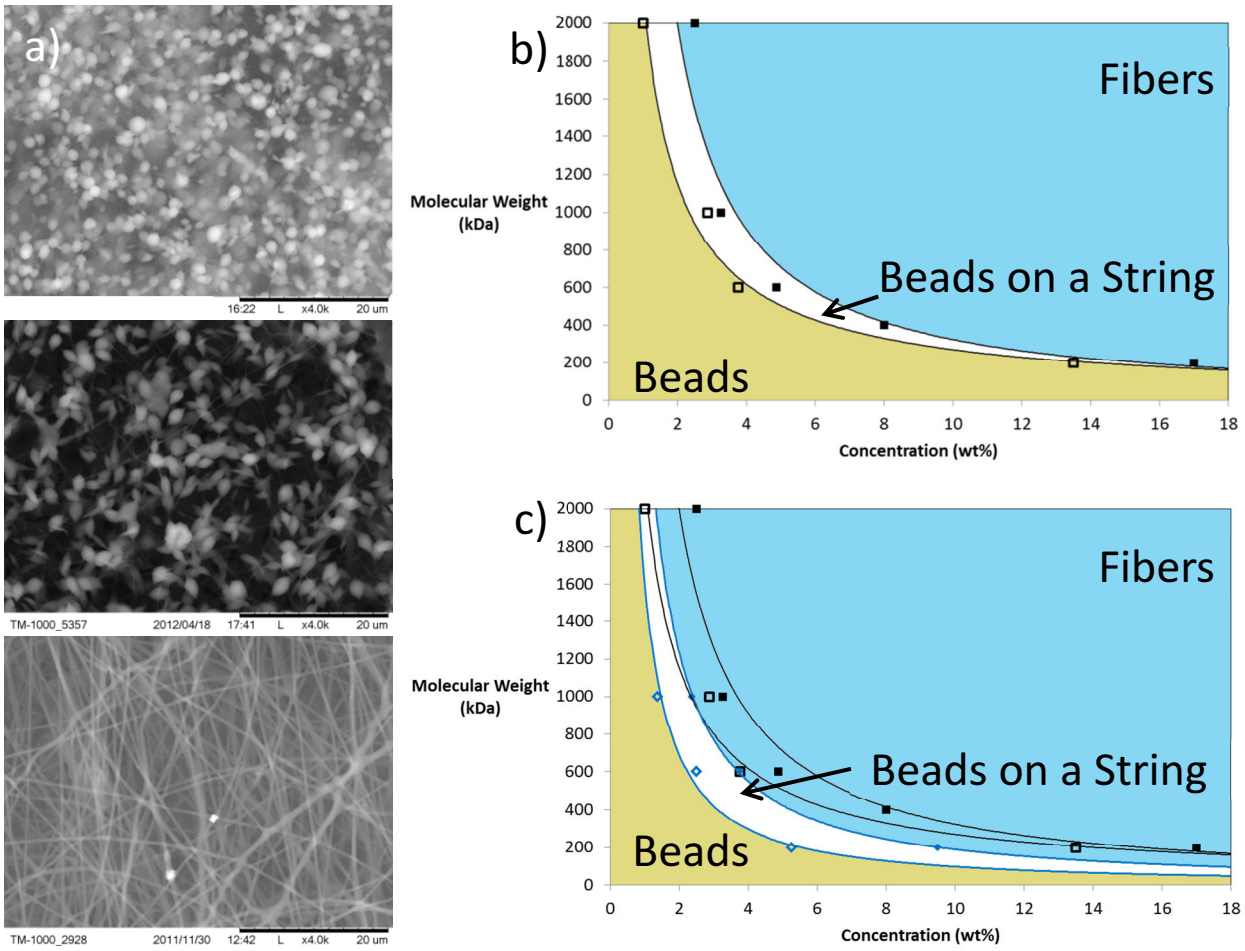

Figure 5.4. a) Representative images of the three electrospun morphologies. All images are 1 MDa pEG. From top to bottom, beads resulting from a 2 wt% solution, beads on a string from a 2.5 wt% solution and fibers from a 4 wt% solution. b) and c) Phase diagrams of the different morphologies obtained before (b) and after (c) addition of 0.5 wt% 600 kDa HyA. The solid symbols represent the lowest concentration at which unbeaded fibers were formed. The empty symbols represent the highest concentration at which only beads were formed. The fiber-forming region is colored blue and the beads region is yellow, with the beads on a string region white. In c), the phase diagram without HyA is provided in black as a reference.

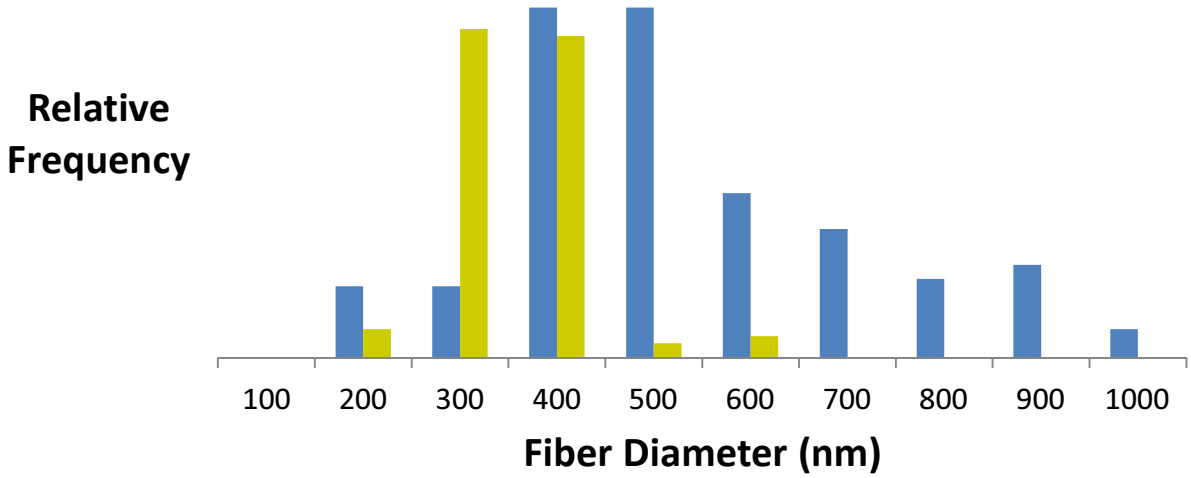

Figure 5.5. Histogram of the distribution of fiber diameters with and without the addition of PEGDA. Fibers without PEGDA are shown in gold and fibers with 5% PEGDA are shown in blue.

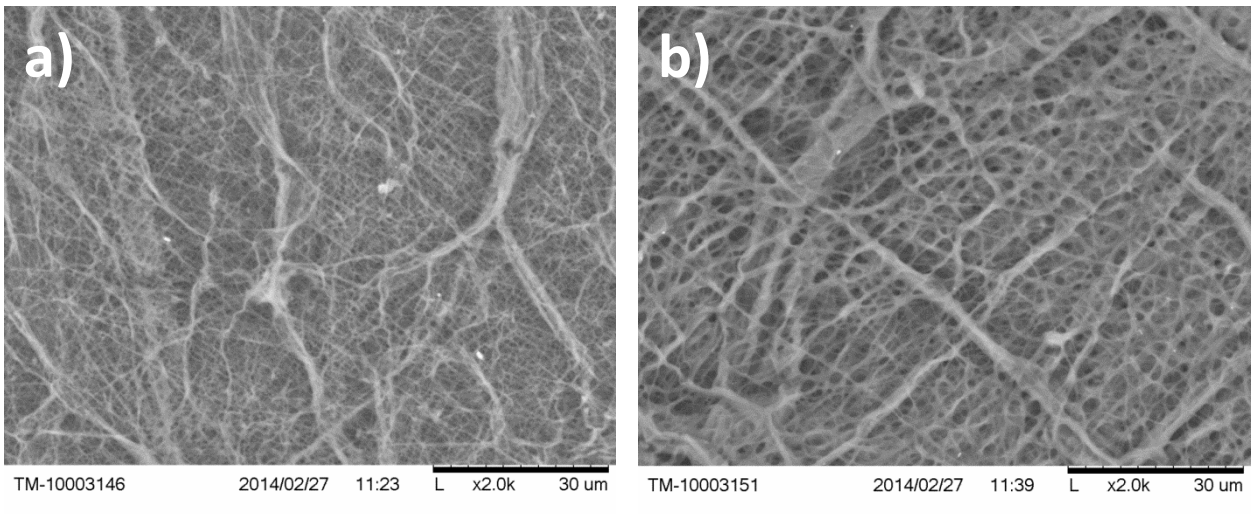

Figure 5.6. Comparison of the morphologies of electrospun fibers containing a) 1% and b) 5% PEGDA in the electrospinning solution. For the conditions in a), the average fiber diameter was 336±134 nm. For the conditions in b), the fiber diameter increased to 538±262 nm.

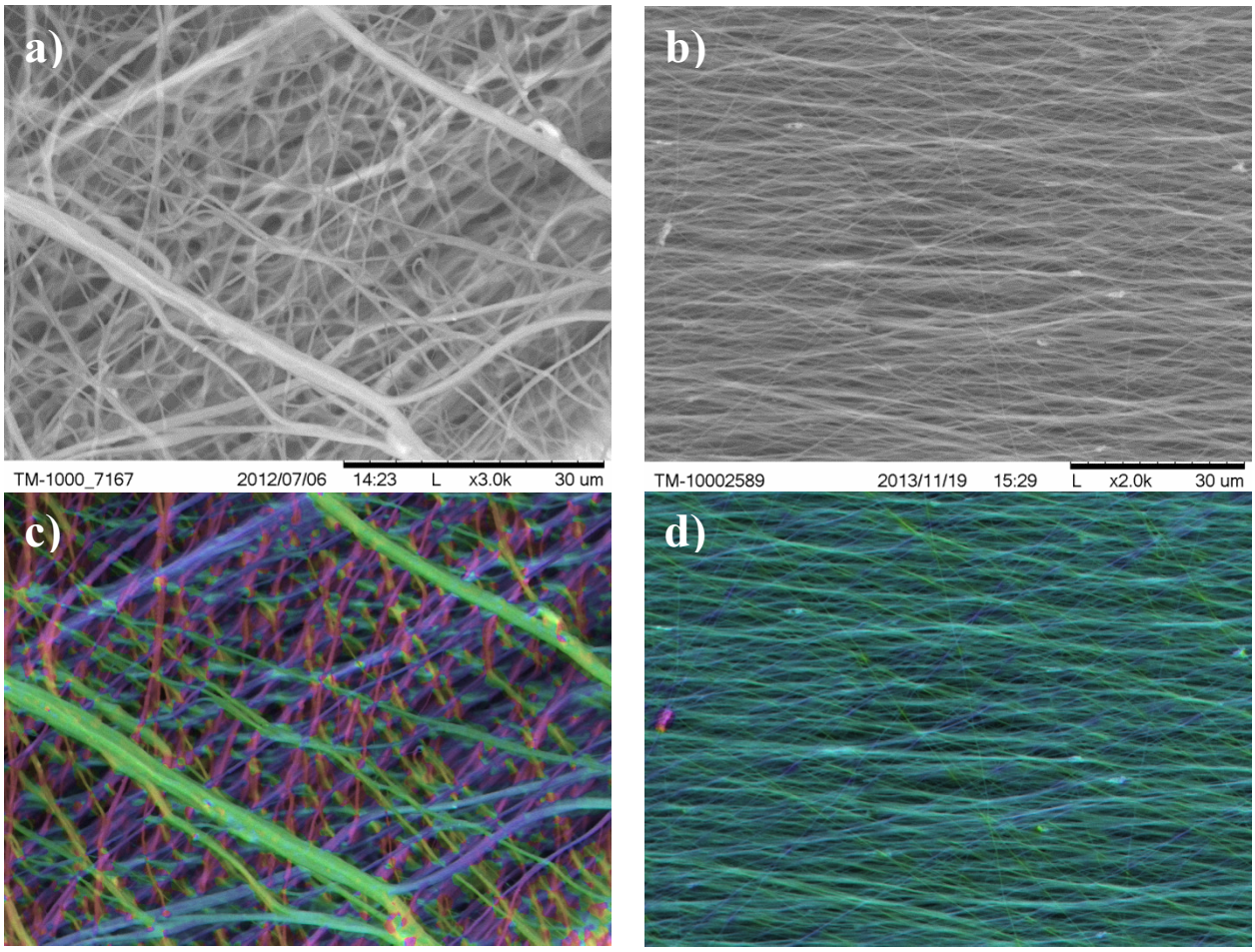

Figure 5.7. SEM images of unaligned (a, c) and aligned (b,d) electrospun fibers. a) Representative SEM image of electrospun fibers on slowly rotating mandrel. b) Representative SEM image of electrospun fibers on 140 mm disk target rotating at 5000 rpm. c,d) False colored versions of the images in a) and b) created using the OrientationJ plugin for ImageJ. The hue of the fibers in the image corresponds to their orientation, with blue fibers oriented horizontally and red fibers oriented vertically.

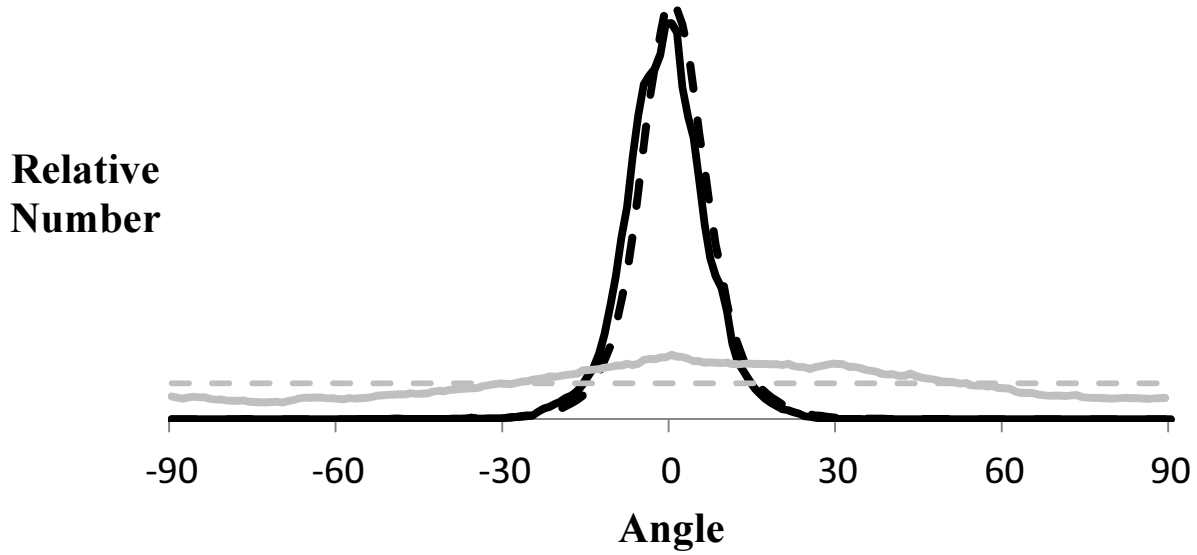

Figure 5.8. Distribution of the orientation of electrospun fibers under varying conditions. The light gray dashed line represents perfectly randomly oriented fibers. The solid gray line represents the experimentally "unaligned" fibers spun with a small mandrel rotating slowly. The solid black line represents fibers spun onto a 75 mm diameter barrel rotating at 5000 rpm and the dashed black line represents fibers spun onto a 140 mm diameter disk rotating at 5000 rpm. The degree of alignment achieved under both "aligned" conditions is comparable, and significantly more pronounced than that from the "unaligned" conditions.

Chapter 6

Physical and chemical characterization of electrospun semi-interpenetrating hydrogel networks (sIPNs) containing multivalent peptide conjugates

6.1. Abstract

A novel electrospun hydrogel material containing embedded peptide-hyaluronic acid conjugates was designed as a scaffold for tissue engineering. In this chapter I report on the physical and chemical characterization to assess its ability to serve as a synthetic extracellular matrix for tissue repair, specifically as a 'patch' for repair of myocardium. Using uniaxial tensile testing, the material's modulus was measured to be 4.3 MDa for materials spun from solutions containing 1 v% pEGDA, and 6.04 MDa for solutions containing 5 v% pEGDA. While this is higher than the modulus of the myocardial extracellular matrix, it is significantly lower than the modulus of most other electrospun materials. Alignment of the fibers caused the modulus of 1 v% pEGDA fibers measured parallel to the aligned fibers to increase to 8.35 MDa, while the modulus perpendicular to the alignment was dropped to 2.16 MDa. BET analysis measured the specific surface area of the fibrous material to be 1.1 m^2g^{-1} when 5 v% pEGDA was used, increasing to 6.1 m^2g^{-1} when 1 v% pEGDA was used. This correlates to the decreased fiber diameter for materials spun with less pEGDA (Chapter 5). The surface density of available peptides on the fiber surface was 46.5 $pmol/m^2$, as measured via cleavage by trypsin. This concentration is high enough to expect the material to be capable of supporting cell adhesion and spreading. This characterization and analysis demonstrates that this electrospun hydrogel is capable of mimicking the structure of the extracellular matrix, as well as providing more relevant biomimetic mechanical and chemical properties when compared to other electrospun polymer materials intended for tissue engineering.

6.2. Introduction

As biomaterials technology evolves, artificial tissue scaffolds come closer to mimicking the native extracellular matrix (ECM)[1,2,3,4]. The inclusion of cell adhesion and signaling molecules in the scaffolding material has greatly increased the ability to control and recreate the biochemical environment of the ECM[5,6]. More recently, the importance of the matrix's physical properties has come to the fore[7,8,9]. The mechanical modulus of the material has profound implications on cell behavior, influencing their adhesion[10,11], shape[12,13], differentiation[14,15], and function[16,17]. Materials also influence undifferentiated stem cells toward lineages that experience their modulus *in vivo*, such as under certain media conditions soft materials favoring adipocyte differentiation and stiffer materials favoring osteocyte differentiation[14]. However, the effect of scaffold surface topography has been less explored, but has been shown to have a similarly profound effect on cell spreading[18,19], shape[20], differentiation[21,22], and function[23,24]. One method to impart topographical control over scaffolding materials is the use of electrospinning to generate aligned nanofibers. Electrospun materials provide control over the fiber diameters to mimic the ECM, as well as over the alignment of the fibers for mimicry of anisotropic tissues[1].

One drawback of electrospinning for scaffold synthesis is the limited number of materials that have been successfully spun, predominantly polyesters and polyurethanes[25]. These materials fail to provide the proper mechanical environment for biomimetic scaffolds. Cardiac tissue, as an example, has a modulus in the range of 10 to 20 kPa at the beginning of diastole and 200-500

kPa at the end of diastole[26]. For example, bulk poly(lactic acid) has a modulus of 3-4 GPa[27], and in electrospun form, the nanofibrous poly(lactic acid) has a modulus ranging from 2-200 MPa[28,29], many orders of magnitude stiffer than natural tissue. Electrospun polyurethane exhibits a similar range of properties[30]. Hydrogels provide a much more attractive option to approach the mechanical properties of native tissue. Not only do hydrogels generally have modulus values much closer to ECM[31], they are also easily tunable[32]. Bulk hydrogels, however, do not allow for the topographical control seen in electrospun materials. It is only by combining the topography of an electrospun material with the mechanical properties of a hydrogel that we can recreate the physical environment of the ECM.

The topography of electrospin hydrogels alters the effective chemical environment of the material surface as well. Cells chemically interact only with the surface of the material, making control of the scaffold material surface chemistry critical. For traditional cell culture on plates of tissue culture polystyrene (TCPS), this surface is largely flat and uncontrolled. A hydrophilic two dimensional surface is presented to the cells, and adhesion occurs only after the adhesion of proteins to the TCPS, either from the cell culture media or deposition from the cells themselves[33]. Peptides and proteins have been pre-attached to TCPS or glass through various methods, such as silane deposition[34], gold-thiol interation[35,36], or formation of an interpenetrating polymer network[37,38], to provide a more defined surface chemistry. Nanostructured materials like electrospun fibers present a greatly increased specific surface area compared to monolithic materials[39], improving cell adhesion and proliferation[40,41]. However, common electrospun materials such as polyesters and polyurethanes allow for very limited control over surface chemistry[42,43], and are difficult to modify to covalently graft biological molecules[44].

By using an electrospun semi-interpenetrating polymer network (sIPN) containing peptide-conjugated macromolecules, this limitation can be bypassed and specific chemistry and biological signals can be engineered into the material and presented to the cell from a nanostructured surface[45,46]. In this work, I created and characterized such an electrospun matrix, consisting of hyaluronic acid (HyA) multivalently conjugated with peptides and entrapped within a hydrogel network based on poly(ethylene glycol) (pEGDA) diacrylate. The mechanical properties of the material were explored by altering the concentration of pEGDA in the electrospinning solution, as well as the photoinitiator used to crosslink the network. The availability of the included peptide on the surface of the material was then quantified by cleaving a fluorescently labeled peptide and measuring the solvent fluorescence. In this way, we have quantified the mechanical and chemical signals being provided by this novel biomaterial.

6.3. Materials and methods

Hyaluronic acid sodium salts (HyA) of 600 kDa molecular weight were obtained from Genzyme. Polyethylene glycol (pEG) polymers of molecular weight 1 MDa was purchased from Sigma-Aldrich. Polyethylene glycol diacrylate (pEGDA) of 200 Da molecular weight was obtained from Polysciences. Irgacure 2959 and Irgacure 819DW were provided by BASF. All chemicals used in the conjugation reaction, including 1-ethyl-3-(3-dimethylaminoproyl) carbodiimide hydrochloride (EDC), N-hydroxysulfosuccinimide (sulfoNHS) and 3,3'-N-(ε-maleimidocaproic acid)hydrazide trifluoroacetic acid (EMCH), tris(2-carboxyethyl) phosphine (TCEP), and the buffers phosphate buffered saline (PBS) and 2-(N-morpholino)ethanesulfonic acid (MES) were purchased from Thermo Scientific. SnakeSkin dialysis tubing with 10k

molecular weight cutoff was also purchased from Thermo Scientific. A FITC-containing fluorescent cysteine-terminated polyargenine peptide was purchased from American Peptide.

6.3.1. Electrospinning of hydrogels

Polymer solutions for electrospinning were prepared by mixing 3 wt% 1 MDa pEG, 0.5 wt% 600 kDa HyA, 1-5 v% 200 Da pEGDA, and 3 mg/mL Irgacure in ultra-pure ASTM type I reagent grade water (<18.2 MΩcm, pyrogen free, UPW). This solution was allowed to homogenize for 24 hours before use. The electrospinning process was carried out on a custom electrospinning apparatus. The solutions were loaded into a 3 mL plastic syringe (Becton-Dickinson) and delivered to a 22g needle through a length of 1/16" inner diameter polyvinyl chloride tubing (McMaster Carr) by a syringe pump (Chemyx) at 0.1 mL/h. A rotating mandrel or barrel was used as a collector (NaBond). For unaligned fibers, a 20 mm diameter mandrel rotating at 1000 rpm was used at the target. For aligned fibers, a 75 mm diameter barrel rotating at 5000 rpm was used as the collector. The needle was charged to +10.5 kV, and the collector was charged to -1.5 kV using a high voltage power supply (Gamma High Voltage). After electrospinning, the fibers were exposed to 365 nm UV light at 7 mW/cm^2 for 90 s to initiate crosslinking. After fabrication, the materials were stored at -20^oC until used.

6.3.2. Mechanical characterization of nanofiber materials

The modulus of the electrospun fibers was measured using a Bose Electroforce 3000. Samples were cut to an initial height of between 4 and 7.5 mm and a width of between 20 and 28 mm. The initial thickness of the fiber mats varied between 10 μm and 1.2 mm. The samples were fastened between two vice grips and pre-stretched until a measurable amount of pre-stress was achieved. Once in this state, their initial length, width and thickness were measured. The samples were then stretched at a constant strain rate of 0.5 percent per second until either the sample failed or the tensile tester reached the limit of its range of motion. For aligned fibers, samples for parallel and perpendicular testing were cut from adjacent sections of the electrospun material. Samples were tested under identical conditions with the direction of alignment running either parallel to or perpendicular to the direction of strain.

6.3.3. Conjugation of fluorescent peptide to hyaluronic acid

The carboxylic acid residue on the HyA chain was activated by the addition of a maleimide for conjugation to a cysteine-terminated peptide. First, HyA was dissolved in MES buffer and gently stirred overnight to ensure complete homogenization. EDC, sulfoNHS and EMCH were dissolved in MES buffer and added to the HyA solution. The final concentrations for all reagents were 5 mg/mL HyA, 10 mg/mL EDC, 2.8 mg/mL sulfoNHS, and 1.2 mg/mL EMCH. The reaction was allowed to proceed for two hours in the dark with gentle stirring. The product was then purified through dialysis in a 10k MWCO SnakeSkin dialysis tube against PBS. Dialysis lasted for 24h in 2L of buffer, with fresh buffer added at the 0h, 2h, and 4h time points.

After dialysis, the activated hyaluronic acid was reacted with 0.08 mg of the cysteine-terminated fluorescent peptide per 1mg of HyA. The peptide was reduced in a solution of 5.7 mg/mL TCEP with 3 mg/mL NaOH in order to disrupt any pre-existing disulfide bonds. This solution was then added to the activated HyA and allowed to react overnight in the dark at 4^oC.

Once the reaction was complete, the peptide-HyA conjugates were purified via dialysis in a 10k MWCO dialysis tube against water. The dialysis was kept at 4°C and lasted for 24h, with fresh water added at the 0h, 2h, and 4h time points. After dialysis, the product was lyophilized and kept at -20°C until used.

6.3.4. Surface characterization of nanofibers

The surface area of the nanofiber materials was measured via 3-point BET analysis by Particle Technology Labs. Briefly, the sample was loaded into a 7 mL glass bulb and conditioned for one hour at 40°C. A known volume of krypton gas was introduced and allowed to adsorb to the sample until the pressure has stabilized. Knowing the volume of gas introduced and the amount of unadsorbed gas as calculated from the temperature, volume and pressure of the chamber, the number of gas molecules adsorbed onto the surface was calculated. With the cross-sectional area of the gas molecules known, this was translated to a surface area.

The availability of the peptide at the surface of the fibers was assessed via cleavage of fluorescent peptides by trypsin. HyA conjugated with fluorescently tagged peptides containing a FITC residue was electrospun and crosslinked. The fibers were then treated with 0.25% trypsin-EDTA for periods of 5 minutes, 10 minutes, 15 minutes, 15 minutes and 1 hour. The concentration of FITC released into the supernatant was measured with a SpectaMax i3 plate reader (Molecular Devices). This concentration of FITC was normalized by the initial dry weight of the sample to calculate a mass fraction of peptide released from the fibers. The peptide surface density was calculated using the known specific surface area from the BET measurements.

6.4. Results and Discussion

6.4.1. Dependence of modulus on pEGDA content of fibers and on photoinitiator

In the dry state, the material exhibited a small "toe" region at low strain, followed by a linear stress/strain relationship. Qualitatively, the curve resembles that seen in mechanical testing of tissues such as ligament or tendon, where the initial toe region arises due to the aligning of the constituent fibers and the subsequent linear region representing the stretching of the aligned fibers[47]. This is consistent with the architecture of the electrospun material, consisting of nanofibers that become aligned with the direction of stretching at low strain values, and become individually loaded at higher strains.

Fibers containing an initial 1 v% pEGDA had an average Young's modulus of 4.3 MDa. This increased to 6.0 MDa in fibers containing an initial 5 v% pEGDA, however the difference was not statistically significant. A comparison of two representative stress/strain curves for the differing pEGDA concentrations is presented in Figure 6.1. Use of the photoinitiator Irgacure 819DW with 5 v% pEGDA rendered the electrospun fibers less stable in solution, and lowered the measured modulus to 769 kPa. While this modulus of fibers crosslinked by Irgacure 819DW was closer to that of the native ECM than those using Irgacure 2959, the decreased stability and reliability reduced their viability as a tissue scaffold material. A summary of the various moduli measured is presented in Table 1.

It is worth noting that the moduli of these materials are considerably higher than that of the ECM. Softer electrospun materials with moduli closer to that of the ECM have been shown to be superior for tissue scaffold application[15]. Cardiac tissue, as an example, has a modulus

ranging from 10 kPa to 500 kPa, depending on the stage of contraction. The modulus of these electrospun fibers is between one and two orders of magnitude higher than the stiffest conditions of the ECM. However, these materials exist near the lower limit of what has been observed with other electrospun materials, and thus are closer than other electrospun fibers at mimicking the ECM mechanically. In addition, all of these mechanical measurements were taken with the fibers in the dry state. For a hydrogel material, the mechanical properties are expected to decrease considerably when swollen in water, which is not the case for hydrophobic materials such as polyesters and polyurethanes. Thus, while the modulus reported here is higher than that of the ECM and at the lower limit of other electrospun materials, the modulus that the cells will experience is expected to be considerably lower. In preliminary results, hydrated fibrous scaffolds have a modulus on the order of 10 kPa, which is within the range seen in natural ECM tissue.

6.4.2. Anisotropy of mechanical properties in aligned fibers

Alignment of the electrospun nanofibers by use of a rapidly rotating barrel collector was reflected in the tensile modulus of the fiber mats. The modulus of aligned fibers spun from a solution containing 1 v% pEGDA, when strained parallel to or perpendicular to the direction of alignment, were compared to unaligned samples. Comparative stress/strain curves of unaligned samples and aligned samples tested parallel and perpendicular to the direction of alignment are presented in Figure 6.2. The measured tensile modulus of fibers aligned perpendicular to the direction of strain was lowered from 4.30 MDa in unaligned samples to 2.16 MDa. When the fibers were aligned parallel to the direction of tension, the modulus increased to 8.35 MDa.

The difference in tensile modulus between the two orientations of aligned fibers can be explained by examining the mechanisms by which the material resists reformation. There are two main modes of deformation in response to tension: rearrangement of fibers, and stretching of the fibers themselves. Of the two, stretching the fibers will result in a significantly higher resistive force. When examining rearrangement of the nanofibers, they are capable of sliding past each other with minimal inter-fiber interaction. The only significant resistive force for this sliding or alignment of fibers is the presence of entanglements between the fibers, restricting their motion. If this were the only, or the predominant mode of deformation, the measured modulus would be very low. The stretching of nanofibers will present a much higher modulus value, due to the stretching of the covalent bonds in the crosslinked polymer network.

For aligned nanofiber materials, the change in modulus is due to the change in which mode of deformation is most prevalent. For fibers strained perpendicular to the direction of alignment, the predominant mode of deformation is the sliding and alignment of fibers. Fibers strained parallel to the direction of alignment, on the other hand, will deform primarily via fiber stretching. This results in a much higher tensile modulus in the direction of alignment when compared to the perpendicular alignment. Materials with no preferential direction of alignment will undergo a mixed mode strain, and thus will have an intermediate tensile modulus.

6.4.3. Availability of peptide at nanofiber surface

The specific surface area of the fibers depended largely on their diameter. Fibers spun with an initial 1 v% pEGDA had an average fiber diameter of 336 nm, while fibers spun from a solution with an initial 5 v% pEGDA had an average fiber diameter of 538 nm. BET analysis of

the electrospun fibers showed that material spun from a 1 v% pEGDA solution had a specific surface area of 6.1 m^2g^{-1}. Thicker fibers spun from a 5 v% solution had a lower specific surface area of 1.1 m^2g^{-1}. A representative BET plot is shown in Figure 6.3. This trend is as would be expected for a nanofibrous system. As the size of the features, namely the diameter of the fibers in this instance, decreases, the ratio of surface area to volume, and thus to mass, will increase. Because of this increased surface area, and the smaller fibers more closely resembling ECM fibers, fibers spun from 1 v% pEGDA solutions were used in all experiments moving forward.

SEC-MALS analysis of the FITC peptide conjugated HyA showed that the conjugates contained on average 21 peptides per 570 kDa HyA chain (Chapter 4), comprising a weight percentage of 5.0%. Incubation of electrospun fibers containing FITC tagged HyA with trypsin caused the cleavage of the peptide chain and release of the FITC tag into the supernatant. This release was seen to plateau after the 15 minute time point, suggesting that the majority of available peptides had been cleaved. Because of the size of the trypsin molecule and the small mesh size of the hydrogel network, it is believed that the cleavage of peptides was largely limited to those at the surface of the fibers.

After five minutes of incubation with trypsin, 8 μg of peptide was released per milligram of fiber. This increased to 11.6 μg/mg at 10 minutes and 10.8 μg/mg at 15 minutes. After 60 minutes of incubation, 12.6 μg/mg of FITC had been released from the fibers (Figure 6.4). Given the starting concentration of peptide in the material, 16% of the embedded peptide was released at 5 minutes, increasing to a maximum of 25% released at 60 minutes. This corresponds to a peptide surface density of 29.6 pmol/m^2 of peptide released at 5 minutes and 46.5 pmol/m^2 of peptide at 60 minutes. These values are tabulated in Table 2. These surface densities of RGD containing peptides are in line with those required for strong cell attachment, which have been reported to be between 10 and 100 pmol/m^2 [48].

6.5. Conclusions

Physical and chemical analysis of this novel electrospun hydrogel material confirms that it is capable of serving as a defined synthetic extracellular matrix substitute. Mechanically, this material more closely resembles the modulus of the ECM than other electrospun materials, such as polyesters or polyurethanes. While the match in mechanical properties is not perfect, the use of hydrogels allows for the tailoring of these properties in future studies, such as with the use of a longer pEGDA molecule to reduce the modulus of the polymer network. Alignment of the nanofibers caused the material to exhibit anisotropic mechanical properties. This provides another signal beyond the topography to directionality align cultured cells such as cardiomyocytes. The nanofibrous material exhibited a high specific surface area, ranging from 1.1 to 6.1 m^2g^{-1}. From this surface, the embedded peptide-hyaluronic acid conjugates presented sufficient adhesive ligand to allow for cellular attachment. In future work, the surface density of peptides may be increased by increasing the valency of the embedded conjugates, or increasing their relative prevalence by decreasing the amount of pEG and pEGDA in the electrospinning solution. This material provides a platform for creating a biomimetic tissue scaffold that can recreate the topographical, chemical, and mechanical environment of the extracellular matrix. Further refinements and modification, such as changing the hydrogel modulus or the identity of the conjugated peptide will widen the range of possible applications in which this material may be used.

6.6. Acknowledgements

The authors would like to thank Min Ju Lee for her assistance in mechanical characterization. We would also like to thank Min Ju Lee and Christine Lam for assistance in measurement of peptide surface availability.

6.7. References

1. Wang, X. F.; Ding, B.; Li, B. Y., Biomimetic electrospun nanofibrous structures for tissue engineering. *Mater Today* **2013,** *16* (6), 229-241.

2. Silvestri, A.; Boffito, M.; Sartori, S.; Ciardelli, G., Biomimetic Materials and Scaffolds for Myocardial Tissue Regeneration. *Macromol Biosci* **2013,** *13* (8), 984-1019.

3. Ma, P. X., Biomimetic materials for tissue engineering. *Adv Drug Deliver Rev* **2008,** *60* (2), 184-198.

4. Holzwarth, J. M.; Ma, P. X., Biomimetic nanofibrous scaffolds for bone tissue engineering. *Biomaterials* **2011,** *32* (36), 9622-9629.

5. Yu, J. S.; Lee, A. R.; Lin, W. H.; Lin, C. W.; Wu, Y. K.; Tsai, W. B., Electrospun PLGA Fibers Incorporated with Functionalized Biomolecules for Cardiac Tissue Engineering. *Tissue Eng Pt A* **2014,** *20* (13-14), 1896-1907.

6. Kim, T. G.; Park, T. G., Biomimicking extracellular matrix: Cell adhesive RGD peptide modified electrospun poly(D,L-lactic-Co-glycolic acid) nanofiber mesh. *Tissue Eng* **2006,** *12* (2), 221-233.

7. Guilak, F.; Butler, D. L.; Goldstein, S. A.; Baaijens, F. P. T., Biomechanics and mechanobiology in functional tissue engineering. *J Biomech* **2014,** *47* (9), 1933-1940.

8. Hung, B. P.; Hutton, D. L.; Grayson, W. L., Mechanical control of tissue-engineered bone. *Stem Cell Res Ther* **2013,** *4*.

9. Butler, D. L.; Goldstein, S. A.; Guilak, F., Functional tissue engineering: The role of biomechanics. *J Biomech Eng-T Asme* **2000,** *122* (6), 570-575.

10. Ouasti, S.; Donno, R.; Cellesi, F.; Sherratt, M. J.; Terenghi, G.; Tirelli, N., Network connectivity, mechanical properties and cell adhesion for hyaluronic acid/PEG hydrogels. *Biomaterials* **2011,** *32* (27), 6456-6470.

11. Nemir, S.; West, J. L., Synthetic Materials in the Study of Cell Response to Substrate Rigidity. *Ann Biomed Eng* **2010,** *38* (1), 2-20.

12. Rehfeldt, F.; Brown, A. E. X.; Raab, M.; Cai, S. S.; Zajac, A. L.; Zemel, A.; Discher, D. E., Hyaluronic acid matrices show matrix stiffness in 2D and 3D dictates cytoskeletal order and myosin-II phosphorylation within stem cells. *Integr Biol-Uk* **2012,** *4* (4), 422-430.

13. Mathieu, P. S.; Loboa, E. G., Cytoskeletal and Focal Adhesion Influences on Mesenchymal Stem Cell Shape, Mechanical Properties, and Differentiation Down Osteogenic, Adipogenic, and Chondrogenic Pathways. *Tissue Eng Part B-Re* **2012,** *18* (6), 436-444.

14. Engler, A. J.; Sen, S.; Sweeney, H. L.; Discher, D. E., Matrix elasticity directs stem cell lineage specification. *Cell* **2006,** *126* (4), 677-689.

15. Nam, J.; Johnson, J.; Lannutti, J. J.; Agarwal, S., Modulation of embryonic mesenchymal progenitor cell differentiation via control over pure mechanical modulus in electrospun nanofibers. *Acta Biomater* **2011,** *7* (4), 1516-1524.

16. Bhana, B.; Iyer, R. K.; Chen, W. L. K.; Zhao, R. G.; Sider, K. L.; Likhitpanichkul, M.; Simmons, C. A.; Radisic, M., Influence of Substrate Stiffness on the Phenotype of Heart Cells. *Biotechnol Bioeng* **2010,** *105* (6), 1148-1160.

17. Wang, P. Y.; Yu, J. S.; Lin, J. H.; Tsai, W. B., Modulation of alignment, elongation and contraction of cardiomyocytes through a combination of nanotopography and rigidity of substrates. *Acta Biomater* **2011,** *7* (9), 3285-3293.

18. Ghibaudo, M.; Di Meglio, J. M.; Hersen, P.; Ladoux, B., Mechanics of cell spreading within 3D-micropatterned environments. *Lab Chip* **2011,** *11* (5), 805-812.

19. Le Saux, G.; Magenau, A.; Boecking, T.; Gaus, K.; Gooding, J. J., The Relative Importance of Topography and RGD Ligand Density for Endothelial Cell Adhesion. *Plos One* **2011,** *6* (7).

20. Rape, A. D.; Guo, W. H.; Wang, Y. L., The regulation of traction force in relation to cell shape and focal adhesions. *Biomaterials* **2011,** *32* (8), 2043-2051.

21. McNamara, L. E.; McMurray, R. J.; Biggs, M. J.; Kantawong, F.; Oreffo, R. O.; Dalby, M. J., Nanotopographical control of stem cell differentiation. *J Tissue Eng* **2010,** *2010*, 120623.

22. Wilson, S. L.; Wimpenny, I.; Ahearne, M.; Rauz, S.; El Haj, A. J.; Yang, Y., Chemical and Topographical Effects on Cell Differentiation and Matrix Elasticity in a Corneal Stromal Layer Model. *Adv Funct Mater* **2012,** *22* (17), 3641-3649.

23. Mendonca, D. B. S.; Miguez, P. A.; Mendonca, G.; Yamauchi, M.; Aragao, F. J. L.; Cooper, L. F., Titanium surface topography affects collagen biosynthesis of adherent cells. *Bone* **2011,** *49* (3), 463-472.

24. Min, S. K.; Kim, S. H.; Kim, C. R.; Paik, S. M.; Jung, S. M.; Shin, H. S., Effect of topography of an electrospun nanofiber on modulation of activity of primary rat astrocytes. *Neurosci Lett* **2013,** *534*, 80-84.

25. Chen, Q. Z.; Ishii, H.; Thouas, G. A.; Lyon, A. R.; Wright, J. S.; Blaker, J. J.; Chrzanowski, W.; Boccaccini, A. R.; Ali, N. N.; Knowles, J. C.; Harding, S. E., An elastomeric patch derived from poly(glycerol sebacate) for delivery of embryonic stem cells to the heart. *Biomaterials* **2010,** *31* (14), 3885-3893.

26. Chen, Q. Z.; Bismarck, A.; Hansen, U.; Junaid, S.; Tran, M. Q.; Harding, S. E.; Ali, N. N.; Boccaccini, A. R., Characterisation of a soft elastomer poly(glycerol sebacate) designed to match the mechanical properties of myocardial tissue. *Biomaterials* **2008,** *29* (1), 47-57.

27. Liu, D. Y.; Yuan, X. W.; Bhattacharyya, D., The effects of cellulose nanowhiskers on electrospun poly (lactic acid) nanofibres. *J Mater Sci* **2012,** *47* (7), 3159-3165.

28. Cho, A. R.; Shin, D. M.; Jung, H. W.; Hyun, J. C.; Lee, J. S.; Cho, D.; Joo, Y. L., Effect of Annealing on the Crystallization and Properties of Electrospun Polylatic Acid and Nylon 6 Fibers. *J Appl Polym Sci* **2011,** *120* (2), 752-758.

29. Liu, H.; Wang, S. D.; Qi, N., Controllable structure, properties, and degradation of the electrospun PLGA/PLA-blended nanofibrous scaffolds. *J Appl Polym Sci* **2012,** *125*, E468-E476.

30. Amoroso, N. J.; D'Amore, A.; Hong, Y.; Rivera, C. P.; Sacks, M. S.; Wagner, W. R., Microstructural manipulation of electrospun scaffolds for specific bending stiffness for heart valve tissue engineering. *Acta Biomater* **2012,** *8* (12), 4268-4277.

31. Moon, J. J.; Saik, J. E.; Poche, R. A.; Leslie-Barbick, J. E.; Lee, S. H.; Smith, A. A.; Dickinson, M. E.; West, J. L., Biomimetic hydrogels with pro-angiogenic properties. *Biomaterials* **2010,** *31* (14), 3840-3847.

32. Tse, J. R.; Engler, A. J., Preparation of hydrogel substrates with tunable mechanical properties. *Curr Protoc Cell Biol* **2010,** *Chapter 10*, Unit 10 16.

33. Vanwachem, P. B.; Mallens, B. W. L.; Dekker, A.; Beugeling, T.; Feijen, J.; Bantjes, A.; Detmers, J. P.; Vanaken, W. G., Adsorption of Fibronectin Derived from Serum and from Human-Endothelial Cells onto Tissue-Culture Polystyrene. *J Biomed Mater Res* **1987,** *21* (11), 1317-1327.

34. Senyah, N.; Hildebrand, G.; Liefeith, K., Comparison between RGD-peptide-modified titanium and borosilicate surfaces. *Anal Bioanal Chem* **2005,** *383* (5), 758-762.

35. Giljohann, D. A.; Seferos, D. S.; Daniel, W. L.; Massich, M. D.; Patel, P. C.; Mirkin, C. A., Gold Nanoparticles for Biology and Medicine. *Angew Chem Int Edit* **2010,** *49* (19), 3280-3294.

36. Liu, Y. L.; Shipton, M. K.; Ryan, J.; Kaufman, E. D.; Franzen, S.; Feldheim, D. L., Synthesis, stability, and cellular internalization of gold nanoparticles containing mixed peptide-poly(ethylene glycol) monolayers. *Anal Chem* **2007,** *79* (6), 2221-2229.

37. Xiao, W. Q.; He, J. K.; Nichol, J. W.; Wang, L. Y.; Hutson, C. B.; Wang, B.; Du, Y. A.; Fan, H. S.; Khademhosseini, A., Synthesis and characterization of photocrosslinkable gelatin and silk fibroin interpenetrating polymer network hydrogels. *Acta Biomater* **2011,** *7* (6), 2384-2393.

38. Bearinger, J. P.; Castner, D. G.; Golledge, S. L.; Rezania, A.; Hubchak, S.; Healy, K. E., P(AAm-co-EG) interpenetrating polymer networks grafted to oxide surfaces: Surface

characterization, protein adsorption, and cell detachment studies. *Langmuir* **1997,** *13* (19), 5175-5183.

39. Yoshimoto, H.; Shin, Y. M.; Terai, H.; Vacanti, J. P., A biodegradable nanofiber scaffold by electrospinning and its potential for bone tissue engineering. *Biomaterials* **2003,** *24* (12), 2077-2082.

40. Bhattarai, S. R.; Bhattarai, N.; Yi, H. K.; Hwang, P. H.; Cha, D. I.; Kim, H. Y., Novel biodegradable electrospun membrane: scaffold for tissue engineering. *Biomaterials* **2004,** *25* (13), 2595-2602.

41. Pant, H. R.; Neupane, M. P.; Pant, B.; Panthi, G.; Oh, H. J.; Lee, M. H.; Kim, H. Y., Fabrication of highly porous poly (epsilon-caprolactone) fibers for novel tissue scaffold via water-bath electrospinning. *Colloid Surface B* **2011,** *88* (2), 587-592.

42. Bhardwaj, N.; Kundu, S. C., Electrospinning: A fascinating fiber fabrication technique. *Biotechnol Adv* **2010,** *28* (3), 325-347.

43. Sill, T. J.; von Recum, H. A., Electro spinning: Applications in drug delivery and tissue engineering. *Biomaterials* **2008,** *29* (13), 1989-2006.

44. Zonca, M. R.; Yune, P. S.; Williams, J. K.; Gu, M.; Unser, A. M.; Imbrogno, J.; Belfort, G.; Xie, Y. B., Enhanced Stem Cell Pluripotency in Surface-Modified Electrospun Fibrous Matrices. *Macromol Biosci* **2014,** *14* (2), 215-224.

45. Liang, D.; Hsiao, B. S.; Chu, B., Functional electrospun nanofibrous scaffolds for biomedical applications. *Adv Drug Deliver Rev* **2007,** *59* (14), 1392-1412.

46. Choi, W. S.; Bae, J. W.; Lim, H. R.; Joung, Y. K.; Park, J. C.; Kwon, I. K.; Park, K. D., RGD peptide-immobilized electrospun matrix of polyurethane for enhanced endothelial cell affinity. *Biomed Mater* **2008,** *3* (4).

47. Hooley, C. J.; Mccrum, N. G.; Cohen, R. E., The Viscoelastic Deformation of Tendon. *J Biomech* **1980,** *13* (6), 521-528.

48. Massia, S. P.; Hubbell, J. A., An Rgd Spacing of 440nm Is Sufficient for Integrin Alpha-V-Beta-3-Mediated Fibroblast Spreading and 140nm for Focal Contact and Stress Fiber Formation. *J Cell Biol* **1991,** *114* (5), 1089-1100.

6.8. Tables

Table 6.1. Summary of measured mechanical moduli under uniaxial tension for various combinations of polymer concentration, photoinitiator, and alignments of nanofibers.

pEGDA Concentration (volume percent)	Photoinitiator	Alignment	Modulus (MPa)
5	IC 819DW	Unaligned	0.77
5	IC 2959	Unaligned	6.04
1	IC 2959	Unaligned	4.30
1	IC 2959	Parallel to tension	8.35
1	IC 2959	Perpendicular to tension	2.16

Table 6.2. Release of FITC tagged peptide from electrospun fibers after incubation with trypsin. The fraction of total embedded peptide released was calculated by comparing the mass of released peptide to the SEC-MALS calculated peptide fraction of the conjugate. The surface density was calculated by comparing the mass of peptide released to the BET calculated specific surface area.

Trypsin Incubation Time (minutes)	**Mass of Peptide Released per Fiber Weight (μg/mg)**	**Percent of Embedded Peptide Released**	**Surface Density of Peptide Released from Fibers ($pmol/m^2$)**
5	8.03	16.1	29.6
10	11.6	23.2	42.8
15	10.8	21.5	39.6
60	12.6	25.3	46.5

6.9. Figures

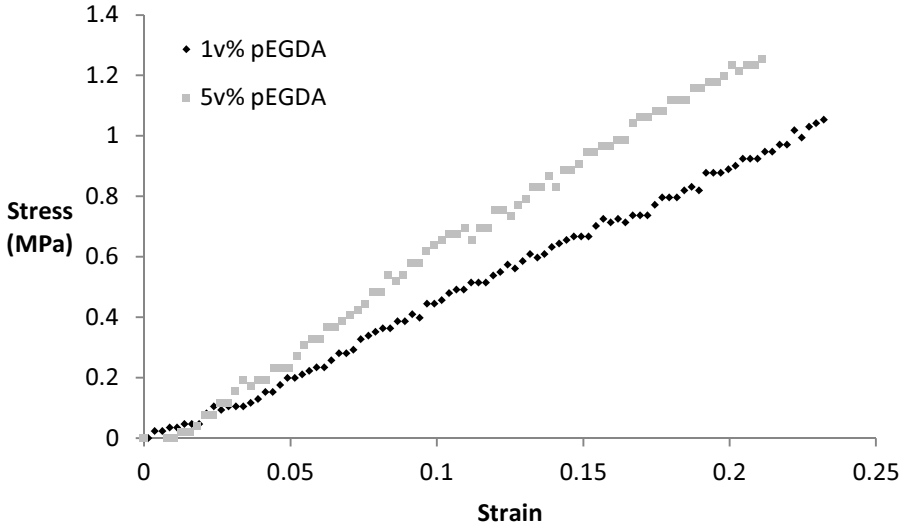

Figure 6.1. Representative stress/strain curves of nanofiber mats electrospun from solutions containing 1 v% pEGDA (black) and 5 v% pEGDA (gray). Unaligned samples were strained in uniaxial tension.

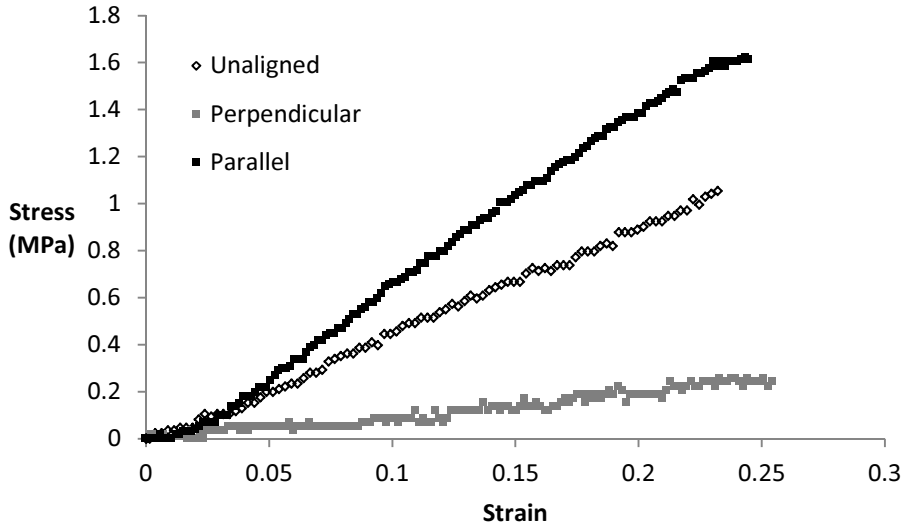

Figure 6.2. Representative stress/strain curves of unaligned (empty markers) and aligned (filled markers) nanofibers electrospun from solutions containing 1 v% pEGDA. Samples were strained in uniaxial tension. Aligned samples were strained parallel to (black) and perpendicular to (gray) the direction of alignment.

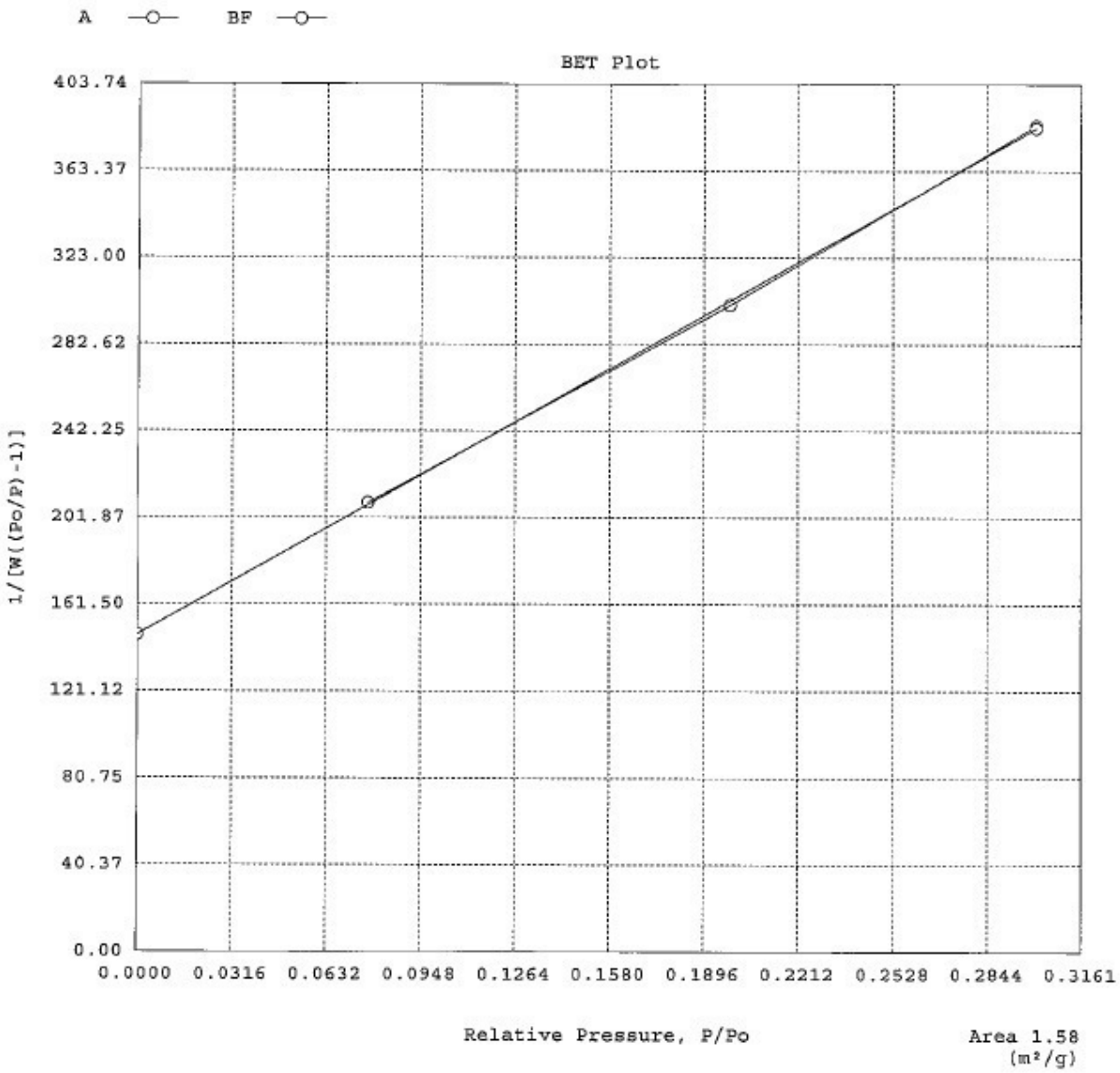

Figure 6.3. BET plot of electrospun fibers spun from a solution with 5 v% pEGDA. Plotted on the abscissa is the relative pressure (equilibrium pressure divided by saturation pressure). On the ordinate is inverse of the adsorbed gas quantity multiplied by the relative pressure divided by one minus the relative pressure. The surface area is calculated from the slope and the intercept of the gas adsorption isotherm.

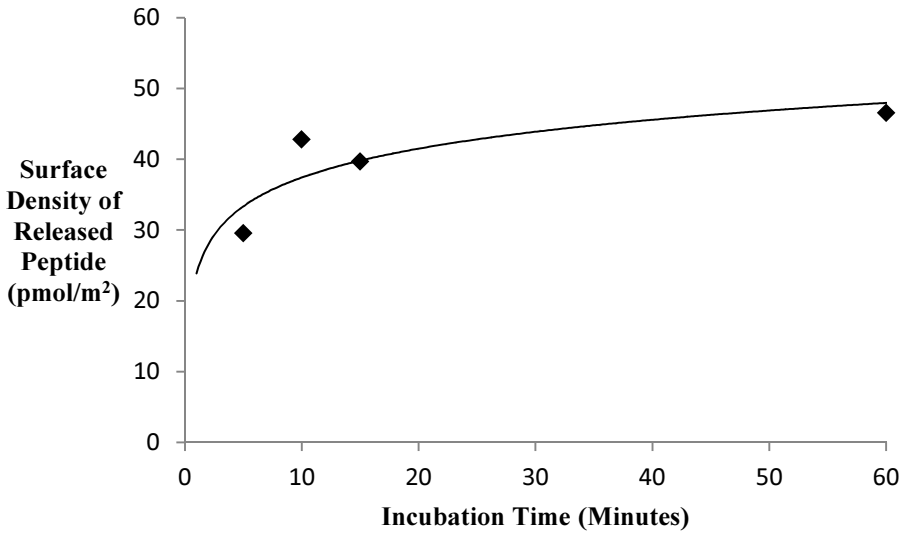

Figure 6.4. Release of bsp-RGD(15) peptide from the surface of electrospun fibers after incubation with trypsin.

Chapter 7

Assessment of the capacity of electrospun poly(ethylene glycol) based hydrogels containing multivalent RGD peptides to support cell adhesion, alignment, and function

7.1. Abstract

The capacity for an electrospun hydrogel scaffold containing embedded multivalently conjugated hyaluronic acid to maintain cardiomyocyte viability and functionality was assessed. An RGD containing peptide derived from bone sialoprotein, bsp-RGD(15) was chosen to mediate cell-material interaction. On materials not containing the peptide, cells were not able to adhere or spread. Cardiomyocytes cultured on scaffolds containing these peptide conjugates were capable of adhering and remaining viable. The cell-material interactions were sufficient to maintain adhesion, but could not generate a uniform cell sheet. Instead, cells more strongly interacted with each other, forming clusters of cells on the material surface. Cardiomyocytes retained contractile functionality on the electrospun fibers. Individual cell clusters beat with internal synchronization, but independently of other clusters. Long-range coordinated contraction was observed, though no source for the contraction was readily apparent, implying the presence of a population of cells outside of the clusters beating in a synchronized fashion. These experiments serve as a proof of concept for use of this material as a cardiomyocyte scaffold, with possible applications as a cardiac patch for treatment of myocardial infarction. Further experiments are necessary to improve cellular adhesion, and to validate the material's capability to align cardiomyocyte cytoskeletal arrangement and contractility.

7.2. Introduction

Heart failure due to cardiovascular disease, and ischemic heart disease in particular, remains the leading cause of death worldwide[1]. Myocardial infarction (MI) caused by the obstruction of blood flow to the heart is one of the major causes of heart failure. The heart is largely incapable of naturally repairing the damaged ventricular wall tissue[2]. This leads to thinning of the ventricular wall and the formation of noncontractile scar tissue[3,4]. This thinned, passive wall will dilate and reduce the heart's capacity to pump blood to the rest of the body[5]. The continual weakening of the heart may lead to complete heart failure and death. Commonly used methods to treat this condition include ventricular reconstruction, stem cell injection, and the use of a synthetic material to reinforce the ventricular wall. During ventricular reconstruction, the infarcted area is removed and the resulting hole is then either sutured closed directly if the defect is small enough, or if the damage was too extensive, a synthetic patch is sutured in place[6]. The removal of the infarcted region may reduce the ventricular remodeling and subsequent dilation of the wall while maintaining the heart's ability to pump[7]. The use of injected stem cells to treat MI has met mixed success[8]. Injection of various undifferentiated cell populations has demonstrated the ability to improve heart function post-MI[9,10]. However, cells injected without a scaffold or other material are quickly cleared from the location of injection[11,12,13], and studies have shown that stem cell treated medium has a similar ability to improve heart function, implying it paracrine signaling from the injected cells is the predominant mode of effect[14]. A synthetic material in the form of a polymer mesh "sock" that is placed around the heart[15,16] or a locally applied patch[17] can also be used to physically reinforce the heart and prevent failure. However, these patches are static and lack the ability to adapt or grow with the patient. This makes them impractical for use in children with congenital heart defects.

In order to address this shortcoming, patch materials have begun using the tissue engineering approach. Rather than introduce a permanent foreign implant, these strategies attempt to use a combination of scaffolding materials, cells, and growth factors to regenerate the myocardium[18]. The key to successful tissue engineering is providing a physical scaffold that can not only support the cells, but replicate the native cell niche[19,20]. The majority of these scaffolds are based on hydrogel materials such as polysaccharides[21], proteins[22], and their blends[23,24]. Many hydrogel tissue scaffolds fail to mimic the structural environment seen *in vivo*. For myocardial tissue in particular, this environment consists of anisotropically aligned protein nanofibers[25]. Electrospinning is a simple and easily scalable method by which to create a similar architecture and has become the subject of recent research in cardiac patch development[26]. Various methods, such as rotating the target[27] or changing the target geometry[28], can align the fibers to recreate the anisotropic environment. Most commonly used polymers in electrospun scaffolds are much stiffer than the extracellular matrix and fail to provide a chemically significant environment[29,30,31,32].

Zimmerman *et al* proposed that a tissue construct for cardiac repair should be contractile and electrophysiologically stable, vascularized or easily vascularized post-implantation, non-immunogenic, and match tissue mechanics[33]. This research project seeks to fulfill those criteria by creating a biologically instructive electrospun cardiac patch to assist in the repair of damaged cardiac tissue after infarction through mechanical stabilization as well as physical and chemical signaling. The use of synthetic polymers and a defined biomolecular suite will limit batch to batch variation and ease regulatory problems seen with natural materials such as Matrigel[34]. The patch will mechanically reinforce the infarcted region to reduce dilation and thinning of the vascular wall. Meanwhile, the material will mimic native ECM through its nanofibrous structure and multivalent presentation of peptides from macromolecules embedded in the fibers in order to recruit native cardiac progenitor cells present in the myocardium[35,36]. A short RGD containing peptide will be used to promote cell attachment to the scaffold material[37,38,39]. Eventually, the infarcted region will be either replaced by or reinforced by healthy tissue, preventing heart weakening and failure.

7.3. Materials and methods

Hyaluronic acid sodium salts (HyA) of 600 kDa molecular weight were obtained from Genzyme. Polyethylene glycol (pEG) polymers of molecular weight 1 MDa was purchased from Sigma-Aldrich. Polyethylene glycol diacrylate (pEGDA) of 200 Da molecular weight was obtained from Polysciences. The photoinitiator Irgacure 2959 was provided by BASF. All chemicals used in the conjugation reaction, including 1-ethyl-3-(3-dimethylaminoproyl) carbodiimide hydrochloride (EDC), N-hydroxysulfosuccinimide (sulfoNHS) and 3,3'-N-(ε-maleimidocaproic acid)hydrazide trifluoroacetic acid (EMCH), tris(2-carboxyethyl) phosphine (TCEP), and the buffers phosphate buffered saline (PBS) and 2-(N-morpholino)ethanesulfonic acid (MES) were purchased from Thermo Scientific. SnakeSkin dialysis tubing with 10k molecular weight cutoff was also purchased from Thermo Scientific. The peptide bsp-RGD(15) (Ac-CGGNGEPRGDTYRAY-NH_2) was synthesized by American Peptide.

7.3.1. Synthesis of electrospun hydrogel scaffolds

RGD peptides were multivalently conjugated to 600 kDa hyaluronic acid as has been described previously[40]. Polymer solutions for electrospinning were prepared by mixing 3 wt% 1

MDa pEG, 0.5 wt% 600 kDa RGD-conjugated HyA, 1-5 v% 200 Da pEGDA, and 3 mg/mL Irgacure 2959 in ultra-pure ASTM type I reagent grade water (<18.2 MΩcm, pyrogen free, UPW). This solution was allowed to homogenize for 24 hours before use. The electrospinning process was carried out on a custom electrospinning apparatus. The solutions were loaded into a 5 mL plastic syringe (Becton-Dickinson) and delivered to a 22g needle through a length of 1/16" inner diameter polyvinyl chloride tubing (McMaster Carr) by a syringe pump (Chemyx) at 0.1 mL/h. A rotating mandrel or barrel was used as a collector (NaBond). For unaligned fibers, a 20 mm diameter mandrel rotating at 1000 rpm was used at the target. For aligned fibers, a 75 mm diameter barrel rotating at 5000 rpm was used as the collector. The needle was charged to +10.5 kV, and the collector was charged to -1.5 kV using a high voltage power supply (Gamma High Voltage). After electrospinning, the fibers were exposed to 365 nm UV light at 7 mW/cm^2 for 90 s to initiate crosslinking. After fabrication, the materials were stored at -20^oC until used.

7.3.2. Wnt mediated cardiac differentiation via small molecules.

The protocol to differentiate either human embryonic stem cells or iPS cells into cardiac myocytes was based on a temporal Wnt induction and inhibition protocol[41]. Episomal human iPS cells (Wtc10) and H-9 cells engineered with an m-cherry reporter to show α myosin heavy chain (αMCH) gene expression were maintained feeder free on Synthemax II plates (Corning) in mTeSR1 medium (STEMCELL Technologies) at 37^oC and 5.0% CO_2. The H-9 cells were a generous gift from the Conklin Lab at UCSF. Stem cells were dissociated into a single cell suspension with Accutase at 37°C for 3 minutes before seeding onto Synthemax II coated 12 well plates (Costar) at a density of 25,000 cells/ml with 10mM ROCK inhibitor (Y-27632; BioVision) solution at 1:1000x. Cells were maintained in mTeSR for 5-7 days, exchanging media daily until reaching the appropriate confluence. Once confluent, cells were treated with 12μM Gsk3 inhibitor CH (CHIR-99021; Selleck) in RPMI-B27 minus insulin (Gibco) for 24 hours (day 0-1). Media was then exchanged on day 1 for RPMI-B27 minus insulin. On day 3 cells were treated with RPMI-B27 minus insulin with 5uM Wnt inhibitor IWP4 (Stemgent) for 24 hours. On day 5 media was exchanged for RPMI-B27 minus insulin. On day 7 the media was exchanged for RPMI-B27 complete and exchanged every 3 days. Beating was observed around day 10. Flow Cytometry confirmed that 54.8% of the differentiated iPS cell population was positive for cTnT (Figure 7.1).

7.3.3. Culture of cardiomyocytes on electrospun material

Cardiomyocytes were dissociated 20 days after differentiation with 0.25%Trypsin for 15 minutes at 37°C and seeded on to both bsp-RGD(15) conjugated HA-PEG electrospun fibers with a seeding density of either 250,000 or 500,000 cells/ml in 48 well plates. Seeded electrospun fibers were maintained in EB20 media composed of Knockout DMEM with 20% FBS (Gibco), 1X non-essential amino acids, 200 nM L-Glutamine, and β-mercaptoethanol. Media was exchanged every three days. Cell seeded scaffolds were imaged using a Nikon Eclipse TE300 Inverted Tissue Culture Microscope with a QImaging QICAM Fast 1394 Digital Camera and a FEI/Philips XL30 SEM in low vacuum.

After one week of culture, samples were moved to glass cover slips for immunostaining. Cells were washed with PBS and fixed with 4% paraformaldehyde for 15 minutes at room temperature before being permeabilized with 0.2% Triton X for 8 minutes. The cells were then

exposed to a solution of 2% BSA, 4% goat serum and 0.1% Triton X as a blocking agent. Mouse anti-cTnT and goat anti-mouse antibodies (Thermo Scientific) were used as the primary and secondary antibodies, respectively. DAPI was used as a nuclear stain. Fluorescent images were acquired using a Nikon Eclipse TE300 Inverted Tissue Culture Microscope with a QImaging QICAM Fast 1394 Digital Camera.

7.4. Results and Discussion

7.4.1. Adhesion of cardiomyocytes on electrospun scaffolds

Cardiomyocytes plated on the electrospun hydrogel scaffold containing RGD-conjugated HyA adhered and remained viable. On materials containing either no HyA, or HyA without the cell-binding peptide, cells did not show any significant adhesion to the material. This difference in cellular adhesion in illustrated in Figure 7.2. Environmental SEM imaging of the scaffolds confirmed the presence of cells adhered to the surface of peptide containing fibers and their absence from non-peptide containing fibers. The nanofibrous nature of the scaffold was evident in the SEM images, and deformation of this matrix in the vicinity of the cells demonstrated the cell's ability to exert tensile force on the underlying substrate.

While the adhesion to the electrospun material was sufficient to maintain cellular attachment and viability, it was not strong. Cardiomyocytes formed individual clusters and did not fully spread on the scaffold, maintaining a rounded morphology. These observations indicate that cell-cell interactions were more favorable than cell-scaffold interactions. During the immunostaining process, this weak adhesion resulted in cells often falling off of the surface during the multiple washing steps. This resulted in immunostaining often showing many fewer cells than were initially present on the scaffold.

This weak adhesion can be tied to the concentration of peptide on the scaffold surface. The fibers possessed a surface peptide density of 46.5 pmol/m^2 (Chapter 6). Surfaces with peptide densities of 10 pmol/m^2 have been shown to be capable of supporting cell adhesion, though maximal spreading wasn't achieved until concentrations of 100 pmol/m^2, and stress fibers do not form until a concentration of 1 nmol/m^2 [42]. The multivalency of the peptide conjugates will increase their potency and improve adhesion, which will lower the peptide concentration necessary for optimal spreading. However, the fibers also contain a significant amount of pEG, which will inhibit adhesion. The combination of these three factors, peptide density, multivalency, and pEG inhibition, will need to be further explored and characterized to create an optimal surface for cardiomyocyte adhesion.

7.4.2. Contractility of cardiomyocytes on electrospun scaffolds

Cells were viable and functional for over two months on the peptide containing fibers. Spontaneous beating of cardiomyocytes was observed on all peptide-containing samples with the contractions becoming more prevalent and more pronounced as cell culture continued. The cell clusters beat independently and asynchronously. Observed beat rates varied from 20 bpm to 64 bpm. In some cases, these contractions were capable of deforming the scaffold hundreds of microns away. Larger, long-range contractions were powerful enough to cause contraction and bending of the electrospun matrix. A series of images showing the deformation of the scaffold due to cardiomyocyte contractility is shown in Figure 7.3. A single colony source for these

contractions could not be identified, suggesting that the cells between clusters were beating as well. After one week, the scaffolds began to twist into curves and helices that continued to beat (data not shown). This was likely caused by asymmetrical cell contractility as cardiomyocytes attached to the top of the fibers and were incapable of full penetration of the mat.

After one week of culture on the electrospun fibers, all of the differentiated cell population expressed cardiac troponin T (cTnT) (Figure 7.4). Live imaging of mcherry expressing cells showed that these αMHC positive cells in the clusters are responsible for the contractile activity of the cell clusters. These beating cells were observed throughout the material surface, as seen in Figure 7.5. As these αMHC positive cells were observed to be the source of contractions while in clusters, this population seen outside of the clusters is likely responsible for the coordinated long-range contractions.

7.5. Conclusions

These experiments serve as a proof of concept for this material to serve as a biomimetic scaffold for cardiomyocyte culture. With the inclusion of cell-adhesive peptides, the hydrogel nanofibers were capable of supporting cardiomyocyte adhesion. Further improvements to the strength of the cell-material interaction are necessary, though they are in principle simply optimization of the amount of peptide and pEG present in the fibers. This and other material improvements are addressed in Section 7.6. In addition to supporting cellular survival, these materials were capable of maintaining cardiomyocyte function. Cardiomyocytes remained metabolically active and underwent spontaneous contraction for over two months on the fibers. These contractions exerted significant force on the underlying material sufficient to cause large deformations over the scale of hundreds of microns. Cells within clusters were electrically independent of other clusters, with no synchronization of their contraction. However, long-range coordinated contraction with no source cluster was observed, implying the activity of a population of cells outside the clusters. These results demonstrate the material's capacity to act as a cell scaffold. Further refinements and improvements may render the material capable of being used as a cardiac patch for treatment of myocardial infarction.

7.6. Future Directions

The experiments and results outlined here should serve as a proof of concept for this promising material system. However, before this material may be put to use in applications such as tissue engineering, additional experiments and refinements are necessary. The synthesis protocol and materials chosen in this dissertation serve as just one possible use of this materials platform, which can be adapted to a wide variety of applications. For the purpose of use as a cardiomyocyte scaffold, three further experiments and alterations are of particular interest and importance: improving cell-material adhesion, quantifying cellular alignment on the material, and making a quantitative assessment of the cardiomyocyte contractility.

To the first point, several methods are available to improve cell-scaffold interaction. One possibility is the use of a different peptide in the conjugate. In this work, bsp-RGD(15) was chosen, as it is a simple peptide that is widely used and well understood, and is capable of binding and supporting a wide variety of cell types. Changing this peptide to one that is more adhesive, such as a cyclic RGD containing peptide, could further improve cellular adhesion. Another possibility is to increase the surface peptide density. This can be accomplished in three

ways: increasing the valency of the conjugates to increase the number of peptides per hyaluronic acid backbone molecule, increasing the concentration of hyaluronic acid conjugate in the electrospinning solution, or decreasing the amount of pEG and pEGDA in the electrospinning solution. Any of these three methods will increase the relative amount of peptide in the system, which should have positive implications on cellular adhesion.

Once cellular adhesion has been improved such that cells will adhere and spread on the surface, the capability of the material to induce alignment of the cell cytoskeleton must be addressed. In Chapter 6, we showed that by electrospinning onto a rapidly rotating target, we can induce alignment of the nanofibers. Other labs have shown that cells cultured on aligned substrates, including nanofibers, will spontaneously align with this substrate. This result must be confirmed on this novel material.

The functionality of cardiomyocytes on the material, namely their spontaneous contraction, has been assessed qualitatively here in Chapter 7.4.2. To fully characterize the material and its interaction with cells, cardiomyocyte contractility should be quantitatively measured. Namely, cell beat frequency and contractile strength must be measured. A video tracking software currently in use by our lab is capable of tracking the motion of individual components of a beating cell cluster independently of any labeling mechanism. This method can be used to quantify both the beat frequency and the displacement caused by these contractions without disturbing the system. With the known mechanics of the scaffold, these data can be translated to a contractile force. We can use these data to assess the capability of the material to mimic the myocardial extracellular matrix in a quantitative fashion by comparing cellular function on the scaffold to that in the native myocardium. Once the material has been optimized in this way, experiments in animals will be necessary to assess possible clinical implications.

7.7. Acknowledgements

The authors would like to thank Min Ju Lee and Christine Lam for assistance with material synthesis. Special thanks to Natalie Marks for her help with cell maintenance, culture, immunostaining, and imaging.

7.8. References

1. Gaziano, T. A., Cardiovascular disease in the developing world and its cost-effective management. *Circulation* **2005,** *112* (23), 3547-3553.

2. Ruvinov, E.; Leor, J.; Cohen, S., The promotion of myocardial repair by the sequential delivery of IGF-1 and HGF from an injectable alginate biomaterial in a model of acute myocardial infarction. *Biomaterials* **2011,** *32* (2), 565-578.

3. Shah, D. J.; Kim, H. W.; James, O.; Parker, M.; Wu, E.; Bonow, R. O.; Judd, R. M.; Kim, R. J., Prevalence of Regional Myocardial Thinning and Relationship With Myocardial Scarring in Patients With Coronary Artery Disease. *Jama-J Am Med Assoc* **2013,** *309* (9), 909-918.

4. van den Borne, S. W. M.; Diez, J.; Blankesteijn, W. M.; Verjans, J.; Hofstra, L.; Narula, J., Myocardial remodeling after infarction: the role of myofibroblasts. *Nat Rev Cardiol* **2010,** *7* (1), 30-37.

5. Pfeffer, M. A.; Braunwald, E., Ventricular Remodeling after Myocardial-Infarction - Experimental-Observations and Clinical Implications. *Circulation* **1990,** *81* (4), 1161-1172.

6. Dor, V.; Sabatier, M.; Montiglio, F.; Civaia, F.; Di Donato, M., Endoventricular patch reconstruction of ischemic failing ventricle. A single Center with 20 years experience. Advantages of magnetic resonance imaging assessment. *Heart Fail Rev* **2004,** *9* (4), 269-286.

7. Oh, J. K.; Velazquez, E. J.; Menicanti, L.; Pohost, G. M.; Bonow, R. O.; Lin, G.; Hellkamp, A. S.; Ferrazzi, P.; Wos, S.; Rao, V.; Berman, D.; Bochenek, A.; Cherniavsky, A.; Rogowski, J.; Rouleau, J. L.; Lee, K. L.; Investigators, S., Influence of baseline left ventricular function on the clinical outcome of surgical ventricular reconstruction in patients with ischaemic cardiomyopathy. *Eur Heart J* **2013,** *34* (1), 39-47.

8. Clifford, D. M.; Fisher, S. A.; Brunskill, S. J.; Doree, C.; Mathur, A.; Watt, S.; Martin-Rendon, E., Stem cell treatment for acute myocardial infarction. *Cochrane Db Syst Rev* **2012,** (2).

9. Williams, A. R.; Hatzistergos, K. E.; Addicott, B.; McCall, F.; Carvalho, D.; Suncion, V.; Morales, A. R.; Da Silva, J.; Sussman, M. A.; Heldman, A. W.; Hare, J. M., Enhanced Effect of Combining Human Cardiac Stem Cells and Bone Marrow Mesenchymal Stem Cells to Reduce Infarct Size and to Restore Cardiac Function After Myocardial Infarction. *Circulation* **2013,** *127* (2), 213-223.

10. Williams, A. R.; Trachtenberg, B.; Velazquez, D. L.; McNiece, I.; Altman, P.; Rouy, D.; Mendizabal, A. M.; Pattany, P. M.; Lopera, G. A.; Fishman, J.; Zambrano, J. P.; Heldman, A. W.; Hare, J. M., Intramyocardial Stem Cell Injection in Patients With Ischemic Cardiomyopathy Functional Recovery and Reverse Remodeling. *Circ Res* **2011,** *108* (7), 792-U30.

11. Freyman, T.; Polin, G.; Osman, H.; Crary, J.; Lu, M. M.; Cheng, L.; Palasis, M.; Wilensky, R. L., A quantitative, randomized study evaluating three methods of mesenchymal stem cell delivery following myocardial infarction. *Eur Heart J* **2006,** *27* (9), 1114-1122.

12. Jackson, K. A.; Majka, S. M.; Wang, H. G.; Pocius, J.; Hartley, C. J.; Majesky, M. W.; Entman, M. L.; Michael, L. H.; Hirschi, K. K.; Goodell, M. A., Regeneration of ischemic cardiac muscle and vascular endothelium by adult stem cells. *J Clin Invest* **2001,** *107* (11), 1395-1402.

13. Zhang, M.; Methot, D.; Poppa, V.; Fujio, Y.; Walsh, K.; Murry, C. E., Cardiomyocyte grafting for cardiac repair: Graft cell death and anti-death strategies. *J Mol Cell Cardiol* **2001,** *33* (5), 907-921.

14. Timmers, L.; Lim, S. K.; Hoefer, I. E.; Arslan, F.; Lai, R. C.; van Oorschot, A. A. M.; Goumans, M. J.; Strijder, C.; Sze, S. K.; Choo, A.; Piek, J. J.; Doevendans, P. A.; Pasterkamp, G.; de Kleijn, D. P. V., Human mesenchymal stem cell-conditioned medium improves cardiac function following myocardial infarction. *Stem Cell Res* **2011,** *6* (3), 206-214.

15. Chaudhry, P. A.; Mishima, T.; Sharov, V. G.; Hawkins, J.; Alferness, C.; Paone, G.; Sabbah, H. N., Passive epicardial containment prevents ventricular remodeling in heart failure. *Ann Thorac Surg* **2000,** *70* (4), 1275-1280.

16. Blom, A. S.; Mukherjee, R.; Pilla, J. J.; Lowry, A. S.; Yarbrough, W. M.; Mingoia, J. T.; Hendrick, J. W.; Stroud, R. E.; McLean, J. E.; Affuso, J.; Gorman, R. C.; Gorman, J. H.; Acker, M. A.; Spinale, F. G., Cardiac support device modifies left ventricular geometry and myocardial structure after myocardial infarction. *Circulation* **2005,** *112* (9), 1274-1283.

17. Fujimoto, K. L.; Tobita, K.; Merryman, W. D.; Guan, J. J.; Momoi, N.; Stolz, D. B.; Sacks, M. S.; Keller, B. B.; Wagner, W. R., An elastic, biodegradable cardiac patch induces contractile smooth muscle and improves cardiac remodeling and function in subacute myocardial infarction. *J Am Coll Cardiol* **2007,** *49* (23), 2292-2300.

18. Leor, J.; Amsalem, Y.; Cohen, S., Cells, scaffolds, and molecules for myocardial tissue engineering. *Pharmacol Therapeut* **2005,** *105* (2), 151-163.

19. Lutolf, M. P.; Hubbell, J. A., Synthetic biomaterials as instructive extracellular microenvironments for morphogenesis in tissue engineering. *Nat Biotechnol* **2005,** *23* (1), 47-55.

20. Langer, R.; Tirrell, D. A., Designing materials for biology and medicine. *Nature* **2004,** *428* (6982), 487-492.

21. Kirker, K. R.; Luo, Y.; Nielson, J. H.; Shelby, J.; Prestwich, G. D., Glycosaminoglycan hydrogel films as bio-interactive dressings for wound healing. *Biomaterials* **2002,** *23* (17), 3661-3671.

22. Yeo, I. S.; Oh, J. E.; Jeong, L.; Lee, T. S.; Lee, S. J.; Park, W. H.; Min, B. M., Collagen-based biomimetic nanofibrous scaffolds: Preparation and characterization of collagen/silk fibroin bicomponent nanofibrous structures. *Biomacromolecules* **2008,** *9* (4), 1106-1116.

23. Daamen, W. F.; van Moerkerk, H. T. B.; Hafmans, T.; Buttafoco, L.; Poot, A. A.; Veerkamp, J. H.; van Kuppevelt, T. H., Preparation and evaluation of molecularly-defined collagen-elastin-glycosaminoglycan scaffolds for tissue engineering. *Biomaterials* **2003,** *24* (22), 4001-4009.

24. Pieper, J. S.; van Wachem, P. B.; van Luyn, M. J. A.; Brouwer, L. A.; Hafmans, T.; Veerkamp, J. H.; van Kuppevelt, T. H., Attachment of glycosaminoglycans to collagenous matrices modulates the tissue response in rats. *Biomaterials* **2000,** *21* (16), 1689-1699.

25. Lunkenheimer, P. P.; Redmann, K.; Kling, N.; Jiang, X. J.; Rothaus, K.; Cryer, C. W.; Wubbeling, F.; Niederer, P.; Heitz, P. U.; Ho, S. Y.; Anderson, R. H., Three-dimensional architecture of the left ventricular myocardium. *Anat Rec Part A* **2006,** *288A* (6), 565-578.

26. Kenar, H.; Kose, G. T.; Hasirci, V., Design of a 3D aligned myocardial tissue construct from biodegradable polyesters. *J Mater Sci-Mater M* **2010,** *21* (3), 989-997.

27. Dang, J. M.; Leong, K. W., Myogenic induction of aligned mesenchymal stem cell sheets by culture on thermally responsive electrospun nanofibers. *Adv Mater* **2007,** *19* (19), 2775-+.

28. Mincheva, R.; Manolova, N.; Rashkov, I., Bicomponent aligned nanofibers of N-carboxyethylchitosan and poly(vinyl alcohol). *Eur Polym J* **2007,** *43* (7), 2809-2818.

29. Cho, A. R.; Shin, D. M.; Jung, H. W.; Hyun, J. C.; Lee, J. S.; Cho, D.; Joo, Y. L., Effect of Annealing on the Crystallization and Properties of Electrospun Polylatic Acid and Nylon 6 Fibers. *J Appl Polym Sci* **2011,** *120* (2), 752-758.

30. Liu, D. Y.; Yuan, X. W.; Bhattacharyya, D., The effects of cellulose nanowhiskers on electrospun poly (lactic acid) nanofibres. *J Mater Sci* **2012,** *47* (7), 3159-3165.

31. Bhardwaj, N.; Kundu, S. C., Electrospinning: A fascinating fiber fabrication technique. *Biotechnol Adv* **2010,** *28* (3), 325-347.

32. Sill, T. J.; von Recum, H. A., Electro spinning: Applications in drug delivery and tissue engineering. *Biomaterials* **2008,** *29* (13), 1989-2006.

33. Zimmermann, W. H.; Melnychenko, I.; Eschenhagen, T., Engineered heart tissue for regeneration of diseased hearts. *Biomaterials* **2004,** *25* (9), 1639-1647.

34. Hughes, C. S.; Postovit, L. M.; Lajoie, G. A., Matrigel: A complex protein mixture required for optimal growth of cell culture. *Proteomics* **2010,** *10* (9), 1886-1890.

35. Minatoguchi, S.; Takemura, G.; Chen, X. H.; Wang, N. Y.; Uno, Y.; Koda, M.; Arai, M.; Misao, Y.; Lu, C. J.; Suzuki, K.; Goto, K.; Komada, A.; Takahashi, T.; Kosai, K.; Fujiwara, T.; Fujiwara, H., Acceleration of the healing process and myocardial regeneration may be important as a mechanism of improvement of cardiac function and remodeling by postinfarction granulocyte colony-stimulating factor treatment. *Circulation* **2004,** *109* (21), 2572-2580.

36. Beltrami, A. P.; Barlucchi, L.; Torella, D.; Baker, M.; Limana, F.; Chimenti, S.; Kasahara, H.; Rota, M.; Musso, E.; Urbanek, K.; Leri, A.; Kajstura, J.; Nadal-Ginard, B.; Anversa, P., Adult cardiac stem cells are multipotent and support myocardial regeneration. *Cell* **2003,** *114* (6), 763-776.

37. Humphries, M. J.; Akiyama, S. K.; Komoriya, A.; Olden, K.; Yamada, K. M., Identification of an Alternatively Spliced Site in Human-Plasma Fibronectin That Mediates Cell Type-Specific Adhesion. *J Cell Biol* **1986,** *103* (6), 2637-2647.

38. Tiwari, A.; Salacinski, H. J.; Punshon, G.; Hamilton, G.; Seifalian, A. M., Development of a hybrid cardiovascular graft using a tissue engineering approach. *Faseb J* **2002,** *16* (8).

39. Pratt, A. B.; Weber, F. E.; Schmoekel, H. G.; Muller, R.; Hubbell, J. A., Synthetic extracellular matrices for in situ tissue engineering. *Biotechnol Bioeng* **2004,** *86* (1), 27-36.

40. Pollock, J. F.; Ashton, R. S.; Rode, N. A.; Schaffer, D. V.; Healy, K. E., Molecular Characterization of Multivalent Bioconjugates by Size-Exclusion Chromatography with Multiangle Laser Light Scattering. *Bioconjugate Chem* **2012,** *23* (9), 1794-1801.

41. Lian, X. J.; Hsiao, C.; Wilson, G.; Zhu, K. X.; Hazeltine, L. B.; Azarin, S. M.; Raval, K. K.; Zhang, J. H.; Kamp, T. J.; Palecek, S. P., Robust cardiomyocyte differentiation from human pluripotent stem cells via temporal modulation of canonical Wnt signaling. *P Natl Acad Sci USA* **2012,** *109* (27), E1848-E1857.

42. Massia, S. P.; Hubbell, J. A., An Rgd Spacing of 440nm Is Sufficient for Integrin Alpha-V-Beta-3-Mediated Fibroblast Spreading and 140nm for Focal Contact and Stress Fiber Formation. *J Cell Biol* **1991,** *114* (5), 1089-1100.

7.9. Figures

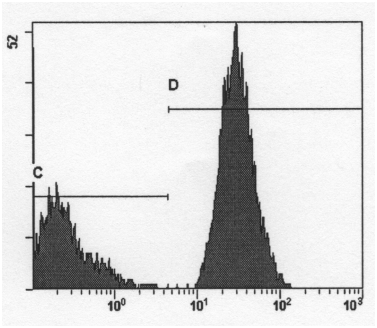

Figure 7.1. Flow cytometry of iPS cell population post-differentiation. 55% of the cell population stained positive for cardiac troponin T (cTnT).

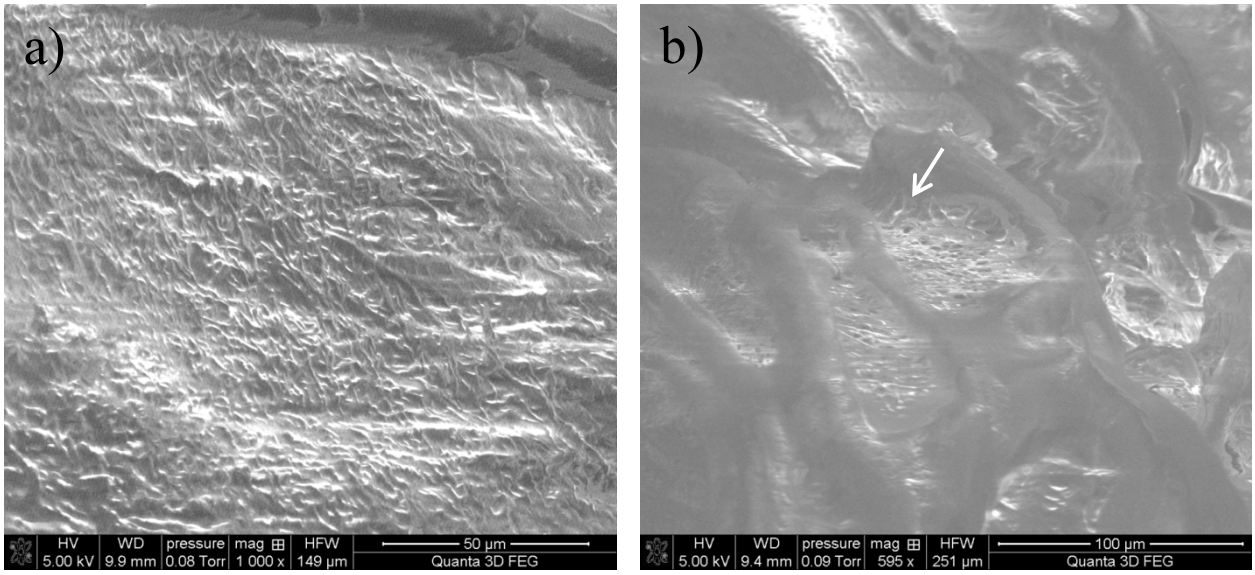

Figure 7.2. Environmental SEM image of cardiomyocytes cultured on electrospun fibers without (a) and with (b) RGD-conjugated HyA. Cells in the image are seen as large, dark mounds on top of the fibrous substrate. In image (b), cells can be seen adhered to, and putting tension on, the underlying fibers. These interactions are indicated with a white arrow.

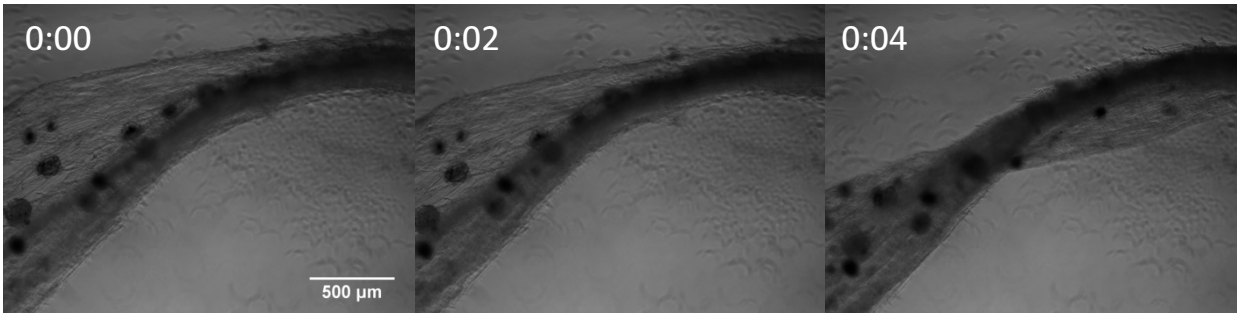

Figure 7.3. Series of optical microscopy images of deformation of electrospun scaffold due to cardiomyocyte contractility. None of the cell clusters seen on the surface of the materials could be identified as the center of contraction, implying the action of a less visible layer of inter-cluster cells.

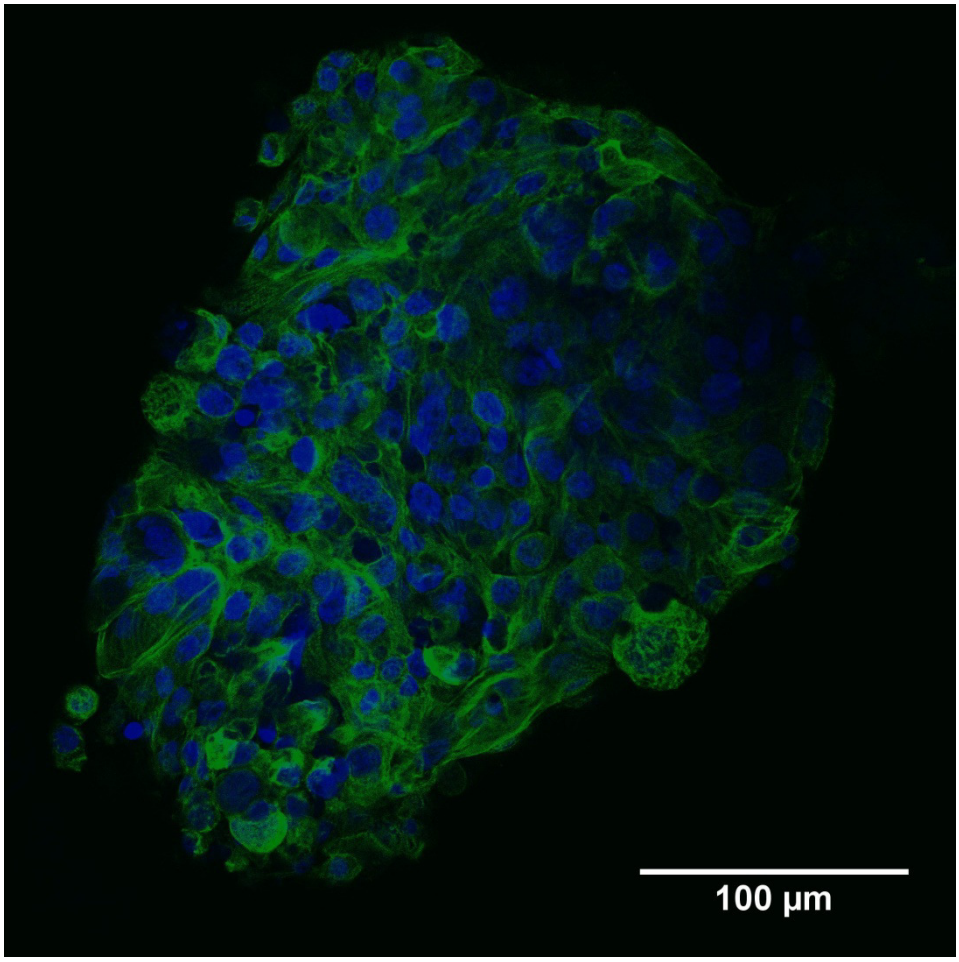

Figure 7.4. Immunostaining of cardiomyocytes on electrospun fibers. Cardiac troponin T is stained green. DAPI is stained blue.

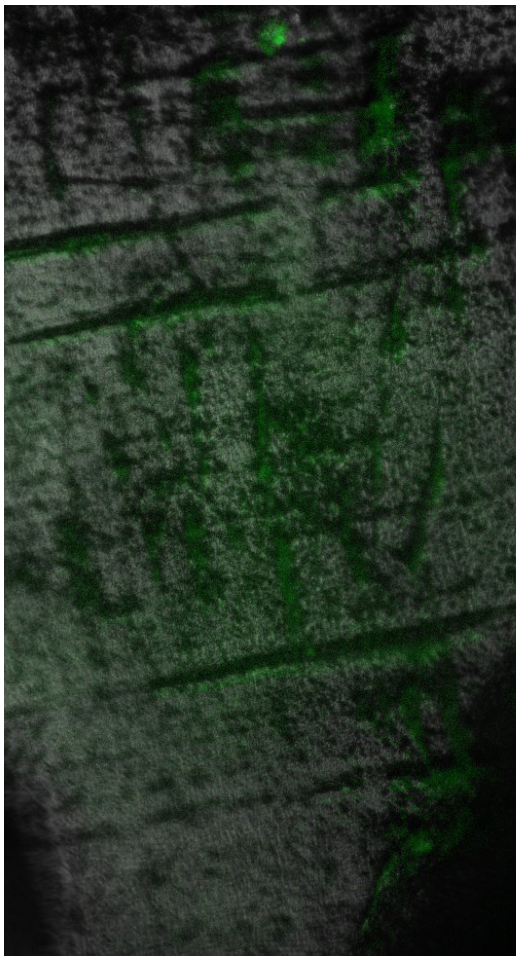

Figure 7.5. mCherry imaging of αMHC in cardiomyocytes on electrospun fibers. These αMHC positive cells are seen distributed on the scaffold and not isolated to cell clusters.